TRITA-FYS 2013:45
ISSN 0280-316X
ISRN KTH/FYS/--13:45—SE

Royal Institute of Technology
School of Engineering Sciences
Nuclear Energy Engineering
Nuclear Power Safety

Coupled 3D Thermo-mechanical Analysis of Nordic BWR Lower Head Failure in case of Core Melt Severe Accident

Master of Science Thesis by:

Claudio Torregrosa Martín

Supervisor:

Dr. Pavel Kudinov

Stockholm, Sweden, June 2013

ABSTRACT

In the present Master Thesis a hypothetical core melt severe accident in a Nordic BWR is considered. The molten core material is assumed to be relocated and quenched in the lower head of the reactor vessel forming an internally heated debris bed and eventually a melt pool of corium, which will inflict thermal and mechanical loads to the vessel wall and penetrations leading to its failure. The mode and timing of the vessel failure determine melt ejection characteristics and the success of ex-vessel melt retention strategy proposed in Nordic BWR as a means of terminate the severe accident progression.

A coupled thermo-mechanical approach using plant-scale 3D models of the lower head geometry with penetrations is followed in the present work in order to reduce uncertainties in the mode and timing of vessel failure. The calculations are performed coupling the Phase change Effective Convectivity Model (PECM), which simulates the debris bed heat transient and thermal load to the lower head, with ANSYS finite element structural models of the vessel wall and penetrations. Furthermore, several scenarios are considered in terms of (i) implementation of control rod guide tube (CRGTs) cooling as a severe accident management strategy, and (ii) different amounts of the core relocated in the lower plenum, with the aim to investigate the influence of these factors on the mode and timing of (a) failure through the vessel penetrations, and (b) failure through the vessel wall by creep.

A total of four possible modes of vessel failure at different times have been identified depending on the scenario. (i) The failure through instrumentation guide tube (IGT) ejection is the earliest mode of failure for both cooling scenarios. In addition, two different modes of vessel wall failure depending on the amount of core relocated in the lower head were found; (ii) vessel wall creep failure by “localized creep” at the vicinity top periphery of the wall, and (iii) vessel wall creep failure by “ballooning” of the vessel bottom. These results are consistent with previously obtained results from analytical calculations using 3D-slice models of the reactor lower head, although slight differences in the timing of failure as a consequence of considering a 3D quadrant model are obtained. Finally, a new possible mode of failure that was not previously being identified was found, that is, (iv) Failure by accelerated creep at the CRGTs penetrations, which can take place earlier than the vessel wall failure for the scenarios without CRGTs cooling.

ACKNOWLEDGEMENTS

I would like to express my deep gratitude to Professor Pavel Kudinov for providing me the chance to carry out this project at the Nuclear Power Safety Division at Royal Institute of Technology, for his always fruitful supervision, clarity of ideas, and dedicated teaching in this interesting and challenging topic.

My special thanks and sincere appreciation to my co-supervisor Dr. Walter Villanueva for his almost daily guidelines, encouragements, and consideration for listening and answering all my comments and concerns.

My dedicated thanks to my Master Thesis colleague, Andrei Goronovski, for our discussions and his observations, as well as to all the other people at the Nuclear Power Safety Division for making a friendly and confidence environment during these months of work.

Finally, I want express my warmest gratitude to my parents and my sister, for their love, encouragements and endless support during my studies and this project. This work would never have been possible without their support, and for this reason it is dedicated to them.

This work was supported in the framework of MSWI-APRI project by the Swedish Nuclear Safety Radiation Authority (SSM, the former SKI), Swedish Power Companies, Swiss Federal Nuclear Safety Inspectorate (ENSI, the former HSK), Nordic Nuclear Safety Research (NKS), and by European Commission in the framework of SARNET Project.

Claudio Torregrosa Martin

TABLE OF CONTENTS

Abstract I

Acknowledgments II

List of Acronyms V

Nomenclature VI

List of Figures VII

List of Tables VIII

1 Introduction ..... - 1 -

1.1 Motivation ..... - 1 -

1.2 Background ..... - 3 -

1.2.1 Core Melt Scenarios and Ex-vessel Retention ..... - 3 -

1.2.2 In-vessel Severe Accident Progression in Nordic BWR ..... - 4 -

1.3 Conclusions about the state-of-the-art: ..... - 15 -

1.4 Goals and Tasks ..... - 16 -

1.4.1 Scope of Task I ..... - 16 -

1.4.2 Scope of Task II ..... - 17 -

2 Approach and Methodology ..... - 19 -

2.1 Thermal and Mechanical Aspects ..... - 19 -

2.1.1 The PECM Model for the Debris Bed and Melt Pool Heat Transfer ..... - 19 -

2.1.2 Debris Bed and Melt Pool Material Properties ..... - 22 -

2.1.3 Material properties for the Vessel Wall Structural Models ..... - 22 -

2.1.4 Creep Model for the Vessel Wall Structural Analysis ..... - 23 -

2.1.5 Boundary and Initial Conditions ..... - 24 -

2.1.6 Boundary Conditions of Debris Bed and Melt Pool Heat Transfer Models ..... - 25 -

2.1.7 Boundary Conditions of the ANSYS Structural Models ..... - 25 -

2.2 Specific Approach and Methodology of Task I ..... - 26 -

2.2.1 Approach ..... - 26 -
2.2.2 Debris Bed and Melt Pool Heat Transfer Models ..... - 29 -
2.2.3 Finite Element Structural Models ..... - 33 -
2.3 Specific Approach and Methodology of Task II ..... - 36 -
2.3.1 Approach ..... - 36 -
2.3.2 Implementation of PECM in 3D Quadrant Geometry ..... - 37 -
2.3.3 3D Quadrant Structural Model ..... - 38 -
3 Results and Discussions ..... - 40 -
3.1 Task I: Study of the Instrumentation Guide Tube Failure ..... - 40 -
3.1.1 Debris Bed Heat Transfer Solution in the Unitary Volume ..... - 40 -
3.1.2 Results of the IGTs Penetrations' Housing Local Analysis ..... - 50 -
3.2 Task II: Study of the Vessel Wall Failure using 3D Quadrant Geometries ..... - 55 -
3.2.1 Debris Bed and Melt Pool Heat Transfer Solution ..... - 55 -
3.2.2 Structural Creep Analysis ..... - 64 -
4 Conclusions ..... - 72 -
5 Bibliography ..... - 76 -

LIST OF ACRONYMS

ADS	Automatic Depressurization System
APRI	Accident Phenomena of Risk Importance
BWR	Boiling Water Reactor
CDA	Core Disruptive Accident
CFD	Computational Fluid Dynamics
CMA	Core Melt Accident
CRGT	Control Rod Guide Tube
DB	Debris Bed
DBA	Design Basis Accident
FOREVER	Failure of REactor VEssel Retention
ECCS	Emergency Core Cooling System
EVMR	Ex-Vessel Melt Retention
IGT	Instrumentation Guide Tube
IVMR	In-Vessel Melt Retention
NPS	Nuclear Power Safety Division
LOCA	Loss of Coolant Accident
NPP	Nuclear Power Plant
PECM	Phase change Effective Convectivity Model
PWR	Pressurized Water Reactor
SA	Severe Accident
SAM	Severe Accident Management
SARNET	Severe Accident Research NETwork of Excellence
SBO	Station Black Out
SSM	Swedish Nuclear Radiation Protection Authority
USNRC	U.S Nuclear Regulatory Commission

NOMENCLATURE

C_p	Specific heat capacity, J/(kg.K)
T	Temperature
t	Time, s
g	Gravitational acceleration, m/s^2
h	Enthalpy, J/kg
H, H_{pool}	Height of the melt pool, m
k	Thermal Conductivity, W/(mK)
Nu	Nusselt number, $Nu = \frac{qHpool}{k\,\Delta T}$
Pr	Prandtl number, $Pr = \nu / \alpha$
Q_v	Volumetric heat source, W/m^3
Q	Heat flux, W/m^2
Sc	Source term
Ra'	Rayleigh number (internal) $Ra' = \frac{g\beta Q_v {H_{pool}}^5}{k\,\nu\,\alpha}$
u,v	Fluid velocity, m/s
U	Characteristic velocity, m/s
W	Width of pool volume, m
α	Thermal diffusivity, m^2/s, $\alpha = \frac{k}{Cp\,\rho}$
β	Thermal expansion coefficient, 1/K
ε_{cr}	Creep strain
σ	Mechanical stress, Pa
ΔT	Temperature difference, K
ρ	Density, kg/m^3
ν	Kinematics viscosity, m^2/s
μ	Dynamic viscosity, Pa.s

LIST OF FIGURES

Figure 1: Scheme of ex-vessel coolability strategy implemented in Nordic BWR..... - 2 -
Figure 2: Modes of core damage depending on “dry conditions” or ·wet conditions”..... - 6 -
Figure 3: Scheme of molten pool formation from a non-coolable debirs bed. ..... - 7 -
Figure 4: Model of a BWR 75 kokvattenreaktor ASEA ATOM, ... - 10 -
Figure 5: Layout of the lower head of a Nordic BWR..... - 11 -
Figure 6: Scheme of the IGT vessel penetration. ..... - 12 -
Figure 7: ANSYS creep model validation results ..... - 24 -
Figure 8: Scheme of the methodology employed to investigate the IGT failure ..... - 28 -
Figure 9: 3D Slice geometry model where the PECM was implemented..... - 29 -
Figure 11(a): Scheme of the slice of the lower head geometry..... - 30 -
Figure 11(b): Top View of the virtual geometry represented by the 3D slice model ..... - 30 -
Figure 12: Unitary Volume Model where PECM was implemented in Fluent..... - 32 -
Figure 13: 2D axi-symmetric structural model used for the step II in figure 8,..... - 34 -
Figure 14: Structural 3D IGTs Penetrations Housing Models implemented in ANYS ..... - 35 -
Figure 15: Scheme of the flow limiter in the IGT housing penetrations..... - 35 -
Figure 16: Scheme of the methodology employed in the Task II of the present work. ..... - 36 -
Figure 17: 3D quadrant models where the PECM was implemented in FLUENT..... - 37 -
Figure 18: ANSYS 3D Quadrant Structural model used in the the Task II ..... - 39 -
Figure 19: Averaged temperature in the IGT welding as a function of time ..... - 41 -
Figure 21: Snapshot of the debris bed temperature distribution at the IGT surrounding..... - 43 -
Figure 22: Snapshot of the debris bed temperature distribution at the IGT surrounding..... - 44 -
Figure 23: Snapshot of the debris bed temperature distribution at the IGT surrounding..... - 45 -
Figure 24: Debris bed bulk temperature distribution as a function of depth..... - 46 -
Figure 25: Debris bed bulk temperature distribution as a function of depth..... - 46 -
Figure 26: Snapshot of the IGT and CRGTs melt mass fractions at 1.9h. ..... - 47 -
Figure 27: Spatial distribution melt fraction of the IGTs as a function of its height ..... - 48 -
Figure 28: Spatial distribution melt fraction of the IGTs as a function of its height ..... - 48 -
Figure 29: Spatial distribution melt fraction of the CRGTs as a function of its height, ... - 49 -
Figure 30: Averaged temperature in the IGT (red) and CRGTs (black) welding ..... - 49 -
Figure 32: Deformation of the flow limiter at 2.5 hours, ... - 51 -
Figure 33: Distance of the diametrical opposite pairs of nodes selected in the flow limiter. ... - 52 -
Figure 34: Distance of the diametrical opposite pairs of nodes selected in the flow limiter. ... - 52 -
Figure 35: Temperature distribution at the surroundings of the IGT farthest to the center ..... - 53 -
Figure 36: Distance of the diametrical opposite pairs of nodes selected in the flow limiter. ... - 54 -
Figure 37: Distance of the diametrical opposite pairs of nodes selected in the flow limiter .... - 54 -
Figure 38: Average temperature in the debris bed/melt pool volume as a function of time..... - 56 -
Figure 39: Average melt mass fraction in the debris bed/melt pool volume ..... - 57 -
Figure 40: Snapshots the melt mass fraction in the debris bed at t=3.47 h..... - 58 -

Figure 41: Snapshots of the temperature distribution in the debris bed at t=3.47 h,..... - 58 -
Figure 42: Temperature distribution on the vessel surface as a function of the angle..... - 60 -
Figure 43: Average temperature in the debris bed/melt pool volume as a function of time..... - 61 -
Figure 44: Average melt mass fraction in the debris bed/melt pool volume. ..... - 62 -
Figure 45: Snapshots the melt mass fraction in the debris bed at t=3.61 h..... - 62 -
Figure 46: Snapshots of the temperature distribution in the debris bed at t=3.61 h..... - 63 -
Figure 47: Maximum creep strain as a function of time for scenarios I (blue) and II (red),..... - 64 -
Figure 48: Snapshot of the Von Mises creep strain (a) and Temperature (b) at t=3.47 h..... - 65 -
Figure 49: Snapshot of the Von Mises creep strain (a) and Temperature (b) at t=3.75 h..... - 65 -
Figure 50: Snapshot of the Von Mises creep strain (a) and Temperature (b) at t=3.47 h..... - 66 -
Figure 51: Snapshot of the Von Mises creep strain (a) and Temperature (b) at t=3.7 h..... - 67 -
Figure 52: Snapshot of the Von Mises creep strain (a) and Temperature (b) at t=4.7 h..... - 68 -
Figure 53: Snapshot of the Von Mises creep strain (a) and Temperature (b) at t=3.3 h..... - 68 -
Figure 54: Snapshots of the Von Mises creep strain and displacements ..... - 69 -
Figure 55: Vertical dislpacement of the bottom of the vessel as a function of time..... - 70 -

LIST OF TABLES

Table 1: Summary of time and mode of vessel wall failure previously predicted. ..... - 14 -
Table 2: Debris Bed properties used in the PECM simulations..... - 22 -
Table 3: Coefficients used in the primary hardering creep model ..... - 23 -
Table 4: Mesh Parameters of the 3D Slice PECM model implemented in Fluent..... - 30 -
Table 5: Mesh Parameters of the 3D Unitary Volume Geometry PECM..... - 31 -
Table 6: Mesh Parameters of the 2D axi-symmetric structural model..... - 33 -
Table 7: Mesh Parameters of the 2D axi-symmetric structural model..... - 34 -
Table 8: Mesh information for the three different 3D Quadrant PECM ……..- 38 -
Table 9: Mesh information of the ANSYS 3D Quadrant Structural Model..... - 38 -
Table 10: Summary of time and mode of vessel wall failure..... - 71 -

1 Introduction

1.1 Motivation

Nuclear power has proven to be a reliable and economic source of energy. By the end of 2012 there were over 430 commercial nuclear power reactors operating in 31 countries with 372 GWe of total capacity [1]. However, the future of nuclear energy is subjected to the capability to ensure the safety of Nuclear Power Plants (NPP). History has shown that, despite the accident prevention and management measures adopted in NPPs, it is still possible that unexpected combination of events and failures will develop into severe accident with core melting. Robust mitigation strategy is necessary in order to prevent further propagation of the accident and subsequent release of radionuclides into the environment. The Fukushima accident occurred in Japan in 2012 strongly underlined this fact. It is mandatory for the worldwide nuclear energy enterprise, in order to survive, to join efforts for adopting the necessary engineering solutions to prevent such kind of accidents. Society and regulatory authorities demand for future nuclear power plants no consequences for the environment and no evacuation of the population in any conceivable scenario, as well as to promote the implementation of possible strategies in current plants to get close to this desirable situation. In this context, the knowledge of the phenomena that may occur during severe accidents in a nuclear power plant is an essential prerequisite to predict the plant behavior and design the proper procedures and instructions for accident management.

The Nuclear Power Safety Division at KTH (KTH-NPS) has made an important contribution to the state-of-the-art in the area of core melting severe accident progression over the past 20 years. This research has been carried out under the APRI Accident Phenomena of Risk Importance framework, supported by the Swedish Nuclear Radiation Protection Authority (SSM) as well as the SARNET Severe Accident Research NETwork of Excellence of the European Commission. The ultimate goal of this ongoing severe accident research is to help reduce uncertainties in the accident progression and acquire valuable knowledge for the application of proper Severe Accident Management (SAM) strategies in current reactors as well as for the safety design of future reactors [2].

One of these SAM strategies proposed in Nordic BWR is to apply ex-vessel melt coolability as a means to terminate severe core melting accident progression. This strategy will be achieved by flooding the reactor cavity in such a way that a coolable porous debris bed of the melted core is formed on the containment basemat as is shown in Figure 1. However, the success of this strategy

depends strongly on the melt ejection characteristics which determine formation and coolability of the debris bed in the flooded cavity. In the most desirable situation, the solidification of the debris bed would terminate the accident without any significant fission products release to environment, as long as the containment integrity is ensured. On the other hand, a non-coolable debris will be reheated, re-melted, and will attack the containment basemat [3], [4], [5], [6], [7] [8]. Besides, there is a risk of energetic melt-coolant interactions (steam explosions) which can also threaten containment integrity and would occur if, for example, the melt jet size and superheat are large.

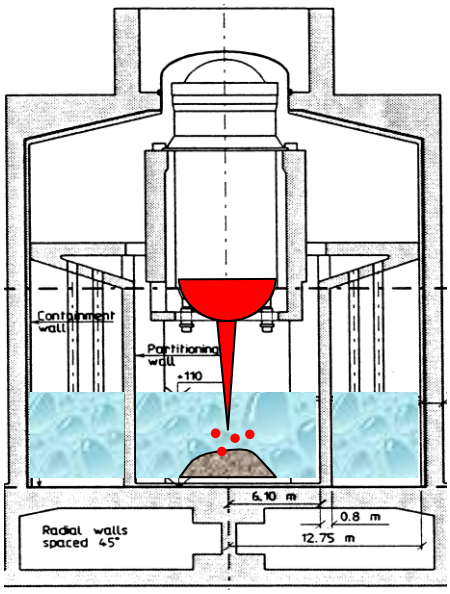

Figure 1: Scheme of ex-vessel coolability strategy implemented in Nordic BWR by flooding the reactor cavity.

The melt ejection characteristics, key factor of the ex-vessel coolability success, will be determined by the mode and timing of vessel failure, which depends on the in-vessel accident progression. Decay heated debris bed formed in the lower head of the reactor vessel inflicts thermal and mechanical loads to the vessel wall and penetrations determining their failure mode and timing. At the same time, this in-vessel progression is full of uncertainties due to the large amount of factors and possible scenarios in the development of the accident stages. For instance, the overheating and core damage process at the beginning of the accident will affect, among other things, the amount of debris relocated in the lower head, its material properties, decay heat and eventually the time and mode of vessel failure. The reduction of these uncertainties is a challenge. Detailed analysis of all the in-vessel stages and the physics involved is practically not feasible due to extreme complexity and strong dependencies on the history of accident.

The main motivation of the present work is the need to identify and consider major sources of uncertainties in the vessel failure modes and timing. Numerical simulations with developed computational tools are used to address the possible modes and timing of the vessel failure for selected accident scenarios.

1.2 Background

In this section we will introduce the reader to the core melt severe accident phenomenology, and the necessary background in order to understand the context, purpose and scope of the present work. Furthermore, we will highlight the importance of predicting the mode and timing of vessel failure for the success the ex-vessel SAM strategy. In addition we will present the state-of-the-art in the lower head failure phenomenology and identify the gaps in the knowledge which will help us establish the goals and tasks of our present work.

1.2.1 Core Melt Scenarios and Ex-vessel Retention

Severe accident definition includes the accidents that are beyond the Design Basis Accidents (DBAs), i.e. accidents that are not postulated as a basis for the design of the safety systems. There are two types of severe accidents that may occur, core melt accidents (CMAs) and core disruptive accidents (CDAs). The last is caused by rapid reactivity insertion that leads to an abrupt increase of the temperature in the core, causing its disintegration in a time scale of seconds. The Chernobyl accident (Ukraine 1986) belonged to this type of accident, which is considered practically impossible in light water power reactors due to inherent negative reactivity feedbacks and engineered safety features.

Core melt accidents, which are the focus of the present work, are initiated due to inadequate core cooling, caused by Loss of Coolant Accidents (LOCA) or station black out (SBO) and failure of emergency core cooling systems (ECCS). The cause of this kind of accident is that, even if the fission reaction stops when the reactor is shut down, energy continues to be released from the decay of the fission products. This decay heat represents a 7% of the operating reactor power and decreases about 1% after one hour. In larger power reactors this heat is more than substantial and the absence of water cooling will increase fuel cladding leading to dry-out. Furthermore, the sudden increase of the cladding by several hundred degrees will cause oxidation of the zirconium present in the cladding. This reaction is very exothermic and at high temperatures can release as much as energy as the initial decay heat. Under this situation meltdown of the core will happen in a time scale of hours [9]. Three Mile Island Unit 2 TMI-2 Accident (March 1979) and Fukushima (March 2011) belong to this core melting type of severe accident.

In this context, the severe accident management (SAM) consists of actions that would prevent the subsequent release of radionuclides by avoiding the failure of the physical safety barriers, i.e. fuel cladding, reactor vessel and containment. In the postulated core melting severe accident, the cladding barrier has already failed since the core is melted. Therefore the termination of the accident will be only achieved when the molten core has re-solidified, cooled and stabilized while the integrity of at least one of the remaining physical barriers is ensured. Two types of SAM depending on where the corium has stabilized; In-vessel Retention (IVMR) and ex-vessel melt retention (EVMR)

In the IVMR strategy the vessel cavity would be completely filled with water. Thus, the molten core relocated in the lower head would be stabilized inside the vessel, and cooled from the outer vessel surface. The possibility of in-vessel retention was contemplated for the considered Nordic BWR with a combination of control rod guide tube (CRGTs) cooling and external cooling by flooding the reactor cavity [10], [11]. However, the high Nordic BWR cavity depth (7-12m) makes external vessel cooling unfeasible at the early stage of the severe accident since flooding the entire cavity will take a long time [12]. This feature and the possible failure through the penetrations work against the implementation of IVMR in Nordic BWR.

In the EVMR strategy, on the other hand, the reactor vessel is assumed to fail leading to melt flow outside the vessel, to the reactor cavity. Then, the corium will be located, cooled down and stabilized there by specially designed strategies. In some new GenIII+ reactors this is achieved by a specially designed core catcher. Alternatively, in the case of Nordic BWR ex-vessel melt retention SAM strategy is currently adopted by flooding the reactor cavity with water coming from the suppression pool, with the aim to quench and stabilize the ejected corium upon vessel failure. However, the success of this strategy relies on the formation of a coolable bed in the flooded cavity as well as avoiding high energy steam explosions when the melt jet from the failed vessel interacts with water. Melt ejection characteristics determine conditions for both steam explosion and formation of debris bed. Thus the mode and timing of vessel failure which, at the same time, depends on the in-vessel accident progression, determines success of the accident mitigation strategy.

1.2.2 In-vessel Severe Accident Progression in Nordic BWR

In this section we include a description of the core degradation, relocation, in-vessel debris bed formation, and identified modes of vessel failure. It is worth noting that the accident progression will be dependent on the possible scenario, SAM activation and cooling capability. The aim of the this section is not to assess a detailed analysis of all possible situations but to introduce the reader to the scenario considered in the present study and provide the justification of the assumptions that were made in the present work.

Core degradation and debris bed formation in a lower head of BWR

The core melt accident starts due to inadequate core cooling as a consequence, for example, of a SBO. In the absence of power supply to the pumps to cool the decay heated core from the auxiliary feedwater system, the water level in the reactor will start decreasing as the water starts evaporating and result to core overheating and melting. The behavior of the core and heating is very dependent on its composition and configuration, as well as the zircaloy cladding oxidation rate. Calculations implemented with the MELCOR code [13] for SBO scenario show that this process can be a very fast (order of 2 o 3 hours) if high rates of oxidation takes place [14].

The decrease of the water level will lead to core uncovery from the top. At this point, two different accident paths that may influence the accident progression and debris bed formation have been identified [15]. These two paths are defined depending if the core damage occurs under “dry core” or “wet core” conditions. For the present study “dry core” scenario is assumed, as it is considered more probable in BWR [12].

In the accident progression with core damage under “dry core” core conditions, the ADS (automatic depressurization system) can be activated and it willopen the reactor relief valves connected to the main steam lines to discharge and cool down the generated steam into the suppression pool. This procedure is intended to cool down the reactor by making use of the steam blowdown cooling effect, and to permit the activation of any potentially available low pressure coolant injection systems [15]. In the event that any of these injection systems is available and core cooling is not regained, the water level in the vessel is expected to be below the core lower plate but still filling the reactor lower plenum. The uncovered fuel rods and reactor core materials (including reactor internal structures, control rods, instrumentation tubes, etc.) will overheat, melt and drain by gravity to the lower plenum. It appears that in BWR early melting of the cruciform control rods and metallic structures, with considerable lower melting point than ceramic fuel, will drain and accumulate on the lower core plate, leading to its failure. The channel boxes of the fuel bundles in a BWR core do not promote core-wide blockages, and melt from individual bundles may dribble down to the lower head. This relocating mode is called “small jets” mode (Figure 2-a).

It must be mentioned that in a “wet core” degradation scenario the mode of core relocation and debris bed formation may be different than the behavior explained above. In “wet core” conditions no depressurization of the vessel is considered and therefore water level is assumed to be above the lower core plate. Under this situation, a metal blockage is expected to happen on the core lower plate due to quenching and relocation of molten metallic materials with the presence of water in the lower regions of the core, forming a dense crust. Subsequent melt collects upon the crust blockage leading to the formation of a molten pool above the lower core plate. This pool, consisting mainly of molten ceramic fuel, will grow progressively until it reaches the peripheral regions of the core. Thus, the melt will overflow to the lower plenum following sideward relocation in the so called “candling” mode (Figure 2-b). The TMI-2 accident is an example of this mode of relocation mechanism [16]. Finally, there is third mechanism of core material relocation called “big jet mode” that may happen after a dramatic failure of the core plate that is below the core melt pool.

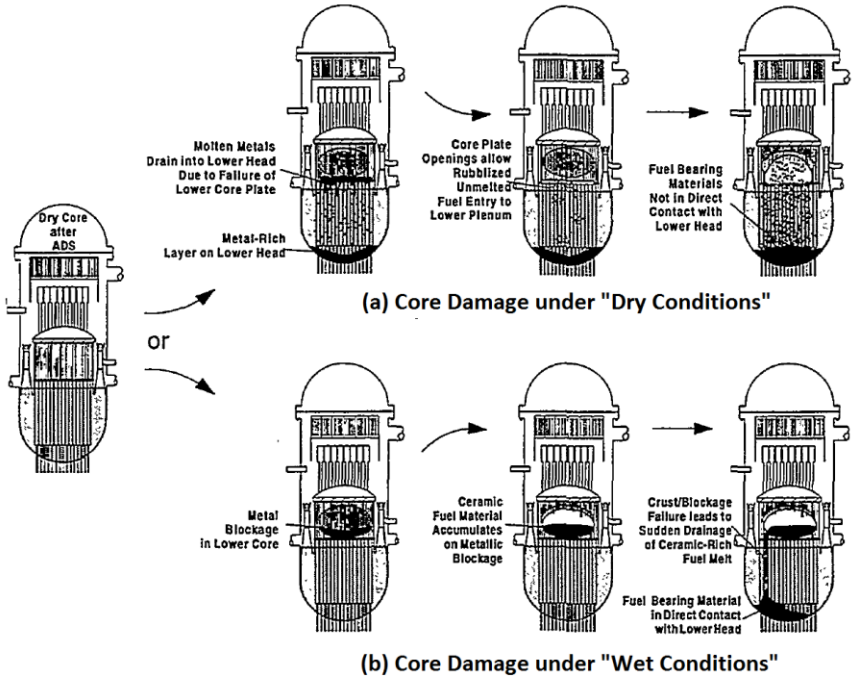

Figure 2: Modes of core damage depending on "dry conditions" or ·wet conditions". The mode of core degradation can affect the mode or relocation of debris bed and eventually failure of the vessel. Drawing obtained from: The XR-2-1 BWR Metallic Melt Relocation Experiment [15]

The characteristics and load inflicted to the vessel and penetrations can be quite different depending on these three relocation mode mechanisms; small jets, candling, of big jet. Nevertheless, we assume for the present calculations that the relocation mode takes place in a mode where no direct impingement to the vessel wall occurs, i.e., the relocation is produced in sufficiently small jets that they are effectively quenched in the water filling the lower plenum, leading to the formation of a solid debris bed.

Melt pool in the lower plenum

In the presence of water in the lower head, the melt jets coming from the progressively melted core will quench, break up, fragment into small particles and form a debris bed in the lower plenum [17]. A large quantity of water in the lower head of a BWR is expected to be more than sufficient to quench an entire mass of molten core and associated structural material [18]. The assumption that water is filling the lower plenum while the molten material from the core is draining down is supported by the fact that water in the lower head can be reduced only by intensive evaporation caused by the relocation of hot materials or leakage through the failed penetrations. The probability of these events before the formation of the previously stated debris bed is considered very low. Besides, the assumption of water filling the lower plenum is reinforced if control rod guide tube (CRGT) cooling is implemented as SAM strategy.

The lower head of a BWR contains a forest of CRGTs. During normal operation a small total flow rate of 15 kg/s is injected to cool them. It is proposed that these tubes could be used as an effective measure to inject water in the reactor in case of accident and improve debris bed coolability in the lower plenum [19]. Furthermore, the flow rate of 15 kg/s is so small that could be provided by a battery driven pump, working even in case of SBO. The suitability of strategy is also enhanced by the large cooling surface provided by the forest of CRGTs and the fact that cooling from the bottom does not interfere with the counter current steam flow limitation, as happens when flooding the vessel from the top. In addition, cooling from the CRGTs will provide a top layer of water as is shown in Figure 3. In the present work, we will perform several calculations with different scenarios studying the efficiency of CRGTs and top cooling. It must be mentioned from now on, that for simplicity sometimes we will refer to it only as CRGTs cooling, but it always means CRGTs and top cooling (as the top cooling is consequence of the CRGTs cooling).

However, even with presence of water filling the lower plenum and water supply from the CRGTs, a non-coolable decay debris bed will be reheated again. If dry-out of the fragmented particles takes place, the debris bed will be re-melted, leading to the formation of a corium melt pool (Figure 3). The heat transient of this formed melt pool is characterized by a multi-component and multi-phase material under high temperature and complex flow. The composition properties of the mixture containing U, O, Zr, Fe, Ni, Cr is full of uncertainties and it will be function of the phenomena occurred upstream the accident progression, as amount of zircaloy oxidation and molten metal structures.

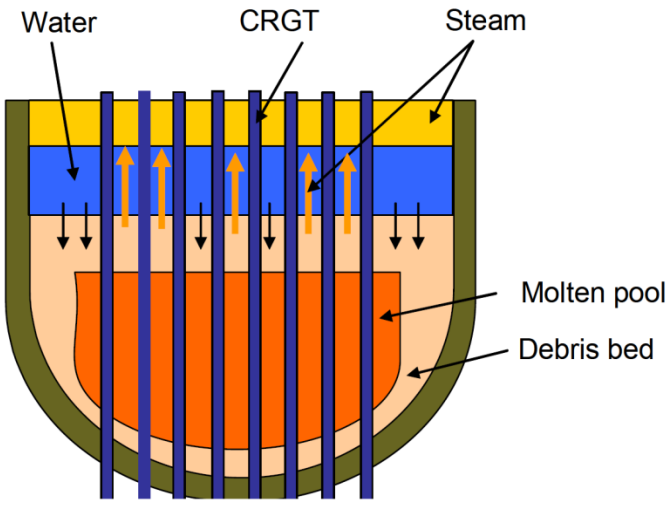

Figure 3: Scheme of molten pool formation from a non-coolable debirs bed. Even if CRGTs cooling is implemented and a layer of water is formed in the top, a non coolable debris bed will melt, leading to molten pool formation.

The melt pool chemistry can also significantly affect the melt pool composition, layer configuration and consequently load to the vessel. For instance, metallic lager stratification in the top of the molten pool (due to its lower density) can lead to concerns to the vessel integrity by the

called “focusing effect” [20]. This is produced when the top metallic layer receives a high amount of heat coming from the internally heated ceramic pool situated downwards. This heat will be mainly evacuated by conduction through the sideward boundaries of the metallic layer, leading to very high heat flux and thermal load to the vessel wall. It is worth noting that this effect was observed when vessel external cooling was applied related to in-vessel retention strategies, which can lead to larger in-vessel melt pool transients. Nevertheless in the present calculations the melt pool is considered with a homogeneous mixture and the “focusing effect” is not taken into account. This hypothesis is done because without external cooling it is assumed that the vessel will fail before the stratification of the melt pool.

Clearly, it is hard to study experimentally the heat transfer of the lower head melt pool due to its multi-component and multi-physics behavior. To assess analytically this debris bed heat transfer progression and melt pool formation is also not trivial at all. The use of Computational Fluid Dynamics (CFD) is limited for predicting the volumetrically heated melt pool behavior due to the corium pool’s high Rayleigh number (10^{15}-10^{17}) and long transients of the accident progression [21]. This difficulty is further increased in a BWR lower plenum complex geometry, which contains a forest of penetrations tubes.

To tackle the issue of computational efficiency in large-scale CFD calculations, a model was developed by Tran et al. [14] [21] called the Phase Change Effectivity Model (PECM). The PECM describes the natural turbulent heat transfer in an internally heated volume based on heat transfer correlations. In this model, the convective terms of the energy conservation equation are described using directional characteristic heat transfer velocities to transport the heat; therefore the need of solving Navier-Stokes equations is eliminated. This assumption makes this model much more computationally-efficient than conventional CFD codes. This model is used in the present work to simulate the debris bed heat transfer, molten pool formation, and to predict thermal load to the vessel wall and penetrations. Further description of this tool will be provided in Chapter 2.

Vessel lower head failure

The accumulation of decay heated debris bed in the lower plenum will start inflicting thermal and mechanical load to the vessel wall and penetrations that can eventually lead to a lower head failure. This failure marks the final stage of the in-vessel accident progression and its mode and timing will have a controlling effect on subsequent consequences of the accident. In particular, it will determine the characteristics of the melt ejection to the reactor cavity and the success of the ex-vessel retention strategy in Nordic BWR. In this section we introduce previous investigations regarding vessel lower head failure. Furthermore, we will present results corresponding to analytical calculations previously carried out at KTH-NPS and the assumptions that were made in these calculations.

Detailed analyses were performed by the U.S Nuclear Regulatory Commission (USNRC) with the aim to investigate the modes of lower head failure in a hypothetical core melting severe accident [22]. These analyses were performed for a wide range and BWR and PWR designs and hypothetical scenarios, including metallic and ceramics debris cases. They found that the failure of the vessel may occur in less than 4 hours for the case of a ceramic debris bed. For the present study, we present a description of these possible failure modes applicable to a Nordic BWR for the stated core melt accident scenario, that is, a non-coolable decay heated debris bed in the lower plenum, eventually leading to formation of a corium molt pool.

Four main mechanisms of lower head failure have been identified; (i) Penetration tube heat up and rupture, (ii) Penetration tube ejection, (iii) Lower

head vessel wall creep failure, and (iv) Lower head vessel wall failure by localized effects such as jet impingements [22]. These four mechanisms can be classified in two main groups;

(i) Failure through the penetrations
(ii) Failure through the vessel wall

Failure through the penetrations

In the lower head of a BWR there is a forest of CRGTs and instrumentation guide tubes (IGTs), see Figure 4. In addition, the lower head of a Nordic BWR design is penetrated by nozzles of the internal recirculation pumps. In the event of a large amount of core relocated to the lower head there is a possibility of melt overflow through the internal pumps when the level of relocated debris is above their nozzles (see Figure 5). Therefore, three different types of failure though the penetrations may happen; failure through the IGTs, CRGTs and pump nozzles. However we will mainly focus our present analysis on the failure of the IGT, in terms of IGT ejection. The motivation of this choice is explained below.

We do not consider in our analysis the possible failure through the recirculation pumps since we assume that even if the level of debris is above the pumps nozzles, the amount of melt that can enter the nozzle is limited and it will be quenched in the water filling the pumps. Furthermore, pumps ejection is considered highly unlikely as they are held by the vessel supporting concrete structure.

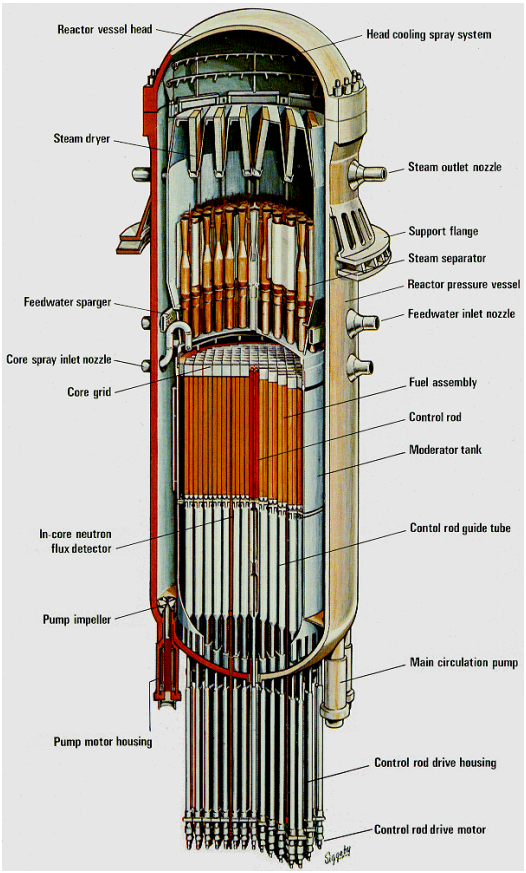

Figure 4: Model of a BWR 75 kokvattenreaktor ASEA ATOM, similar to the ABB-Atom reactor stated for the calculations carried out in the present work.

In case of IGTs and CRGTs, the ablation of the upper part in-vessel tubes is assumed to take place at the same time of melt down of the rest of the core structures. On the other hand, the parts of the in-vessel tubes submerged in the water filling the lower plenum are considered to stand while the melt jets are quenched and form the porous debris bed around them. At this point the internally heated debris bed will start inflicting a thermal and mechanical load to the tubes walls and nozzles internal welding. Two possible modes of failure penetration tubes were identified (i) Tube Heat up and Rupture, and (ii) Tube Ejection.

The tube heat up and rupture could happen as a consequence of corium melt attack and potential melt entering the penetration channel. The in-vessel part of the tubes will start melting as soon as melting temperatures are reached in the surrounding debris bed. Then, debris bed particles (which are considered in a solid state) will replace the position of the progressively melted IGT. Detailed studies about the possibility of melt entering the IGT penetration and drain outside the vessel have been previously carried out [22]. These studies found that the melt flowing through the tubes will probably freeze and plug the IGT when reaches the ex-vessel part of the tube or even before. Then, no re-melting is expected since the ex-vessel tube surface will efficiently remove the melt heat. Besides, this melt is considered to be mainly composed of metal that constitutes the tube and the lack of ceramic material will reduce its internal heat production. This assumption is

made in the present study and therefore melt flowing through the tube is not considered as a mode of failure.

Tube ejection, on the other hand, is considered as one of the dominant modes of vessel failure of BWR for pressures below 2 MPa [12], [22], especially IGTs, which are considered more vulnerable to earlier failure, due to its relatively small size (and hence lower thermal capacity) and lack of external support.

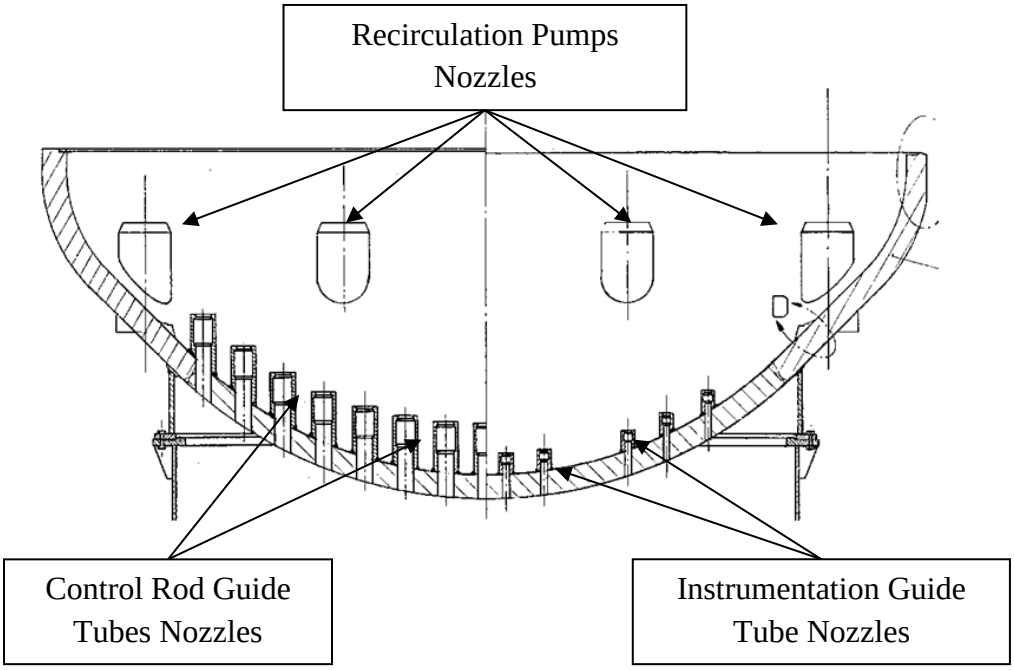

Figure 5: Layout of the lower head of a Nordic BWR, including the CRGTs and IGTs penetrations nozzles, as well as the internal recirculation pumps nozzles. The CRGTs and IGTs are only welded to the vessel through one point, in the penetrations nozzles.

In the Nordic design, the IGTs and CRGTs are welded only at one point inside the vessel Figure 6. It is assumed that the thermal load caused by contact with the heated debris will disable the welding between the penetration housing and the tube. This may happen at an uncertain time between weld creep acceleration (at 1110K) and weld melting (at 1673K). After the welding failure the IG tubes will be ejected out due to the internal vessel pressure. Then, debris or molten corium can enter the penetration´s interior space resulting in a melt jet to the reactor cavity. On the other hand, CRGTs ejection is considered less probable since the tubes are supported from below by the control rod insertion mechanism.

In addition, there is a clamping possibility of the IGTs that can prevent its ejection. The IGTs vessel penetrations in the Nordic BWR design have a flow limiter with a gap size of 0.25 mm between the tube and the vessel (see Figure 6). The objective of this flow limiter is to improve the thermal isolation of the vessel during normal operation by preventing the natural convection air circulation in the IGT-vessel interspace. It has been suggested that the size of this flow limiter

can be reduced during the accident transient due to the global deformation of the vessel. If this reduction is larger than the total size of the gap (0.5 mm) and happens before the welding failure, the IGT will be clamped in the flow limiter. Thus, its ejection would be avoided and IGT failure would be postponed [23]. There are two attributing factors that can affect the displacement of the flow limiter; (i) thermal expansion due to local thermal load, and (ii) applied displacement (normal to the right curved-surface boundary) as consideration of the global deformation.

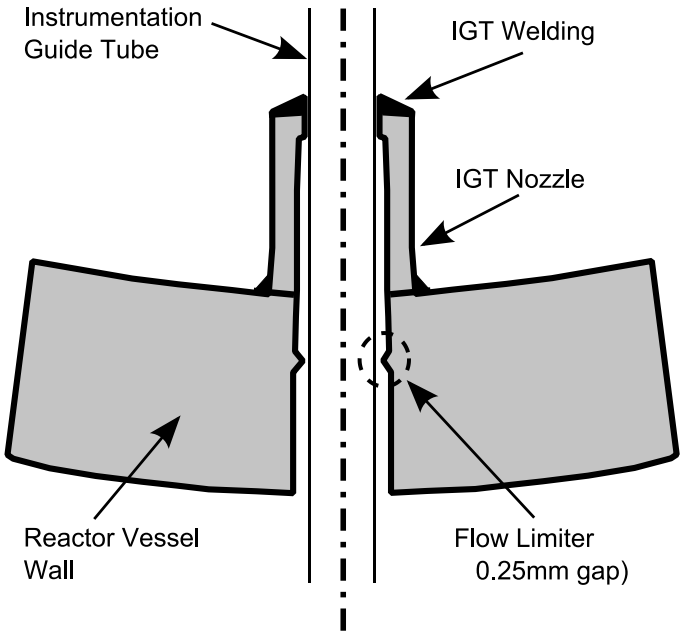

Figure 6: Scheme of the IGT vessel penetration. Including the IGT nozzle, IGT welding and flow limiter of the penetration, where the IGT could be clamped before being ejected.

Previous IGT failure calculations were performed by Villanueva et al. [23]. These calculations were done using the PECM implemented in a 3D slice model of the lower plenum geometry to simulate the debris bed thermal transient and predict the local temperature at IGTs welding. However, this 3D slice model is not taking into account the IGTs in the geometry (they are assumed to be melted and plugged). This assumption is suitable for long transients simulations conceived for structural creep analysis of the vessel (until more than 3 or 4 hours). The IGT welding failure, however, is expected to happen earlier, when the temperatures in the debris bed are lower and the IGTs are not melted yet. Furthermore, the calculations were performed only for one scenario, assuming CRGTs cooling.

Failure through the vessel wall

This mode of failure includes mainly two sub-modes; vessel wall creep failure and wall failure due to localized effects such as jet impingements. However, we only consider the first mode in the present work since the potential for a coherent jet to ablate the lower head is considered limited by the formation of a crust on the vessel surface, especially if there is water filling the lower plenum. Vessel wall creep failure, on the other hand, is expected to be one of the dominating modes of failure due the high temperatures reached during the transient in the vessel wall in contact with the melt pool.

The presence of internally heated debris bed/molten pool in the lower head will inflict load to the vessel wall. In this stage, the lower head vessel wall is considered to be under the following loads:

- The temperature field in the internal vessel surface
- The weight of debris bed/molten pool
- The reactor internal pressure

The combination of these mechanical and thermal stresses on the wall will lead to deformation of the vessel dominantly by creep mechanism. Creep is a time-dependent inelastic deformation process that occurs at stress levels below the yield strength of the material and is greatly accelerated under high temperatures. The progressive deformation and stretch of the vessel material due to the loads mentioned above, will lead to loss of material structural consistency and eventually rupture of the vessel wall at a certain location.

It is worth noting that, in addition to the above stated loads, thermo-chemical attack of the corium (corrosion) may also have a role in the vessel wall failure. However it is hard to assess its influence due to the uncertainties in the melt composition and lack of knowledge of material behavior under such conditions. For this reason, the corrosion effects are not taken into account in the present calculations. Furthermore, we assume that the failure is expected to happen in a time scale order of hours, before this corrosion effects take place.

Several experimental and analytical studies were done in the past addressing the vessel wall failure. For example the FOREVER experiments were performed at KTH [24], [25] with RPV lower head model 1:10 scale on vessel creep failure at pressures at about 25 bars. The melt pool was emulated using an internally heated binary oxide mixture with a melting point of 1270 K. These experiments found that creep process in the vessel walls happens as a consequence of simultaneous presence of high temperature and pressure. The failure position is located where higher temperatures are reached and that the creep deformation process leads to a wall thickness reduction which further accelerates the creep progression. The results of the FOREVER experiment are not directly applicable to the low pressure scenarios considered in this work.

Analytical calculations related to vessel wall creep failure were also previously carried out in the Nuclear Power Safety Division at KTH [26], [27], [10]. In these calculations, the thermal load to the vessel was predicted using the PECM implemented in a 3D slice geometry of the debris bed in the lower plenum (also presented in this Master thesis). Then, the structural response of the vessel wall was studied using a finite element 2D axisymmetric model of the vessel wall. The calculations were performed for different heights of debris beds and scenarios of CRGTs cooling and without CRGTs and top cooling. Table 1 summarizes the timing of creep failure of the vessel and amounts of liquid melt mass fractions of debris beds at time of failure.

Table 1: Summary of time and mode of vessel wall failure as well as the state of the melt pool at this time for different scenarios predicted by simulations performed at KTH-NPS using slices models of the lower head [26],[[27] [10].

CRGTs and Top Cooling implemented as SAM strategy				
H [m]	Time at max ~20 % creep strain, t_1 [h]	Mode of Creep Failure	Amount of liquid melt at t_1 (and after 30 min) [ton]	Average melt superheat at t_2 (and after 30 min) [K]
0.7	4.9	ballooning	18 (20)	160 (168)
1.1	4.9	localized creep	52 (56)	187 (232)
1.5	3.8	localized creep	58 (81)	72 (139)
1.9	3.5	localized creep	68 (112)	23 (103)
No CRGTs and Top Cooling implemented as SAM strategy				
H [m]	Time at max ~20 % creep strain, t_2 [h]	Mode of Creep Failure	Amount of liquid melt at t_2 (and after 30 min) [ton]	Average melt superheat at t_2 (and after 30 min) [K]
0.7	3.5	ballooning	16 (24)	33 (177)
1.9	3.4	ballooning	144 (183)	25 (278)

Two modes of global vessel failure depending on the size of the debris bed and CRTGs cooling supply were identified in these calculations: (i) ‘ballooning’ of the vessel bottom for smaller debris beds, and (ii) ‘localized creep’ concentrated within the vicinity of the top surface of the melt pool, for larger debris beds.

However, all these calculations performed using slices models did not take into account the following; (i) the non-axisymmetric distribution of CRGTs and (ii) the actual cooled surface to heated volume ratio in the debris bed heat transfer analysis, as the only represented one slice of the lower head geometry, and (iii) the influence of the CRGTs penetrations in the structural response of the vessel was not assessed as they were not included in the 2D axisymmetric model of the vessel wall.

1.3 Conclusions about the state-of-the-art:

The above review of the core melting severe accident phenomena, and scenarios leading to core damage, core degradation, debris bed/melt pool formation in the lower plenum, and modes of vessel failure show the complexity and uncertainties associated with the accident progression. Furthermore, we have introduced the importance of predicting the dominant mode of failure and timing in order to assess the successful of the ex-vessel melt retention in Nordic BWR.

Two main modes of vessel failure were identified; instrumentation guide tube failure, in terms of tube ejection, and vessel wall creep failure. In addition, we have shown that the mode and timing of failure depends on the amount of debris bed relocated in the lower head (see Table 1) and the implementation of CRGTs and top cooling as a means of delaying vessel failure.

Previous analytical calculations have been carried out at KTH-NPS in order to study the mentioned modes of failure. The instrumentation guide tube analysis showed that IGT may be the earliest mode of failure due to welding failure and tube ejection. However;

(i) Uncertainties in the prediction of timing of failure of the IGT welding still exits, as the calculations were done using a slice geometry model of the global lower head, which did not resolve the presence IGTs and was not capable of detecting possible local heat transfer effects on the IGTs welding surroundings.
(ii) Possible influence of CRGTs and top cooling on the welding failure timing and IGT clamping possibility was not assessed as the calculations were performed only for one scenario.

In addition, the vessel wall creep failure analysis previously done identified two different modes of wall failure depending on the amount debris relocated in the lower head (i) 'ballooning' of the vessel bottom, and (ii) 'localized creep' concentrated within the vicinity of the top surface of the melt pool. However;

(i) The behaviour of the debris bed heat transfer of the realistic lower head geometry was not fully captured as the calculations were performed using slice models, which could not assess the (i) non-axisymmetric distribution of CRGTs in the lower head geometry and (ii) the actual cooled surface to heated volume ratio in the debris bed. These features may influence the results, especially if CRGTs cooling is implemented as SAM.
(ii) Possible weakening effect on the vessel wall structure due to the penetrations and possible CRGTs failure were not assessed in the structural analyses, as the penetrations were not included in the employed structural 2D axisymmetric model.

1.4 Goals and Tasks

Based on the motivation and review of previous work, the main goal of this Master Thesis is to clarify the influence of:

- Implementation of CRGTs cooling as SAM strategy
- Realistic 3D geometry of the vessel with penetrations

on the mode and timing of:

(i) Penetration failure (IGT and CRGT failure)
(ii) Vessel wall failure.

The present work is divided into two main tasks in order to assess the goal:Task I: Study of the instrumentation guide tube failure, in terms of tube ejectionTask II: Study of the vessel wall failure using 3D quadrant geometry of the lower head with CRGTs penetrations

In the next two subsections we determine the scope and specific objectives of the two above mentioned tasks of the present work.

1.4.1 Scope of Task I: Study of Instrumentation Guide Tube Failure

The IGT failure will take place by tube ejection due to the failure of its nozzle welding, unless clamping in the flow limiter occurs. In this context, our calculations are mainly seeking for:

i. Predicting the time of the IGT welding failure, and
ii. Studying the possibility of clamping of the IGT in the flow limiter due to the global deformation of the vessel and local thermal load in the surroundings of the IGTs penetrations.

In order to assess the first objective above, the PECM is implemented in a geometrical model representing a unitary debris bed volume including a central IGT and four surrounding CRGTs. More details about this model are included in the next chapter. The use of such model will also help us to achieve some secondary objectives, in terms of:

- Obtain the solution of the heat transfer transient in the debris bed when the IGTs are not melted yet.
- Predict locally the time of IGTs and eventually CRGTs melting.
- Predict the state of the debris bed/melt pool when the IGT is eventually ejected.

- Provide the temperature distribution data needed for a possible future experimental study of IGT ejection.

Furthermore, the IGT analysis is performed for two IGTs at two different positions; the one closest from the center of the bottom of the vessel and the one which is farthest, as well as for two different cooling scenarios (i) Assuming CRGTs and top cooling, and (ii) Without CRGTs cooling. The main motivation for selecting these two different positions and different cooling scenarios are:

- Study the influence of IGT location and global deformation of the vessel on the clamping possibility.
- Assess the influence and effectiveness of CRGTs cooling in delaying or preventing IGTs failure.

1.4.2 Scope of Task II: Study of the vessel wall failure using 3D quadrant geometry of the lower head with penetrations

In this second task of the present Master Thesis, we will use a 3D quadrant model of the reactor lower head to simulate the debris bed heat transfer transient and to perform structural creep vessel wall failure analysis. The 3D quadrant model is considered to be more accurate than the 3D slice model previously used [10] [26] [27]. Task II of the present work is divided into two parts.

Part 1:

This part is included in the conference paper titled "Coupled 3D Thermo-mechanical analysis of a Nordic BWR vessel failure and timing" which is attached in Appendix I. There, we provide a comparison of the results obtained with (i) PECM in 3D slice model of the debris bed coupled with ANSYS 2D axisymmetric vessel wall model, and (ii) PECM in 3D quadrant model of the bed coupled with ANSYS 3D quadrant model of the vessel. This comparison attempts to answer the following:

- How actual 3D geometry with non-axisymmetric distribution of CRGTs can affect melt pool heat transfer, and
- How penetrations in the vessel wall (resolved in 3D quadrant model) can affect creep characteristics and eventually timing of failure.

The comparison is performed for the scenarios of 1.9 m debris bed height (~200 tons) relocated in the lower head and assuming that CRGTs cooling is supplied.

Part 2:

In the second part of the Task II we perform several calculations using the 3D quadrant models for four different scenarios, in terms of different amount of debris bed relocated in the lower

plenum, which are 1.9 m (200 tons) and 0.7 m (30 tons), and also the availability of CRGTs cooling. The objectives of these simulations are:

- Study the debris bed heat transfer transient and characteristics of melt pool formation in the lower head for the four considered scenarios,
- Predict the time and mode of failure of the vessel wall for the considered scenarios,
- Identify possible new modes of failure and weakening of the vessel wall not recognized in previous 2D structural calculations due to the CRGTs penetrations, and
- Study the efficiency of CRGTs cooling as means of delaying/preventing creep vessel wall failure.

2 Approach and Methodology

In this chapter we describe the computational approach and models used in the present work. The calculations performed are divided in two Tasks; (I) Study of IGT failure and (II) Study of the vessel wall failure using 3D quadrant geometry of the lower head with penetrations. The specific approach and geometrical models used for these two tasks are different and will be described details in the next sections. However, the computational tools, material properties models, boundary conditions and coupled thermo-mechanical methodology are common for both tasks. This coupled thermo-mechanical methodology consists of two steps:

I. Transient formation of the melt pool and thermal load to the vessel wall are calculated using the phase change effective convectivity model PECM which is implemented in FLUENT® [28].
II. Coupled thermo-mechanical creep analysis of the vessel wall and penetrations are performed using structural models in ANSYS® [29], with imposed temperature distribution on internal vessel walls predicted by PECM in the first step.

The coupling between FLUENT and ANSYS is always performed only in one way since we consider that the global deformation of the vessel has negligible effect on the melt pool heat transfer predicted by the PECM.

In the next sections we will firstly explain used the tools and boundary conditions common for all the calculation performed. Then, we will introduce the specific approach and the characteristic models for the two different tasks performed.

2.1 Thermal and Mechanical Aspects

Although the specific geometrical models used for the two different tasks in the present Master Thesis, the PECM model and debris bed properties for the heat transfer transient simulations as well as creep and material models for the structural ANSYS analysis are the same. In this section we provide the description of such models.

2.1.1 The PECM Model for the Debris Bed and Melt Pool Heat Transfer

The PECM is a model that describes the turbulent natural convection heat transfer in an internally heated fluid volume, as decay-heated debris bed, taking into account the solid-liquid phase change. The PECM was developed by Tran and Dinh [21] using the concept of effective convectivity which was pioneered by Bui and Dinh [30]. The goal of this model is to enable sufficiently accurate simulations of melt pool heat transfer in a computationally efficient way. It

should be noted that, for the mechanical calculations, the detailed temperature distribution within the melt pool are not needed, this enables the use of the proper correlations to efficiently describe heat fluxes at the melt boundaries.

The key concept of the PECM model is the use of directional effective heat-convecting velocities, named characteristics velocities -U_x,U_y, U_z- to transport the heat and represent the convective terms in the energy conservation equation [Eq. (1)]. These characteristics velocities are derived from heat transfer based on Rayleigh number, namely the upward, sideward and downward Steinberner-Reineke correlations [31]. Therefore, the need of solving the full Navier-Stokes equations is eliminated. This assumption makes this model much more computationally-efficient than conventional CFD codes.

In order to implement computationally this method, the heat source Q_v in the energy conservation equation [Eq. (1)] is combined with the convective terms in a modified source term S_c as is showed in Eq. (2).

$$\frac{\partial(\rho C_p T)}{\partial t} + \left(\frac{\partial(\rho C_p U_x T)}{\partial x} + \frac{\partial(\rho C_p U_y T)}{\partial y} + \frac{\partial(\rho C_p U_y T)}{\partial y}\right) = \nabla\left(k\nabla(T)\right) + Q_v \quad (1)$$

$$S_c = Q_v - \left(\frac{\partial(\rho C_p U_x T)}{\partial x} + \frac{\partial(\rho C_p U_y T)}{\partial y} + \frac{\partial(\rho C_p U_y T)}{\partial y}\right) \quad (2)$$

In this way, the energy conservation equation can be expressed as:

$$\frac{\partial(\rho C_p T)}{\partial t} = \nabla\left(k\nabla(T)\right) + S_c \quad (3)$$

Eq. (3) is solved in the commercial code FLUENT® [28] where the modified source term S_c is computed "externally" using the source term of User Defined Function (UDF) option. This enables to utilize all advantages of a CFD commercial code solver such as the pre- and post-processing. It is important to note that, from the point of view of the FLUENT® solver, the fluid is static (only conduction energy equation is computed). Instantaneous fluid velocities (u_x,u_y, u_z) are not required since the convective heat transfer effect is taken into account in the modified source term S_c. The UDF computes when the temperature of the debris bed is higher than the melting point and add these terms when necessary. Furthermore, the PECM uses reduced characteristics velocities as a function of the melt mass fraction to describe the phase change heat transfer and represent the natural convection heat transfer at mushy zones [21].

The correlations used for calculating the characteristics velocities are showed in Eqs (4), (5) (6)

$$U_{up} = \frac{\alpha}{H_{pool}} \times \left(Nu_{up} - \frac{H_{pool}}{H_{up}}\right) \quad (4)$$

$$U_{up} = \frac{\alpha}{H_{pool}} \times \left(Nu_{down} - \frac{H_{pool}}{H_{down}} \right) \quad (5)$$

$$U_{up} = \frac{\alpha}{H_{pool}} \times \left(Nu_{side} - \frac{2 \times H_{pool}}{W_{pool}} \right) \quad (6)$$

Where H_{pool} is the height (or depth) of the melt pool, H_{up} is the thickness of the pool upper mixed region, H_{down} is the thickness of the lower stratified region, W_{pool} is the pool width, and α is the thermal diffusivity.

The upward, sideward and downward Nusselt numbers are respectively obtained from the Rayleigh number based Steinberner-Reineke correlations [31].

$$Nu_{up} = 0.345\, Ra'^{0.233} \quad , 5x10^{12} \leq Ra' \leq 3x10^{13} \, , Pr \approx 7 \quad (7)$$

$$Nu_{side} = 0.85\, Ra'^{0.19} \quad (8)$$

$$Nu_{up} = 1.389\, Ra'^{0.095} \quad (9)$$

The PECM model was validated experimentally and against CFD, confirming that is capable to predict all important parameters of interest for reliable prediction of thermal loads from a melt pool to the vessel wall and structures [14].

2.1.2 Debris Bed and Melt Pool Material Properties

The material properties of the debris bed/ melt pool used for heat transfer analysis were common for all the calculations. These properties were obtained as reference values from calculations carried out previously at KTH [32]. The material properties correspond to a mixture of purely oxidic (UO2 and ZrO2), which can be consider as the lower bound of thermal conductivities of the debris bed.

Table 2: Debris Bed properties used in the PECM simulations

Density *[kg/m3]*	8600
Specific heat *[J/kg-K]*	485
Viscosity *[kg/m-s]*	0.0046
Thermal conductivity of solid debris *[W/m-k]*	1
Thermal conductivity of liquid melt *[W/m-k]*	3
Liquidus Temperature *[K]*	2770
Solidus Temperature (melting range) *[K]*	2750 (20)
Fusion heat *[j/kg]*	277000
Decay Heat Power *[W/m3]*	1e6

For the models without CRGTs cooling, where melt down of the CRGTs is expected, the solidus and liquidus temperatures of steel (material of the vessel wall and CRGTs) are 1671K and 1727K respectively [22].

2.1.3 Material properties for the Vessel Wall Structural Models

For the structural analysis we consider the vessel of the ABB-Atom reactor to be made of steel SA533B1 where material properties such as density, elastic modulus (linear isotropic), thermal conductivity (isotropic), specific heat, and coefficient of thermal expansion (that are all functions of temperature) are taken from Rempe et al. [22]. The Poisson's ratio is set to 0.3. It is important to note that the elastic modulus is highly dependent on temperature, which decreases 2 orders of magnitude as the temperature increases from 300 to 1050 K. Consequently, the strain due to creep increases significantly at high temperatures as the elastic response of the material is inversely proportional to the elastic modulus. These material properties are attached in Appendix I.

2.1.4 Creep Model for the Vessel Wall Structural Analysis

Creep is considered the main cause of failure of the reactor pressure vessel wall given the mechanical and high thermal loads a result of the debris bed/melt pool in the lower head. In this section, we provide description of the creep model used in the ANSYS structural calculations, namely a modified time hardening model.

The creep behaviour of materials is a function of stress, temperature and time. Considering constant temperature and stress, a typical creep curve consists of three stages before rupture; the primary stage (also called transient creep), secondary (steady creep), and tertiary (accelerating creep). This behaviour, however, is difficult to be captured when the temperature and stresses are changing with the time since there are different creep curves for different temperatures and stresses. In order to assess this issue, the creep behavior is described with creep laws which relate the equivalent creep strain with the stress, temperature and time by using a number of free parameters. The time hardening model [Eq. (10)] is one of such models. This assumes a relationship between the equivalent creep rate, the equivalent stress and the time at fixed temperature the for the primary creep stage by the use of three free coefficientsc_1, c_2, c_3 [33]. These coefficients are, in turn, function of temperature.

$$\varepsilon_{cr} = \frac{c_1 \sigma^{c_2} t^{c_3+c_1}}{c_3+1} \qquad (10)$$

In Eq. (10) ε_{cr} is the equivalent creep strain, is the equivalent stress, t is time. The c_1, c_2 and c_3 coefficients are determined by curve fitting with experimental data. For this purpose the experimental creep data for SA533B1 from Rempe et al was used [22]. Table 3 summarizes these coefficients generated for different temperatures. This model was introduced in the FE ANSYS calculations using the user defined material properties.

Table 3: Coefficients used in the primary hardering creep modelas a function of temperature (Eq 10)

Temperature [K]	900	1050	1150	1250	1373
c_1	1.461×10^{-31}	1.867×10^{-42}	7.801×10^{-28}	3.497×10^{-44}	5.383×10^{-47}
c_2	3.0881	4.8171	3.0886	5.5237	6.2092
c_3	-0.0560	0.1609	-0.0180	-0.1219	-0.0554

As a validation test, a uniaxial structural creep analysis was performed by Villanueva et al. [26], using a rectangular block (1 m × 0.2 m) at constant temperature T = 1150 K, clamped on one end,

and applied stress of 26.5 MPa on the opposite. Figure 7 shows the comparison between the theory, numerical and experiments results.

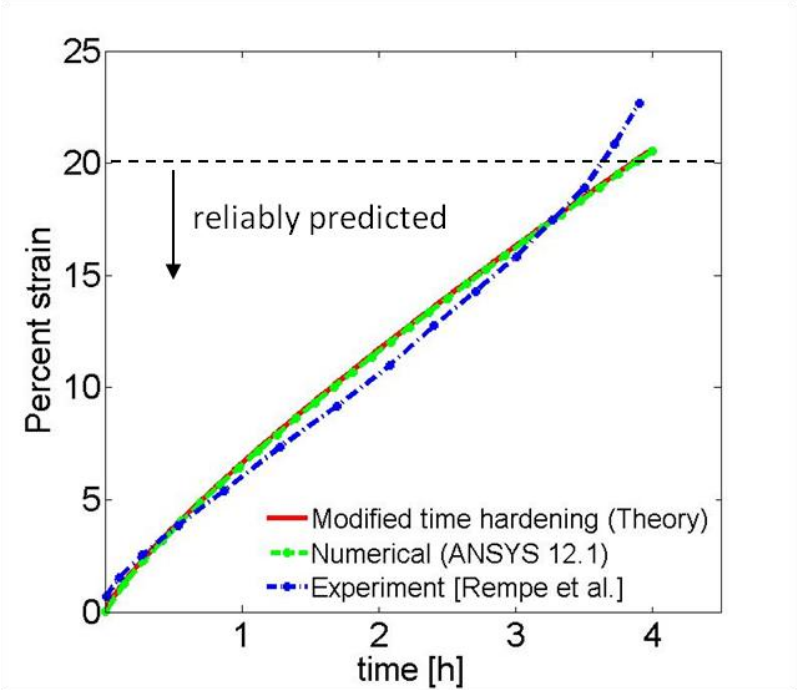

Figure 7: ANSYS creep model validation results carried out by Villanueva et al. [26]. The experimental data is taken from Rempe et al. [22].

It is important to note that this creep model is not able to identify a creep limit as only predicts the equivalent creep strain for the primary creep stage. This is motivated by the fact that creep is a thermally activated process and the material starts to creep even under moderate stresses lying below the yield limit [33]. Instead of defining a creep limit, a range of strain which can be considered reliably predicted by the model was defined. The limit of this reliably predicted range was set at 20% strain, as can be seen in Figure 7. Beyond this range the results are only considered as indicative in a qualitative way meaning that failure may happen in this stage but its exact time and respective deformations cannot be accurately determined. Nevertheless, we adopt the time necessary to reach 20% strain as the minimum estimated vessel wall failure time. Indeed, the structure in such state is very close to its mechanical failure [26].

2.1.5 Boundary and Initial Conditions

The boundary conditions applied for the different models used in this Master Thesis are generally the same, with the exception, of course, of those that corresponds to the specific scenarios (i.e., implementation of CRGTs cooling or different heights of debris bed).

In these subsections we introduce these general boundary conditions which depend on the initial assumptions. Other boundary conditions, which depend specifically on some of the models, such

as symmetry or specific assumptions of the geometry, will be presented together with the specific models.

2.1.6 Boundary Conditions of Debris Bed and Melt Pool Heat Transfer Models

In all the debris bed heat transfer simulations implemented in the PECM it is assumed that the debris bed formed in the lower head is initially in solid state (T=450K) as it has quenched in the remaining water filling the space below the core. Then the debris bed is heated up, dried out and re-melted due to the absence of sufficient cooling. Thus the starting point of all the calculations (time zero) corresponds to a solid debris bed in the lower plenum at 450 K.

In the studied scenarios with CRGTs cooling implemented as SAM strategy, it is assumed that water from inside the CRGTs is supplied. The water is assumed to be ejected from the CRGTs providing a water layer and thus cooling at the top of the debris bed. Dirichlet type isothermal boundary conditions with water saturation temperature (383 K) are therefore applied to the top and the upper part of the vessel inner wall. The CRGTs surfaces in contact with the debris bed are assumed to be at 450 K (taking into account the temperature rising between the CRGT inner and outer walls).

On the other hand, in the scenario without CRGTs cooling implemented as SAM strategy, it is considered that the top of the debris bed will be dry at the beginning of the simulations. Therefore radiation heat transfer is applied on the top debris bed surface with T_∞ equal to saturation temperature and emissivity coefficient is set to 0.8. Adiabatic (no heat flux) boundary conditions are applied in this case on the CRGT inner surfaces.

For the external surface of the vessel wall it is assumed to be covered with insulation therefore only a small heat flux (20 W/m^2) is allowed (for both scenarios with and without CRGTs cooling).

2.1.7 Boundary Conditions of the ANSYS Structural Models

In this section we describe the boundary conditions for the structural calculations of the reactor vessel wall (models showed in Figure 14, 13 and 18). In these calculations, the thermal boundary conditions on the inner surface of the vessel wall in contact with debris are provided by the PECM solution. Other boundary thermal conditions are the same as in section 2.2.1, i.e., the upper part of the vessel inner wall is at saturation temperature and the external vessel is almost completely thermally isolated. The pressure inside the vessel is set at 0.3 MPa (corresponding to the pressure upon activation of the vessel depressurization systems), while atmospheric pressure is imposed outside the vessel.

The hydrostatic pressure due to the weight of the debris bed was taken into account. The specific displacement boundary conditions related with the geometry of the models will be discussed together with such models.

2.2 Specific Approach and Methodology of Task I: Study of the Instrumentation Guide Tube Failure

In Task I of this Master Thesis a detailed analysis of the failure of the IGTs is carried out. This analysis is performed for two IGTs corresponding to two different locations; the one closest from the center of the bottom of the vessel and the one which is the farthest.

The calculations were performed considering a debris bed of 1.9 m height which assumes that almost the whole core (200 tons) was melted and relocated in the lower plenum. Furthermore two different scenarios were studied;

Scenario 1: CRGTs cooling is implemented as SAM.

Scenario 2: No CRGTs in provided.

In the next subsections we provide the approach that was followed for calculating the failure as well as the geometric models used for this purpose.

2.2.1 Approach

Figure 8 shows a scheme of the followed approach for the study of the IGT ejection. The calculations were carried out in 4 different steps and using five different computational models.

I. First, the transient thermal load to the vessel wall was predicted using the PECM implemented in 3D slice geometry of the vessel (Figure 9).

II. Then, the transient of global deformation of the vessel was calculated using a 2D Axisymmetric structural model with the applied thermal load obtained from the step I (Figure 13).

III. After that, local 3D structural analysis of the IGT penetrations sections corresponding to the closest and farthest from the center IGTs were carried out using ANSYS in order to study the deformation of the flow limiter (Figure 14). In these models, the thermal load to the vessel surface was applied from (I) while the displacements in the model boundaries due to the global deformation of the vessel were applied from (II).

IV. Independently, the timing the IGT nozzle welding failure was obtained with the PECM implemented in a geometrical model representing a 3D unitary debris bed volume including the central IGT and the four surrounding CRGTs (Figure 12). The time of failure is estimated by looking at the nozzle welding temperature. This gives a range of time when the failure is expected, which it is when the temperature is between the beginning of welding creep acceleration (at 1110K) and the welding melting point (at 1673K). The reason for using this unitary model and not the global debris bed model of step (I), is that the last is not taking into account the IGTs (they are assumed to be melted and plugged). This assumption is suitable for long transients simulations conceived for structural creep analysis of the vessel (more than 3 or 4 hours). The IGT welding failure, however, is expected to happen much earlier, when the temperatures in the debris bed are lower, and the IGT are not melted yet.

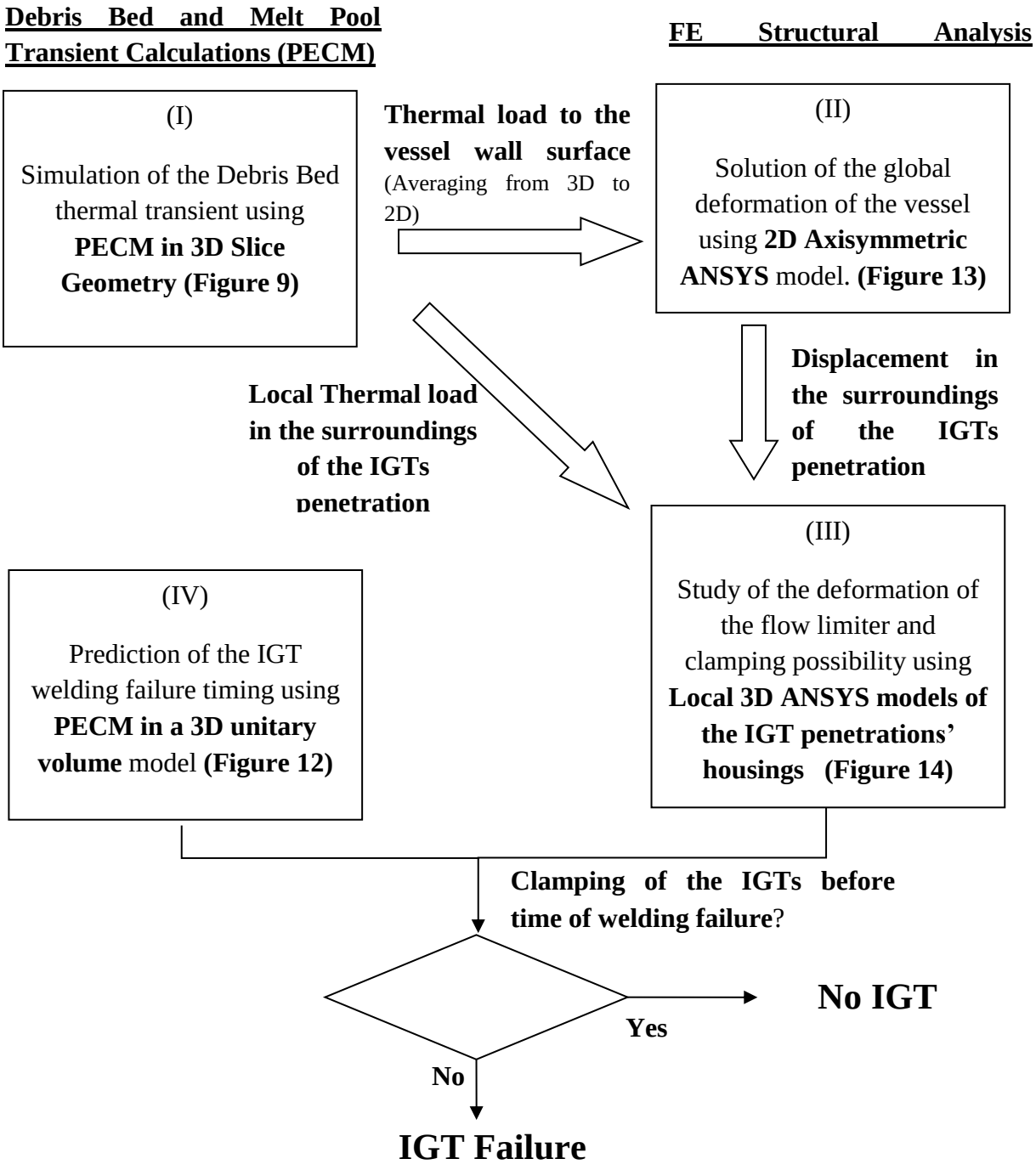

Figure 8: Scheme of the methodology employed to investigate the IGT failure

2.2.2 Debris Bed and Melt Pool Heat Transfer Models

In this section we provide the geometrical models where the PECM was implemented in FLUENT in order to simulate the debris bed transient and welding temperatures for the IGT failure analysis, (steps I and IV in Figure 8).

Implementation of PECM in 3D Slice Geometry

The 3D-slice geometry model is presented in Figure 9. This model consists of a segment of BWR lower plenum filled with decay-heated corium and containing 8 CRGTs as is shown in Figure 11(a).

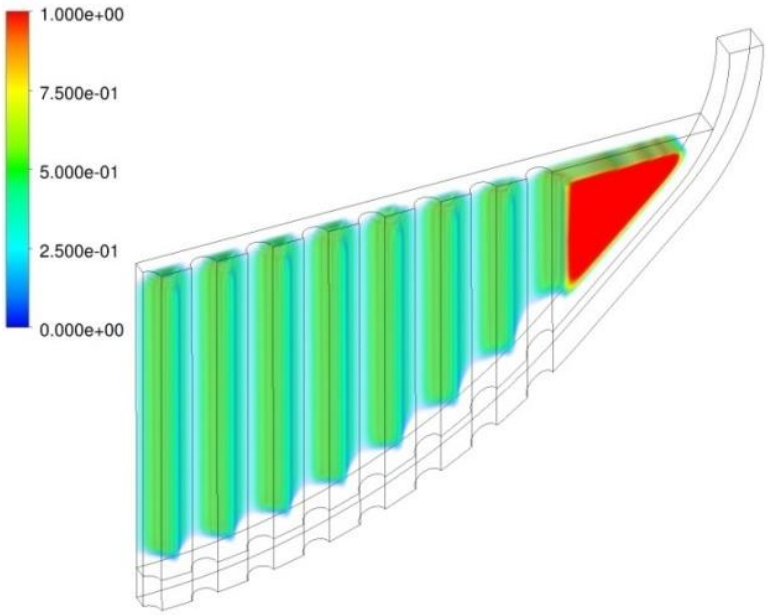

Figure 9: 3D Slice geometry model where the PECM was implemented for the debris bed heat transfer transient calculation in the IGTs failure analysis, as well in previous studies carried out at KTH-NPS [26],[[27] [10].

The IGTs are not included in the model as it is assumed that they are melted and plugged by corium melt during the re-melting of the debris and therefore do not have an influence on melt pool heat transfer.

Symmetry boundary conditions are applied in the front and back walls of the model. It must be noted that because of these boundary conditions, the model will represent a virtual geometry which top view is showed in Figure 11(b). This geometry has a different surface to volume ratio than the real lower plenum geometry, especially if we look at the non-axisymmetric distribution of CRGTs penetrations in the lower plenum (Figure 11(a)). Slightly different results of the debris bed transient and thermal load to the vessel are therefore obtained using this model than the obtained with 3D quadrant model (Figure 17), which represent the actual surface to heated

volume ratio and non-axisymmetric distribution of CRGTs. Detailed discussions about this issues are included in the paper attached in Appendix I, where a comparison of the slice models and 3D quadrant models is provided.

Nevertheless, this 3D slice model is used here for the calculation of the thermal load to the vessel wall in order to check the influence of deformation of the vessel in the IGT clamping possibility. This possibility will happen during the first 2 hours of the transient, where the concerns explained in the last paragraph, in terms of global deformation of the vessel, have not an influence yet, (as can be read in Appendix I).

Finally, in Table 4 we show some parameters of the mesh and computation time corresponding with the PECM implemented in the 3D slice Model.

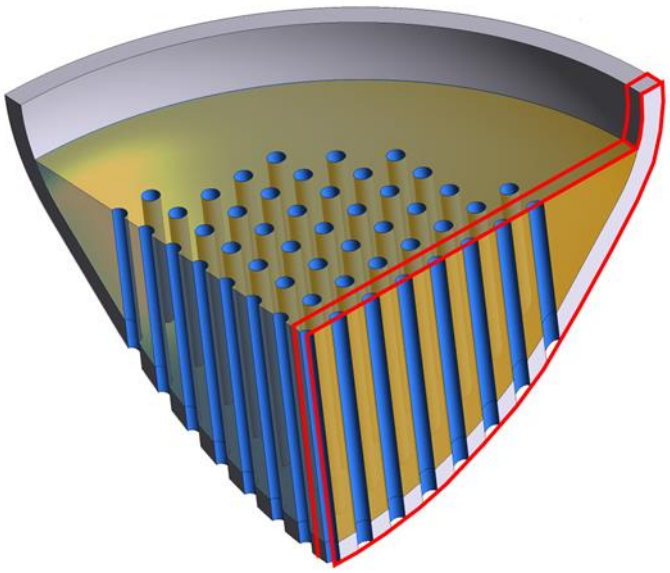

Figure 11(a): Scheme of the slice of the lower head geometry (red) represented by the 3D slice model

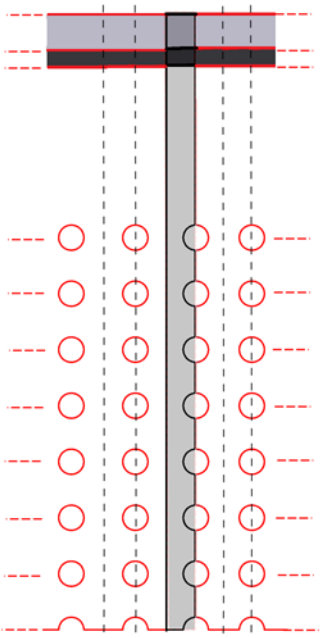

Figure 11(b): Top View of the virtual geometry represented by the 3D slice model as a consequence of its symmetry boundary conditions.

Table 4: Mesh Parameters of the 3D Slice PECM model implemented in Fluent

Feature	3D-Slice Model
Number of elements	293,750
Number of Nodes	332,222
Type of element:	Hexahedra
Typical calculation time	12 hours

Implementation of PECM in 3D Unitary Volume Geometry

In this section we present the unitary volume model which was used in the step (IV) of the methodology showed in Figure 8. This model was made in order to check locally the temperature in the welding of the IGT and study the influence of the IGT presence in the debris bed heat transfer at the beginning of the transient, when the IGT has not been melted yet. The geometry of the model consists on a 3D segment of the debris bed in the lower plenum, surrounded by 4 CRGTs and with a IGT in the center (Figure 12). This piece of debris bed corresponds to the one that is located closest to the center of the vessel, that is, with a 1.9 m debris bed above the vessel wall. For this model, the curvature of the vessel wall was considered to have a negligible effect in the heat transfer transient, therefore the vessel wall is considered flat. The model is taking into account the geometry of the tube nozzles and welding.

Symmetry boundary conditions were applied to the debris bed and vessel walls. Cero heat flux boundary conditions were applied in the inner surface of the IGT. Table 5 shows some parameters of the mesh and computation time corresponding with the PECM implemented in the unitary volume.

Table 5: Mesh Parameters of the 3D Unitary Volume Geometry PECM model implemented in Fluent

Feature	3D-Slice PECM Model
Number of elements	989,584
Number of Nodes	332,222
Type of element:	Tetrahedral
Typical calculation time	4 days

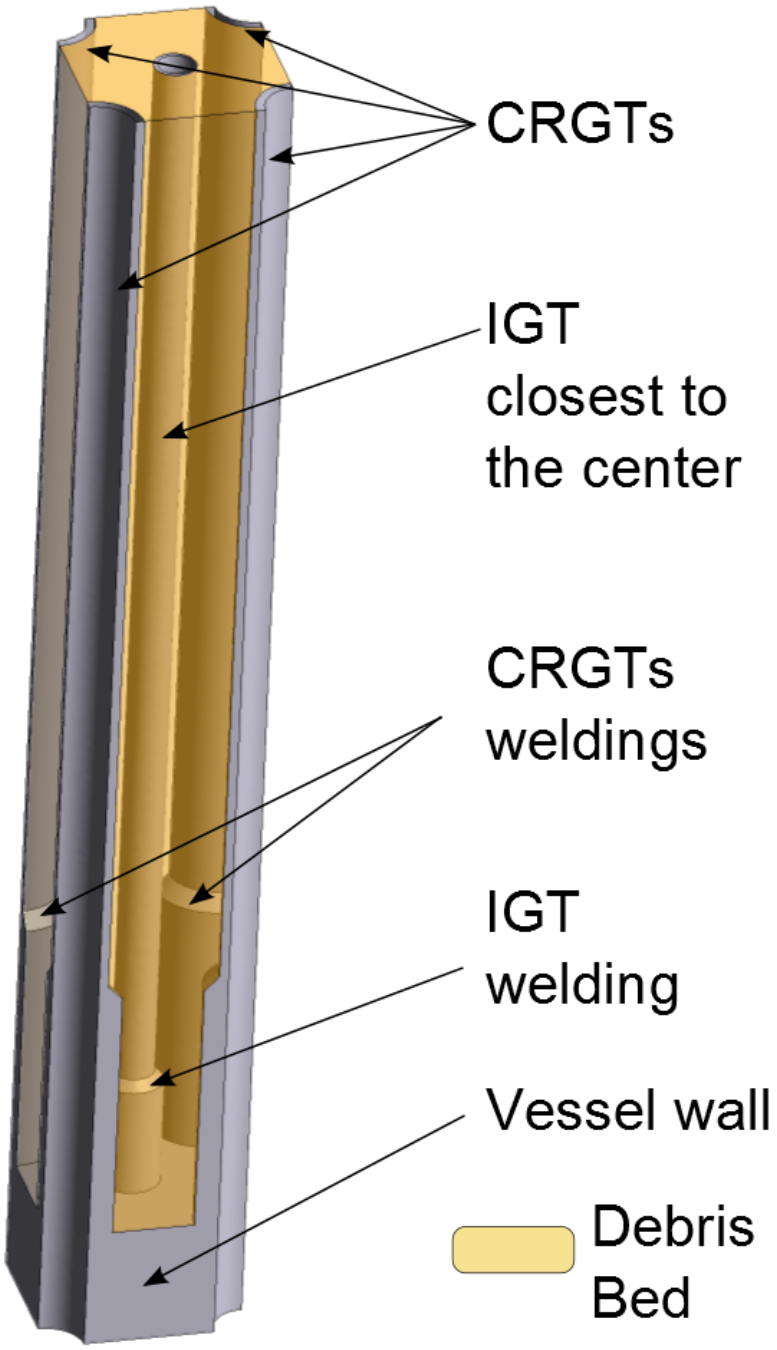

Figure 12: Unitary Volume Model where PECM was implemented in Fluent including one IGT and four CRGTs, for the local analysis of IGT welding failure and unitary volume debris bed heat tranfer calculation.

2.2.3 Finite Element Structural Models

In this section we describe the structural models used in the IGT failure study. Finite element structural simulations were performed using ANSYS in order to; (i) calculate the global deformation of the vessel wall (Step II in Figure 8), and (ii) to study locally the deformation of the flow limiter in the IGTs penetrations (Step III in Figure 8),

2D Axisymmetric Structural Model

Figure 13 shows the 2D model corresponding to one slice of lower part of the ABB-Atom reactor vessel. The element type used in ANSYS is Quad Plane223 which is a 2D 8-nodecoupled-field (structural-thermal) solid. For full transient analyses, a strong structural-thermal coupling is supported. The 2D geometry is meshed with 800 quadrilateral elements and 2731 nodes with an average edge length of 0.04 m. Table 6 summarized the mesh parameters

Table 6: Mesh Parameters of the 2D axi-symmetric structural model used for the step II in figure 8, as well as in the previous studies of vessel wall failure carried out at KTH-NPS [26],[[27] [10]

Feature	ANSYS 2D-Axisymmetric Model
Number of elements	800
Number of Nodes	2901
Type of element:	Quad Plane223
Average edge length (m)	0.04 m
Typical calculation time	0.78h

The boundary conditions applied to this model are the one exposed in section 2.2.2, and are also summarized in Figure 13. These include the pressure load, debris bed weight, and thermal load. Non-horizontal displacement constrain is imposed on the vertical symmetry axis, while non-vertical displacement is imposed in the upper edge of the vessel wall.

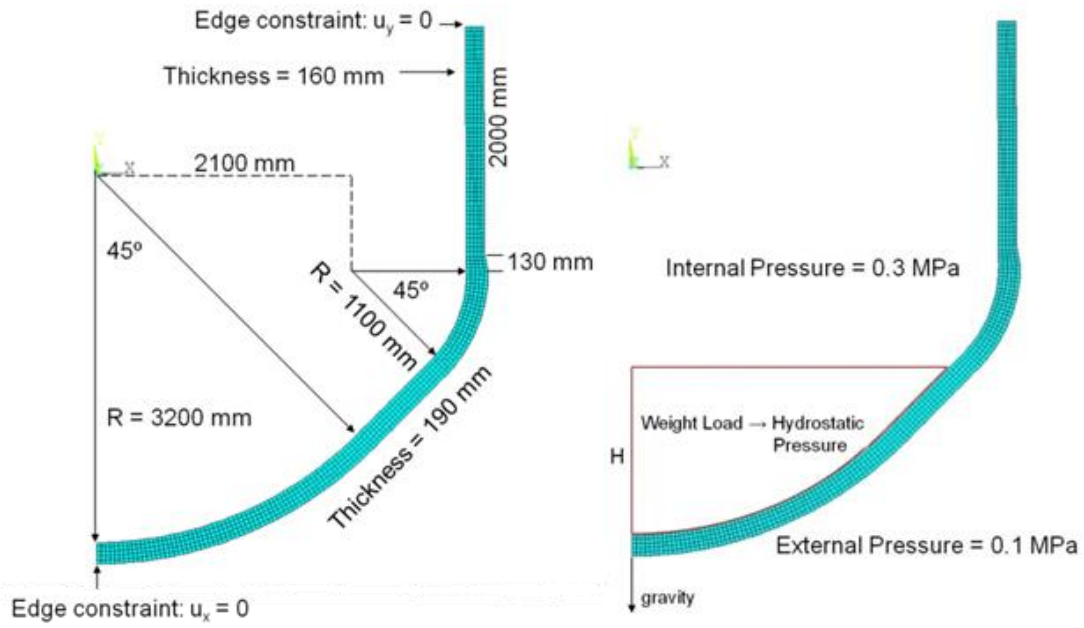

Figure 13: 2D axi-symmetric structural model used for the step II in figure 8, as well as in the previous studies of vessel wall failure carried out at KTH-NPS [26],[[27] [10]. Dimensions, loads and displacement constrains are included in the figure.

3D IGTs Penetrations' Housing Local Models

Figure 14 shows the local 3D ANSYS models used for the local analysis of IGTs penetration deformation and clamping possibility. As can be observed in Figure 14, these models correspond to the penetrations housing of the closest and farthest from the center IGTs. The element type used in ANSYS is Solid 226 which is a 3D 20-node coupled-field (structural-thermal) solid. Full transient analysis with a strong structural-thermal coupling is also implemented. Mesh data of both models is summarized in Table 7.

Table 7: Mesh Parameters of the 3D IGTs Penetrations' Housing Models showed in Figure 14.

Feature	ANSYS 3D Local-Section Closest IGT	ANSYS 3D Local-section Farthest IGT
Number of elements	18102	125111
Number of Nodes	11553	87450
Type of element:	SOLID226	SOLID226
Average edge length (m)	0.015 m	0.015
Typical calculation time	4 days	3 weeks

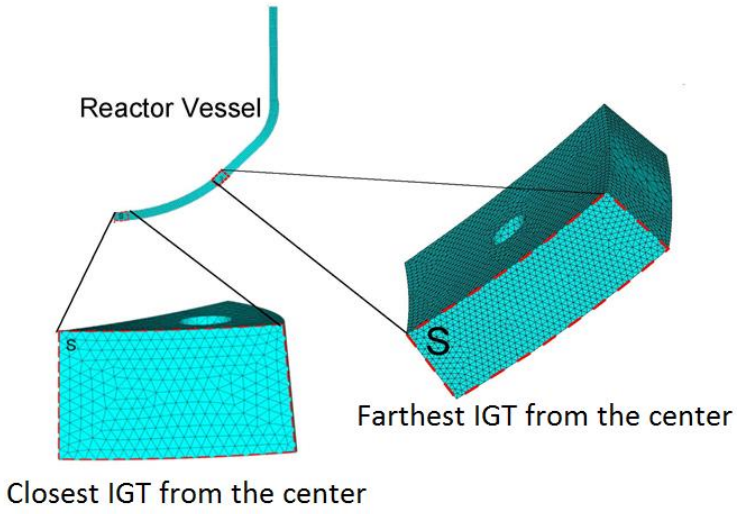

Figure 14: Structural 3D IGTs Penetrations Housing Models implemented in ANYS for the study of the clamping possibility of the IGTs. For the closes and farhest IGTs from thecenter of the vessel

In order to take into account the effect of the global deformation of the vessel, displacements boundary conditions from the structural 2D axisymmetric solution were applied to these models. Therefore, horizontal displacements of the right edge of the corresponding section from the 2D global vessel wall are imposed on the right surfaces of the 3D local IGT sections (marked with "S" in Figure 14). Non-horizontal displacement constraint is imposed on the vertical symmetry axis in the model of the closest IGT. Vertical displacements of the left and right edges of the section from the 2D global vessel wall are almost identical during the first hours of the 2D-Axisymmetric global vessel transient. Hence the left and right sides of the 3D local IGT section are both constrained with non-vertical displacement, since the failure of the penetration welding is expected in this period of time.

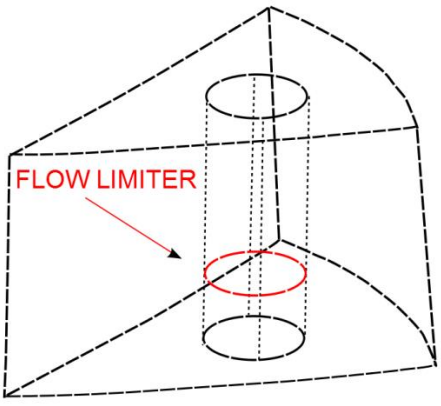

Figure 15: Scheme of the flow limiter in the local 3D strucutral model of the IGT housing penetrations for the study of its deformation and clamping possibility

2.3 Specific Approach and Methodology of Task II: Study Vessel Wall Failure using 3D Quadrant Geometries with Penetrations

In the Task II of the present Master thesis, coupled 3D thermo-mechanical calculations were performed using 3D quadrant models of the reactor vessel lower head. The goal of these calculations was to investigate the influence of the non-axisymmetric distribution of CRGTs in the debris bed/melt pool transient (not included in the 3D slice model presented in Figure 9). Besides, the symmetry boundary conditions applied to the 3D slice model corresponds to a different heated volume to cooled surface ration than in the actual geometry (as was exposed in Figure 11(b)) which may also have an influence in the debris/bed heat transient and thermal load to the vessel. Furthermore, structural calculations were performed using a 3D quadrant model of the vessel wall, which has into account the CRGTs penetrations and its influence in the structural response.

From these 3D thermal and structural models we expect to get accurate solutions of the timing of the creep vessel wall failure and of the state of the melt pool at time of failure, in terms of amount and temperature of the melt available for ejection after such failure.

The calculations were performed for four cases, from the combination of scenarios with 1.9m and 0.7m debris bed and CRGTs cooling or No CRGTs cooling as SAM strategy.

2.3.1 Approach

The approach for the calculations in this part consisted in two steps as is showed in Figure 16:

I) First, the PECM was implemented in FLUENT in a 3D Quadrant geometry of the vessel lower plenum.

II) Then, a structural creep analysis was carried out using ANSYS in 3D quadrant geometry of the reactor vessel wall.

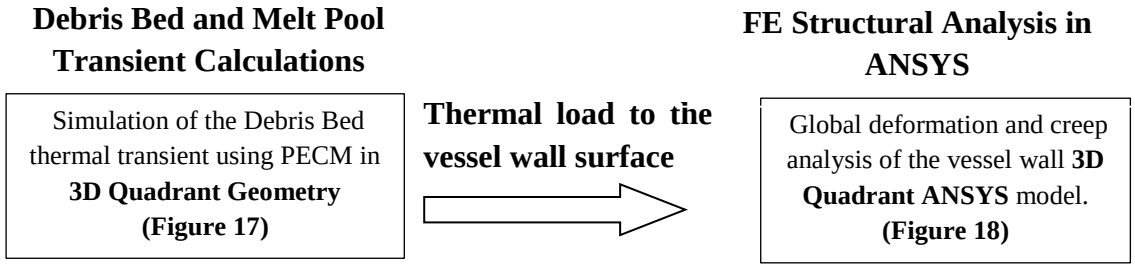

Figure 16: Scheme of the methodology employed in the Task II of the present work.

2.3.2 Implementation of PECM in 3D Quadrant Geometry

Figure 17 shows the quadrant geometry model of the BWR lower plenum used in this part of the work, for two scenarios (a) 0.7 m Debris bed and (b) 1.9 m debris bed. The quadrant geometry includes the penetrations of the 35 CRGTs corresponding to a quarter of the total number of CRGTs present in the RPV. In this model, we assume that the Instrumentation Guide Tubes (IGTs) are melted and plugged by corium melt during the re-melting of the debris and therefore do not have an influence on melt pool heat transfer.

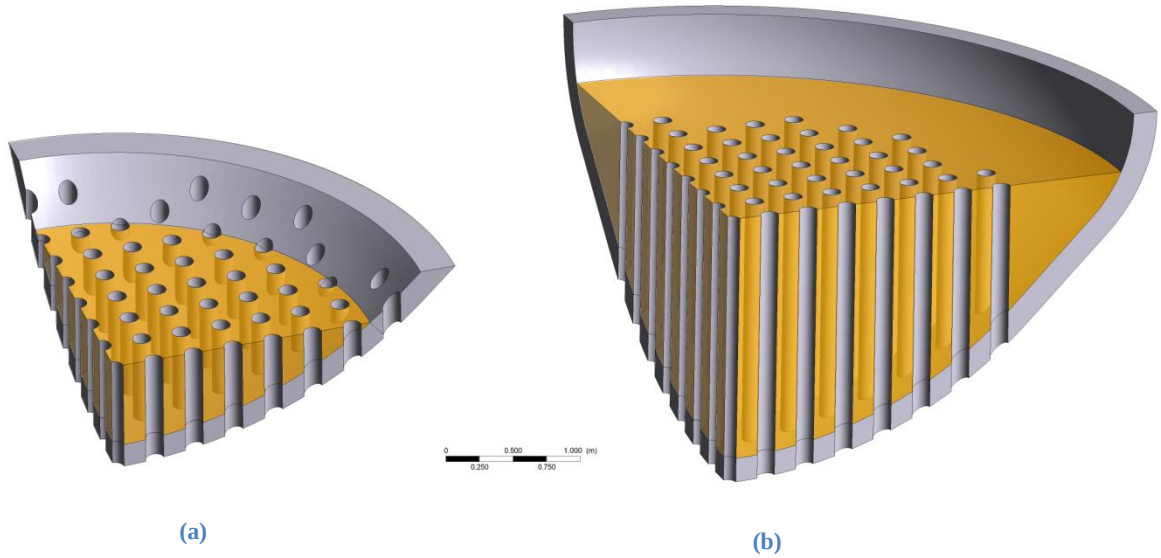

Figure 17: 3D quadrant models where the PECM was implemented in FLUENT in order to simulate the debris bed(melt pool transient, for the scenario of 0.7 m debris bed height -30 tons- (a) and 1.9 m debris bed height -30 tons- (b).

The boundary conditions corresponding to the cases with CRGTs cooling and without CRGTs were the same that the generally exposed in section 2.2.1. Symmetry boundary conditions are applied to the debris and vessel walls in such a way that the entire lower plenum is emulated. Table 8shows mesh parameters of the models with 0.7m and 1.9m of debris bed respectively. Furthermore, an extra simulation of the case with 1.9 m with a much finer mesh was performed. Parameters of this extra simulation are also included in Table 8. The objective of this simulation was to look more accurately to the size of the corium crust at time of the failure of the vessel wall (using a finer mesh). It must be noted, that the thermal load used for the structural simulation corresponds with the model with a coarse mesh. Nevertheless we will show that the refinement of the mesh has not a big influence in terms of total amount of melt and thermal load to the vessel.

Table 8: Mesh information for the three different 3D Quadrant PECM model used in Task II of the present Master Thesis.

Feature	3D Quadrant PECM 0.7 DB	3D Quadrant PECM 1.9 DB	3D Quadrant PECM 1.9 DB (Finer Mesh)
Number of elements	898,715*	3,899,924*	8,9174,679
Number of Nodes	186,723*	1,204,059*	1,778,164
Type of element:	Tetrahedral: 898,715	Tetrahedral: 2,713,254 Wedges: 763,810 Polyhedral: 422,860	Tetrahedral: 8,9174,679
Average edge length (m)	0.025	0.025	0.015
Typical calculation time	3 days	5 days	14 days

*The numbers of elements and nodes in the 3D quadrant are taken at a specific time but are representatives, since adaptive mesh was chosen and these numbers may change during the calculations.

2.3.3 3D Quadrant Structural Model

In this section we present the 3D quadrant model implemented in ANSYS for the creep calculations. The thermal boundary conditions on the inner surface of the vessel wall in contact with debris are provided by the PECM calculation of 3D quadrant model. The pressure inside the vessel is set at 0.3 MPa (corresponding to the pressure after the actuation of the vessel depressurization systems). Also the hydrostatic pressure due to the weight of the debris bed was taken into account. The displacement boundary conditions and geometry of the ANSYS model are summarized in Figure 18. We do not apply displacement boundary conditions on the CRGT penetrations as we consider that they are not strongly attached to the structures of the lower part of the reactor cavity and therefore they will move with some freedom while the vessel is deformed.

Table 9 shows mesh parameters of the 3D quadrant structural model. It important to note the large number of elements present in this model (up to 71,000) in comparison with the 800 elements of 2D axisymmetric model (see Table 6). This fact makes this model quite computationally demanding, with simulation times longer than 3 weeks.

Table 9: Mesh information of the ANSYS 3D Quadrant Structural Model

Feature	ANSYS 3D Quadrant Structural Model
Number of elements	71,343
Number of Nodes	117,362
Type of element:	SOLID226
Average edge length (m)	0.05 m
Typical calculation time	3 weeks

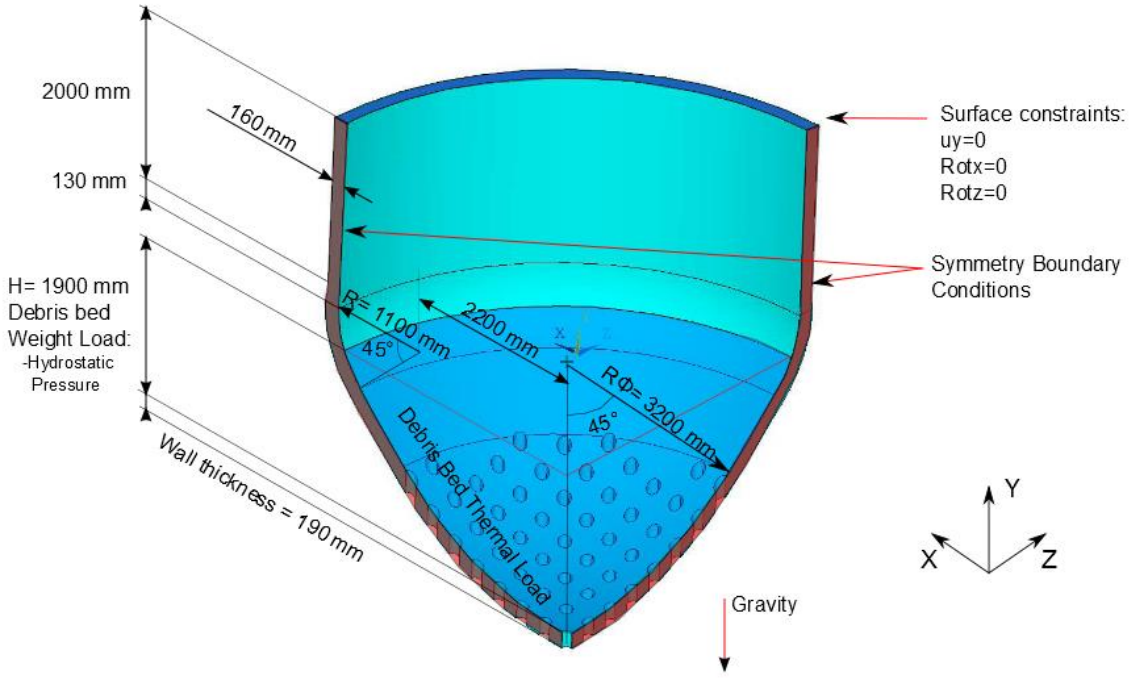

Figure 18: ANSYS 3D Quadrant Structural model used in the the Task II of the present Master Thesis. Dimensions, loads and displacement constrains are included in the figure.

3 Results and Discussions

In this section we present the obtained results for the studies carried out in this Master Thesis. The results are presented in two different sections, corresponding to the two tasks of the work; (I) Study of the instrumentation guide tube failure and (II) Study of the vessel wall failure using the 3D quadrant geometry with penetrations. It is important to note that even if these two parts are independently presented, the final discussion and conclusions will be common.

3.1 Task I: Study of the Instrumentation Guide Tube Failure

In this section the results corresponding to the IGTs failure calculations are presented. As it was stated before, the simulations are performed assuming a debris bed of 1.9 m and for two scenarios (a) CRGTs Cooling and (b) No CRGTs Cooling. The results will be presented in conjunction for these two cooling scenarios, comparing them and discussing the differences.

The calculations respond to the demand for these two main objectives

i. Predict the time of welding failure
ii. Study the possibility of clamping of the IGT in the flow limiter due to the global deformation of the vessel and local thermal load in the surroundings of the IGTs penetrations.

The results will be presented in two steps or subsections; first the results of the PECM implemented in the unitary volume in terms of predicting IGT welding failure, temperature distribution in the unitary volume and melt down of the IGTs. Then, in the second subsection we will present the results corresponding to the 3D local models of the penetrations and the clamping possibility.

3.1.1 Debris Bed Heat Transfer Solution in the Unitary Volume

Figure 19 shows the average temperature in the welding of the IGT as a function of time for scenario (a) With CRGTs and top cooling and (b) Without CRGTs Cooling. The plot shows the timing when accelerated creep and melting temperature is respectively reached (1110K and 1670 K). It can be observed that there is no significant difference in the welding temperature between the two scenarios. The accelerated creep temperature in the welding is reached at 1.02h for scenario (a) and at 1.04h (b). The difference between these times is in the order of one minute and is negligible given the uncertainties associated with the numerical calculations. Besides, the

melting temperature in the welding is reached at 1.8h and 1.85h for scenario (a) and scenario (b) respectively, which is not considered a significant difference either.

Thus we can conclude that the welding of the IGT will fail in an uncertain time between 1 hour and 1.8 hours after the dry out of the debris bed in the lower plenum. The implementation of CRGTs cooling does not have a substantial effect in the IGT welding failure. It should be noted that these results corresponds with the closest IGT from the center of the vessel. Nevertheless we consider that timing of failure of the farthest IGT will be in the same order of magnitude. This assumption is supported by looking locally at the temperature distribution at the respective IGTs nozzle positions in the 3D slice model. It seems that during the first two hours of transient the amount of debris above the nozzle has not a perceptible effect in its temperature distribution (even if the farthest IGT will have less debris above it as it is in a higher position Figure 5).

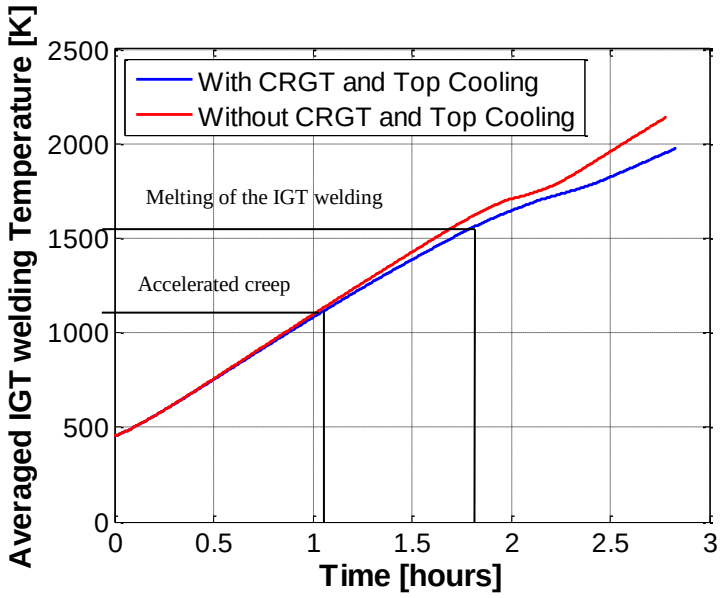

Figure 19: Averaged temperature in the IGT welding as a function of time for (a) With CRGTs and Top Cooling and (b) Without CRGT cooling.

Figure 20, 21, 22 and 23 show snapshots of the temperature distribution at 3500s (0.97h) and 7000s (1.94h) in the unitary debris bed volume. The results are provided corresponding to two studied scenarios (a) With CRGTs and top cooling, and (b) Without CRGTs and top cooling. The time steps shown correspond with the state of the debris bed close to the time when accelerated creep temperature and melting temperature are respectively reached in the IGT welding (Figure 19).

It can be observed in Figure 20 and 21 that the debris bed is still in solid state when the IGT welding fails (maximum temperature are well below 2750 K). The implementation of CRGTs cooling does not have a considerable effect in the bulk debris bed temperatures, where the difference between the maximum temperatures for scenarios (a) and (b) is only 6 K at 0.97h and 50K at 1.94 h. From this tendency we can see that the longer the transient the more influence of

CRGT cooling (as will be observed also in the further in the present work). This effect can also be seen in the temperature stratification at the lower regions, close to the tubes nozzles, where the effect of CRGTs cooling is more visible at 1.9h (Figure 21(a)) than at 0.9 h (Figure 22(a)).

One the other hand the temperature distribution changes locally close to the CRGTs depending on the scenario. When CRGTs cooling is implemented a large temperature gradient (close to 1000K) is observed in the CRGTs surroundings (see top view in Figure 20(a), 21 (a), 22(a) and 23 (a)). For scenario without CRGTs cooling this gradient is less than 100K (see top view in Figure 20(b) and 21 (b), 22(b) and 23 (b)). Much higher temmperatures are therefore reached on the CRGTs surroundigs when CRGTs cooling is not impelemented. The influence of the CRGTs in the unit volume temperature distribution can be clearly observed in Figures 21 and 23 where temperature on the plane containing the CRGTs is shown.

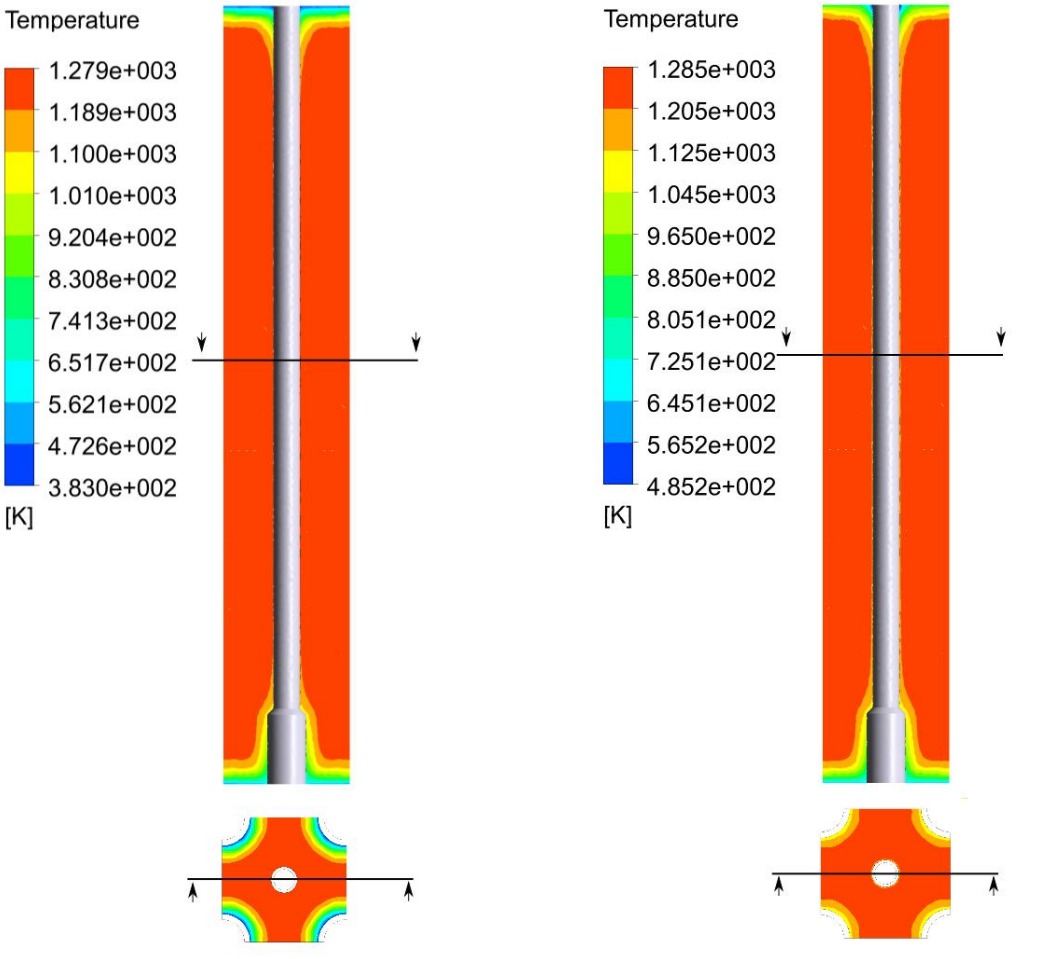

Scenario (a): With CRGTs and top Cooling. t=0.97h

Scenario (b): Without CRGTs and top Cooling. t=0.97h

Figure 20: Snapshot of the debris bed temperature distribution at the IGT surrounding at 0.97h (when accelerated creep temperature is reached in the IGT welding) for (a) With CRGTs and Top Cooling and (b) Without CRGT cooling.

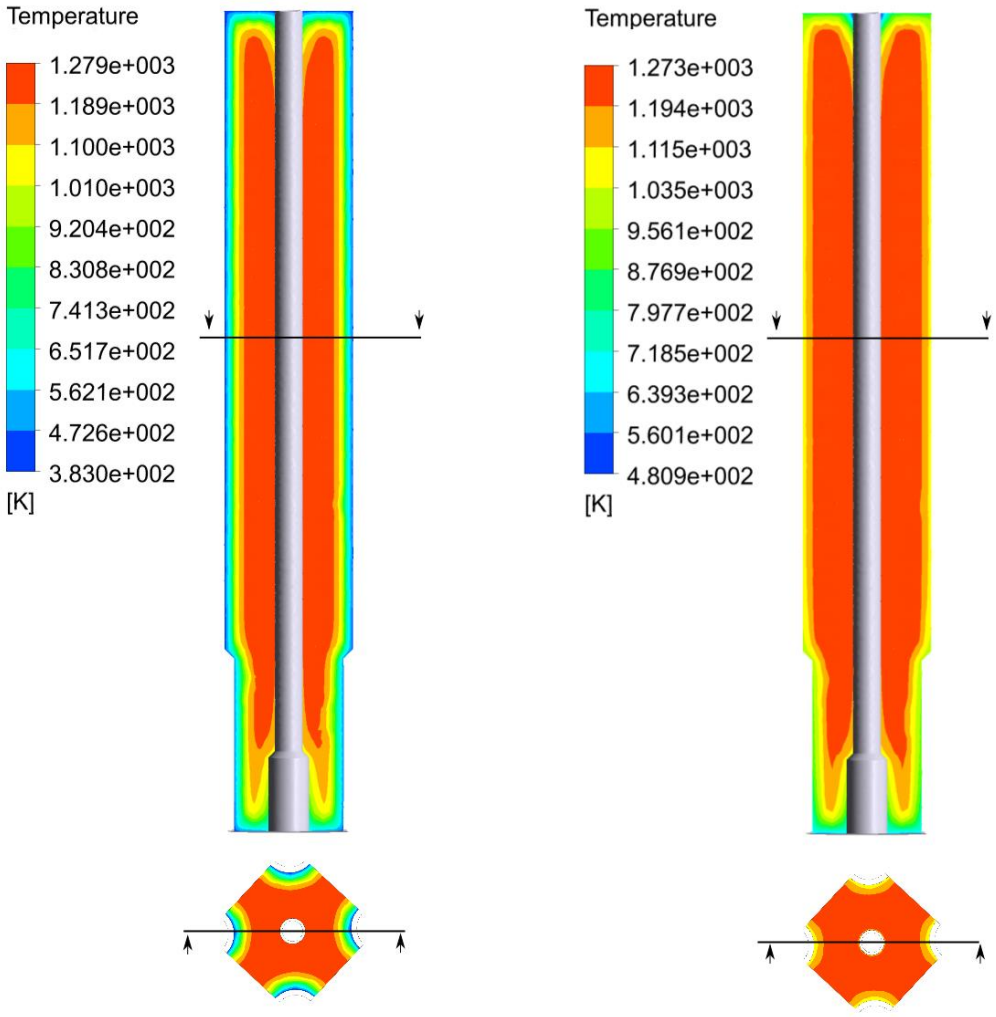

Figure 21: Snapshot of the debris bed temperature distribution at the IGT surrounding at 0.97h. The solution is presented in vertical plane including the two CRGTs. For scenarios (a) With CRGTs and top cooling and (b) Without CRGT cooling

The effect of the top water layer in scenario (a) also can be observed in the temperature distribution at upper regions -Figure 20, 21, 22 and 23-. Larger temperature gradients appear at the top for the scenario (a) while in scenario (b) the top of the debris bed is dry and only radiation heat transfer is allowed.

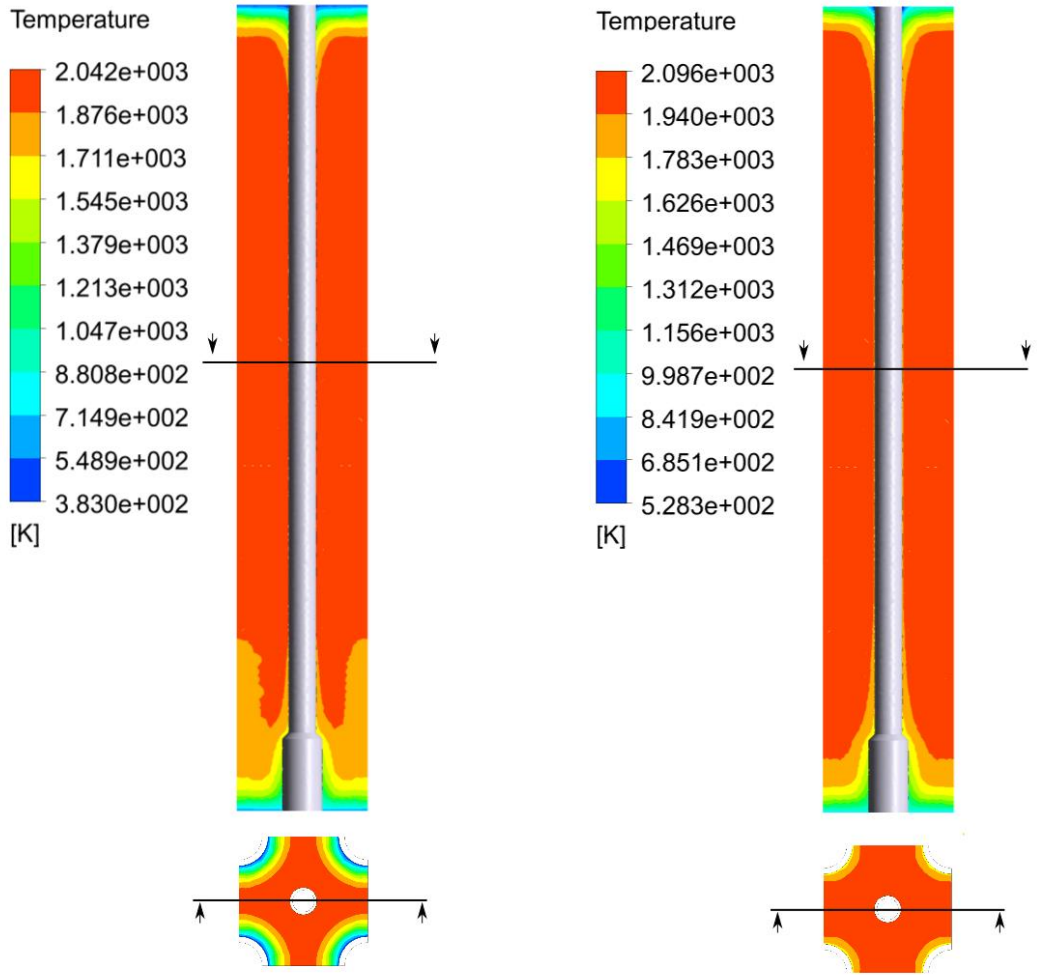

Scenario (a): With CRGTs and top Cooling. t=1.94h

Scenario (b): Without CRGTs and top Cooling. t=1.94h

Figure 22: Snapshot of the debris bed temperature distribution at the IGT surrounding at 1.94h (when melting temperature is reached in the IGT welding) for (a) With CRGTs and Top Cooling and (b) Without CRGT cooling.

Figure 24 and 25 show the bulk temperature distribution at different times as a function of debris bed depth for the scenario with CRGTs and without CRGTs respectively. It can be observe that the spatial temperature shows a flat profile, consequence of the volumetric heat, with a sudden drop in the temperatures close to the top and bottom boundaries of the debris bed. Also it can be observed that there is no significant difference in the bulk temperature profiles between cooling scenarios (Figure 24 and 25).

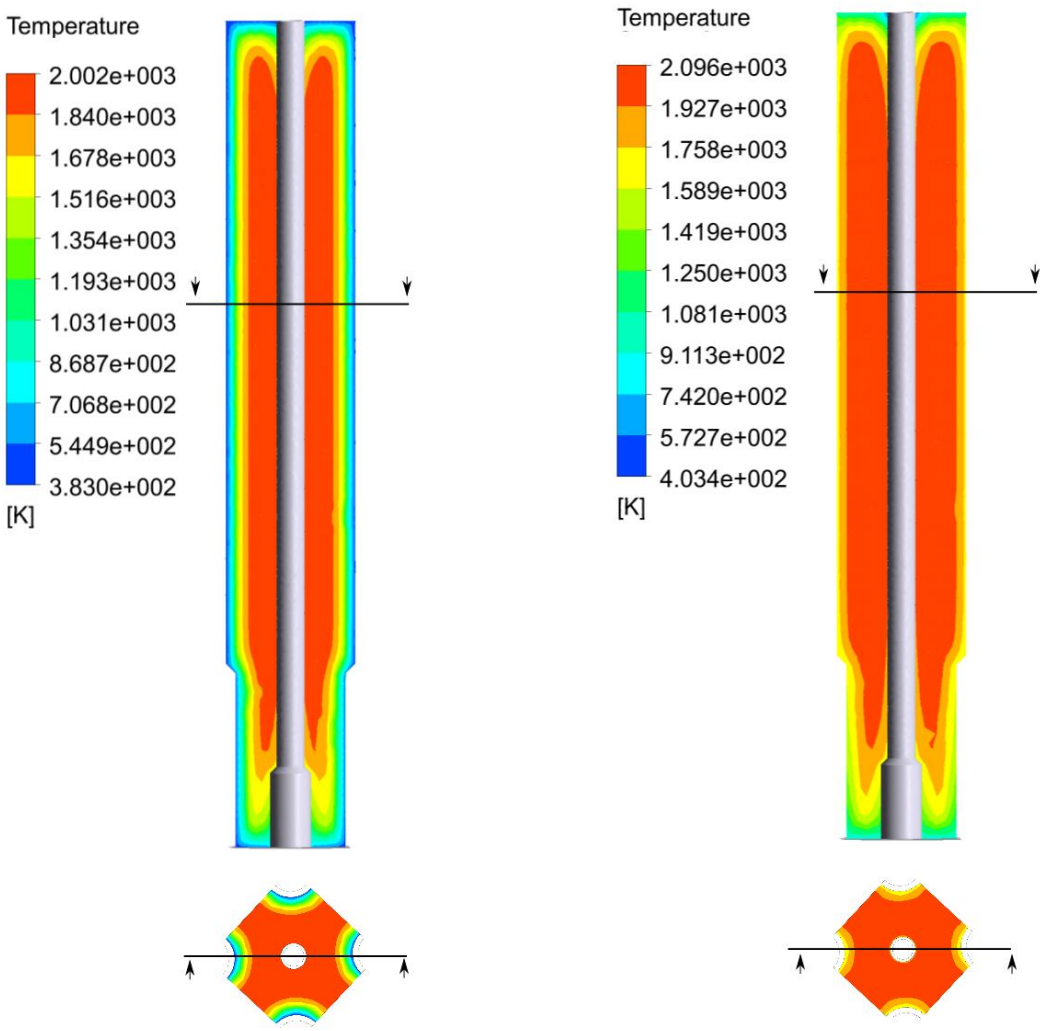

Scenario (a): With CRGTs and top Cooling. t=1.94h

Scenario (b): Without CRGTs and top Cooling. t=1.94h

Figure 23: Snapshot of the debris bed temperature distribution at the IGT surrounding at 0.9h. The solution is presented in vertical plane including the two CRGTs. For scenarios (a) With CRGTs and top cooling and (b) Without CRGT cooling.

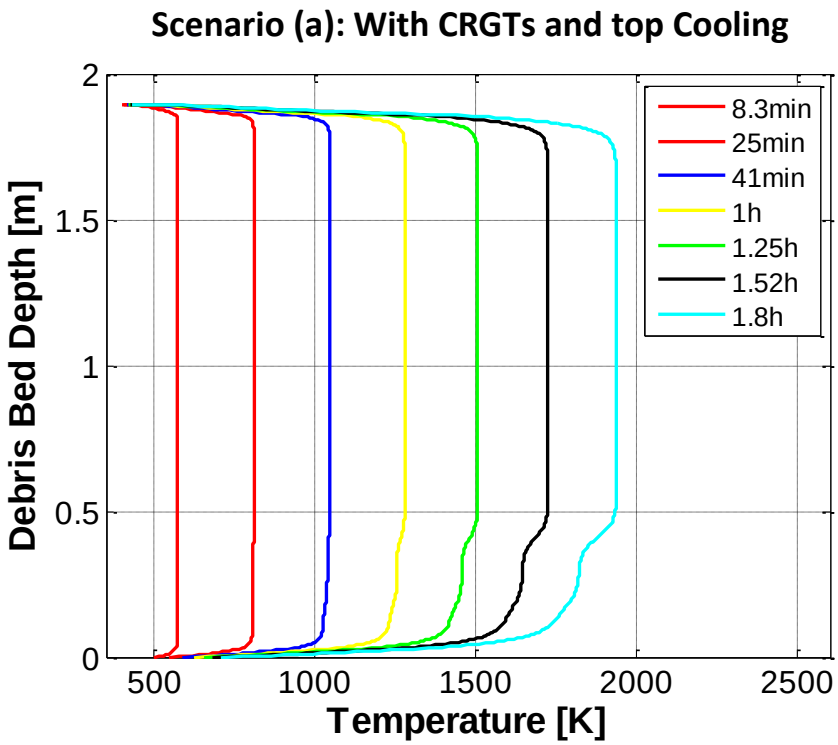

Figure 24: Debris bed bulk temperature distribution as a function of depth at different times for the scenario with CRGTs and top cooling.

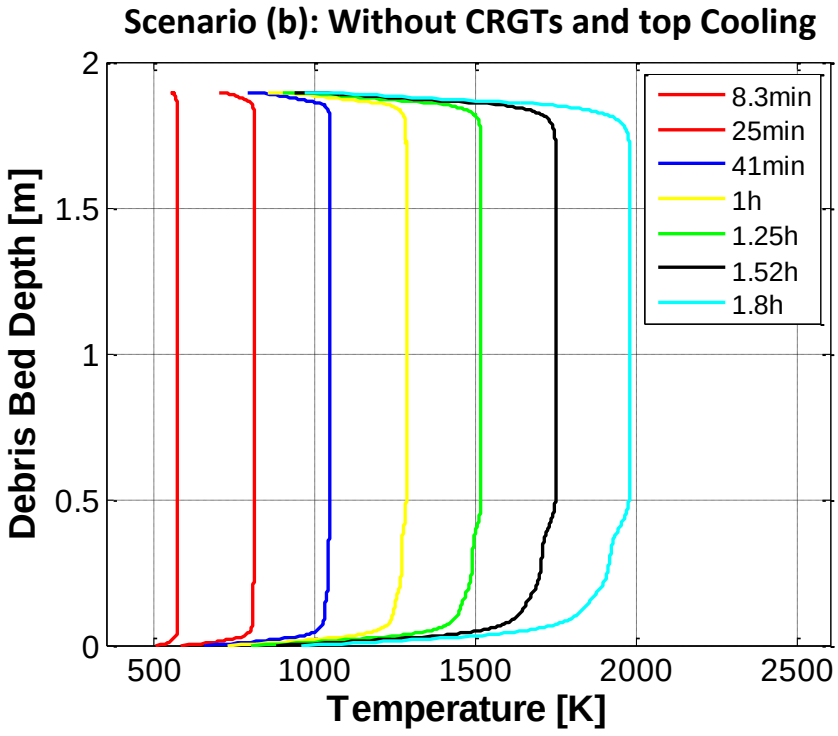

Figure 25: Debris bed bulk temperature distribution as a function of depth at different times for the scenario without CRGTs and top cooling.

Figure 26 shows the melt fraction of the IGT and CRGTs at 1.94 hours. It should be noted that at 1.9 h -time when melting of the IGT welding occurs- the IGT is already completely melted in both scenarios. This can be observed, in Figure 27 and 28, where the melt fraction as a function of IGT height at different times is plotted. These plots show that the melt down of the IGT starts between 1.52 and 1.66 hours at the center of the tubes in both cooling scenarios. The IGT is gradually melted from the center to the bottom and top boundaries. Thus, it is expected that the surrounding debris bed will gradually occupy the space of the melted IGT. The melt down of the IGT occurs slightly faster for the scenario (b) without CRGTs cooling, but the difference is not significant, as happened with the bulk temperature distribution. According to the results, the IGTs have completely melted –except the bottom and the top- at 1.8 h in both scenarios (Figure 27 and 28).

Melting of the CRGTs it is also observed from 1.8 h to 2.2 h for the scenario (b), as can be seen in Figure 29, while it is prevented if CRGTs cooling is implemented –Figure 26-. Melt down of the CRGTs occurs later than the IGT melting due to its larger diameter and amount of material.

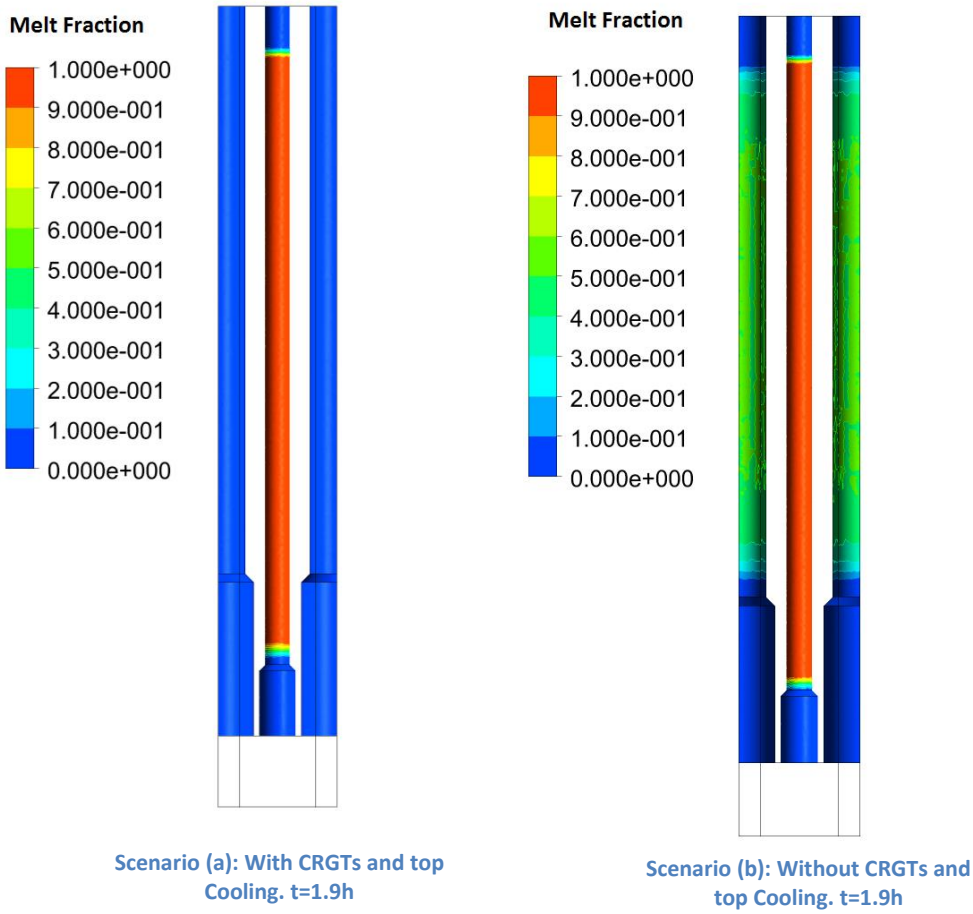

Figure 26: Snapshot of the IGT and CRGTs melt mass fractions at 1.9h. For scenarios (a) With CRGTs and top cooling and (b) Without CRGT cooling.

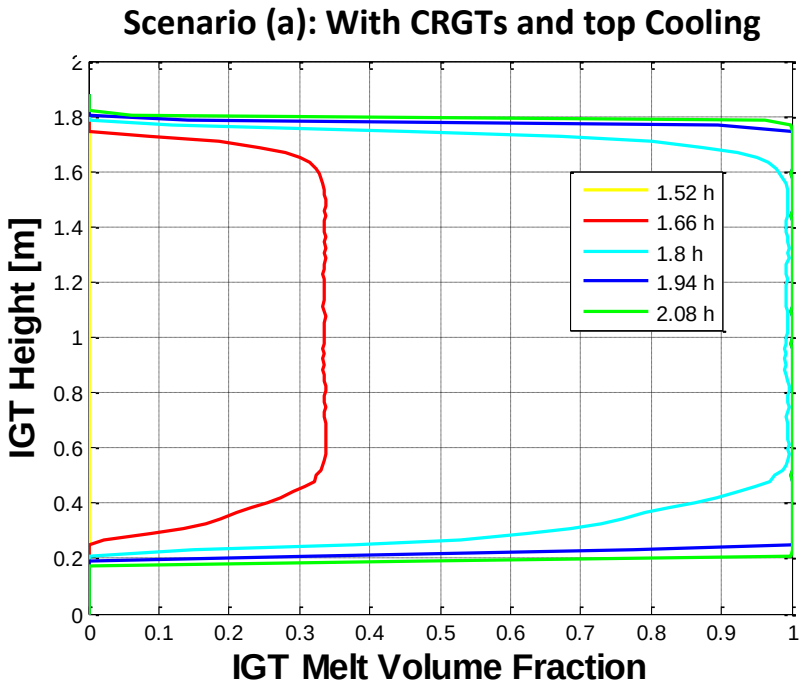

Figure 27: Spatial distribution melt fraction of the IGTs as a function of its height, at different times for the scenario (a) With CRGTs and top Cooling. In the plot it is possible to observe the melting progression of the IGT, from 1.5-1.66 h to 1.8-1.9h.

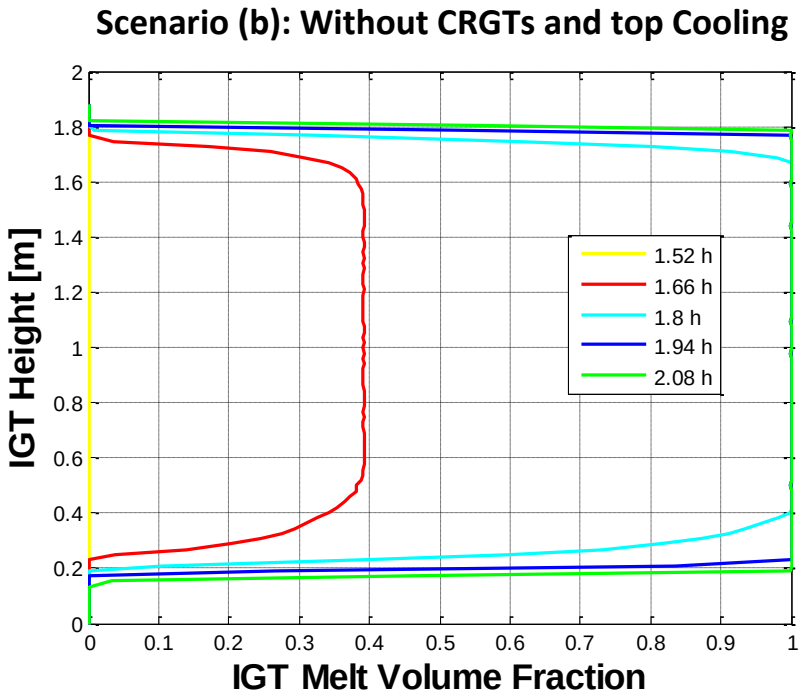

Figure 28: Spatial distribution melt fraction of the IGTs as a function of its height, at different times for the scenario (b) Without CRGTs and top Cooling. In the plot it is possible to observe the melting progression of the IGT, from 1.5-1.66 h to 1.8-1.9h.

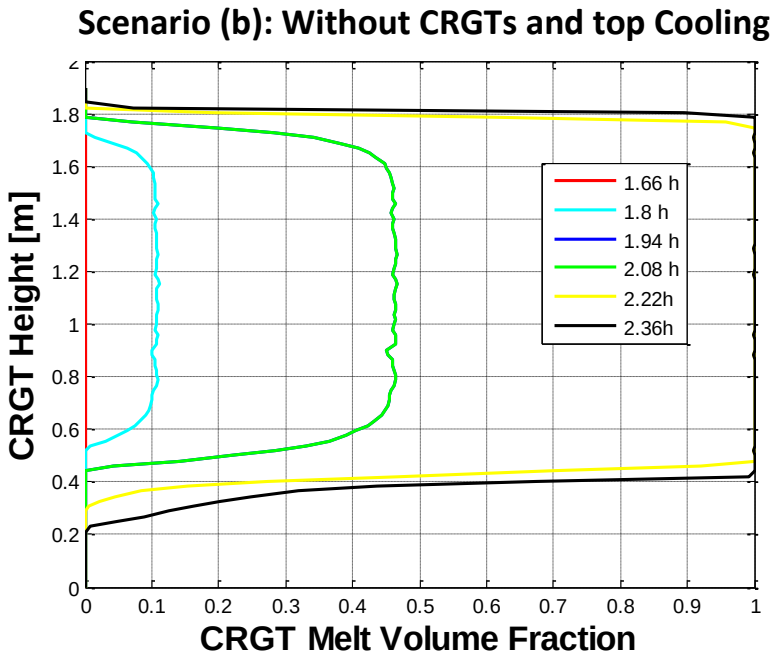

Figure 29: Spatial distribution melt fraction of the CRGTs as a function of its height, at different times for the scenario (b) Without CRGTs and top Cooling. In the plot it is possible to observe the melting progression of the CRGTs, from 1.66-1.8 h to 2.22h.

Finally, Figure 30 shows the average temperature at the CRGTs and IGTs welding for the scenario (b) without CRGTs cooling. The failure of the CRGTs welding is expected in this scenario between 1.2h and 1.95 hours (slightly later than the IGT welding failure). Ejection of the CRGTs however is considered more unlikely than IGT ejection, as the first are supported from below by the control rod insertion mechanisms. Nevertheless, more investigation of CRGTs ejection is necessary.

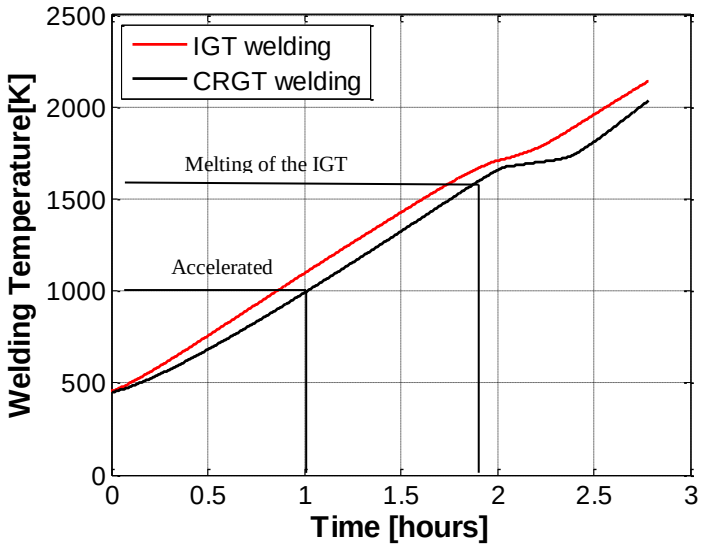

Figure 30: Averaged temperature in the IGT (red) and CRGTs (black) welding as a function of time for scenario (b) Without CRGT cooling.

3.1.2 Results of the IGTs Penetrations' Housing Local Analysis

In this section the results of the local structural analysis of the penetrations' housings for the clamping possibility study are provided. The calculations are presented for the closest and farthest IGTs from the center, for scenarios a) With CRGTs and top cooling and (b) Without CRGTs Cooling.

Closest to the bottom center of the vessel IGT

Figure 31 shows the temperature distribution on the surroundings of the closest from the center IGT penetration, 2 hours after the dry out of the debris bed. At this time the welding of the IGT has already failed according to the calculations shown in the previous section. It can be observed the different distribution of the temperature depending on the scenario (a) and (b) due to the cooling of the CRGTs.

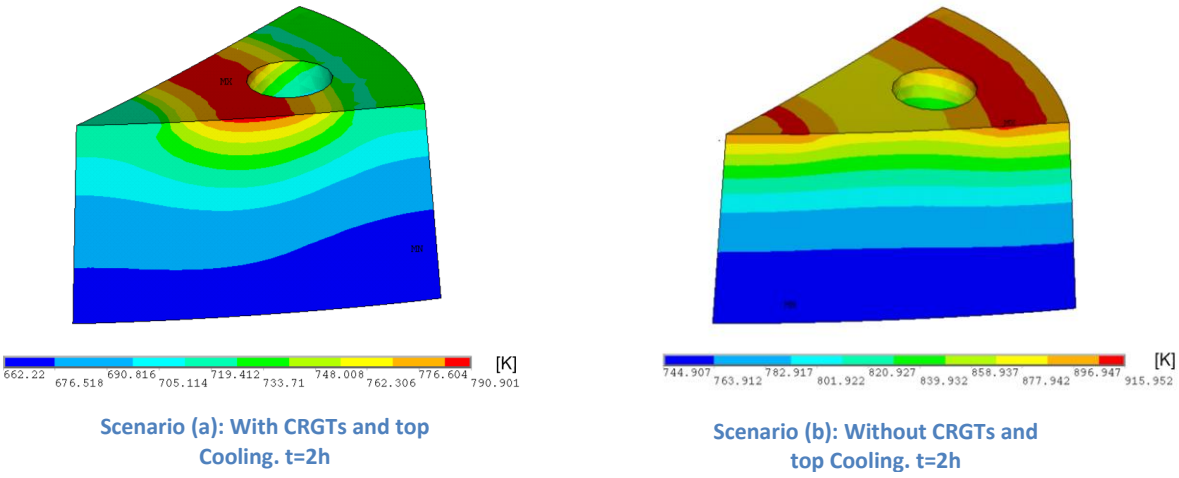

Figure 31: Temperature distribution at the surroundings of the IGT closest to the center at 2 hours, for the scenario (a) With CRGTs and top cooling and (b) Without CRGT cooling

The deformation of the flow limiter is studied by selecting the nodes of the FE models corresponding to the flow limiter and grouping them in diametrically opposite pairs. Then the change in distance between these pairs is checked. if the distance in at least one of these pairs is reduced 0.5 mm –the total size of the gap- during the transient, the IGT will be clamped and its ejection will be avoided (as long as it occurs before the welding failure). Figure 32 shows the displacement of the selected nodes of the flow limiter for the central IGT at 2.5 h for scenarios (a) and (b). It can be observed how the deformation trend is the same in both cases, even though the deformation is slightly more pronounced in (b) because of the higher thermal load corresponding to the scenario without CRGT cooling. From these similar trends we can conclude that the deformation of the flow limiter is more induced by the global vessel deformation than by the local temperature in the surroundings of the IGT penetration.

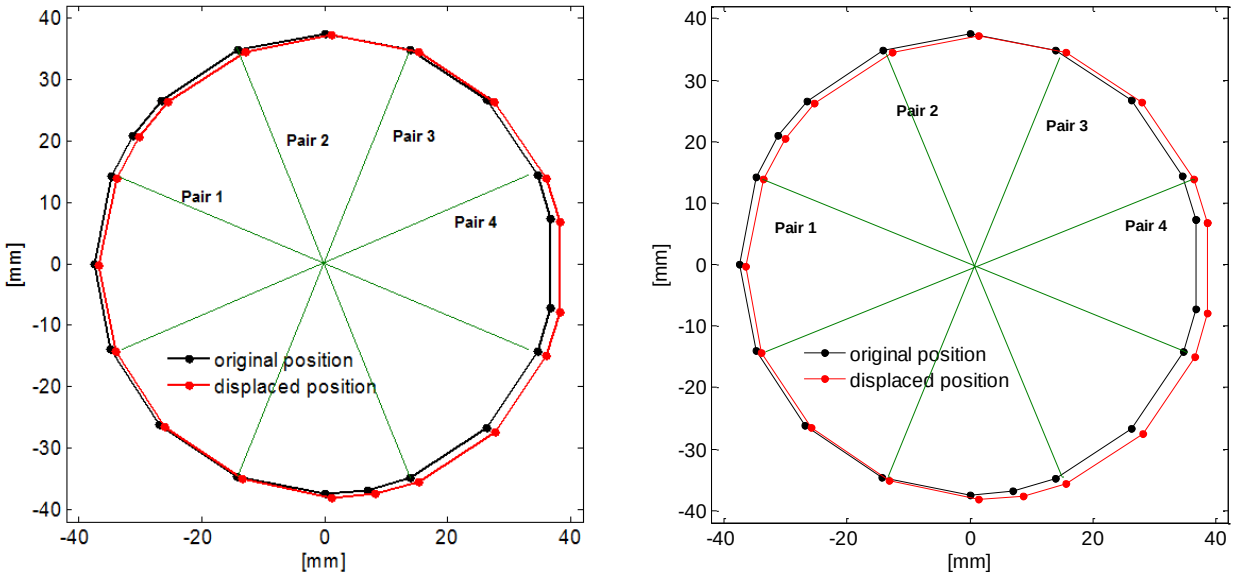

Figure 32: Deformation of the flow limiter at 2.5 hours, in terms of displaced position (red) and original position (black) for the scenario (a) With CRGTs and top cooling and (b) Without CRGT cooling.

Figure 33 and 34 show the change in the distance of the selected pairs of nodes of the flow limiter as a function of time for scenarios (a) and (b) respectively. The plot also includes the clamping threshold, below which clamping will occur. This threshold is also changing with time as it is taking into account the expansion of the IG tube due to the thermal load.

It can be observed that all the distances between pairs increase for both scenarios. Thus the flow limiter size is growing with time and therefore the IGT will not be clamped. The plots also include the timing window of the welding failure.

From Figure 33 and 34, and taking into account the results of the IGT welding failure, we can conclude that the closest IGT to the center will be ejected in an uncertain time between 1 and 1.85 hours, independently if CRGTs cooling is implemented as SAM strategy. Thus CRGT cooling will not prevent the possible failure and ejection of the closest to the center IGT.

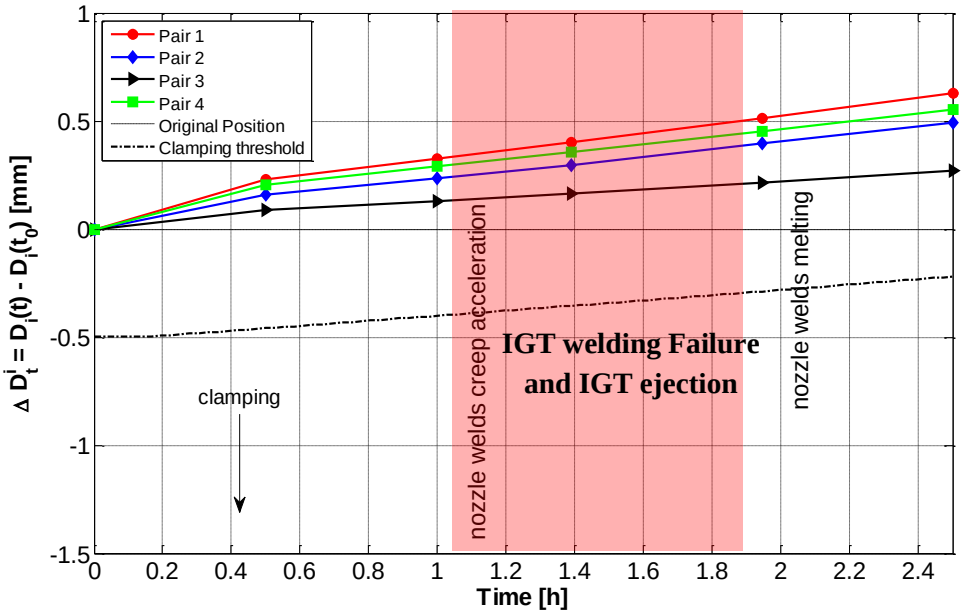

Figure 33: Distance of the diametrical opposite pairs of nodes selected in the flow limiter as a function of time for the closest IGT from the center, scenario (a) With CRGTs and top cooling. It can be observed that the clamping threshold is not crossed and therefore the IGT will be ejected.

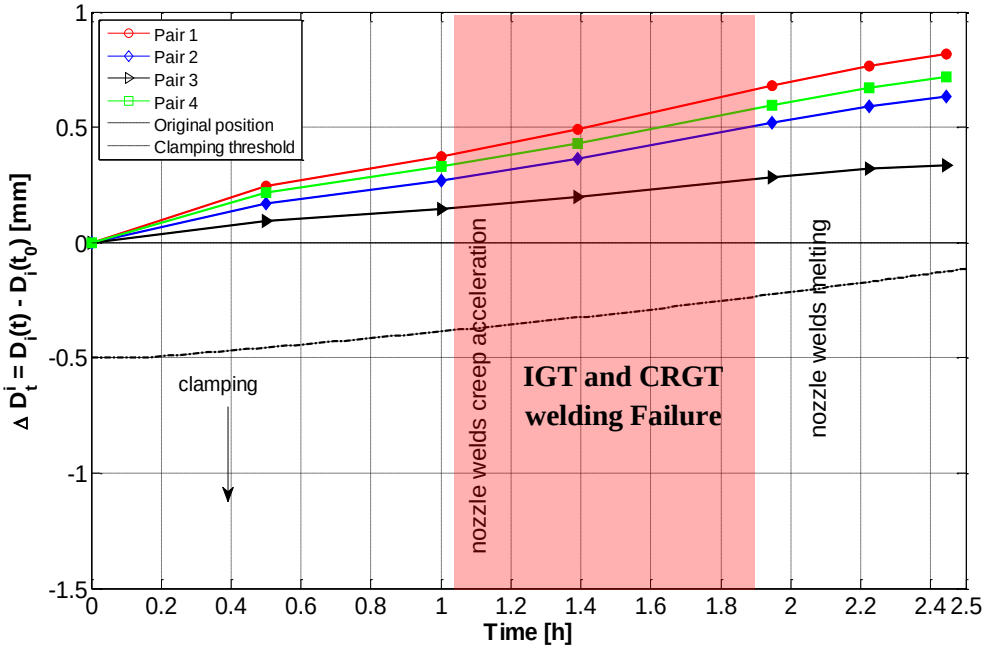

Figure 34: Distance of the diametrical opposite pairs of nodes selected in the flow limiter as a function of time for the closest IGT from the center scenario (b) Without CRGTs and top cooling.

Farthest from the vessel bottom center IGT

Figure 35 shows the temperature distribution on the surroundings of the farthest from the center IGT penetration, 2 hours after the dry out of the debris bed. It can be observed the different distribution of the temperature depending on the scenario (a) and (b) due to the cooling of the CRGTs. On the other hand, this temperature distribution is quite similar to the one present in the closest from the center IGT, which enhances the statement previously made about considering almost the same timing of welding failure for the closest and farthest IGTs.

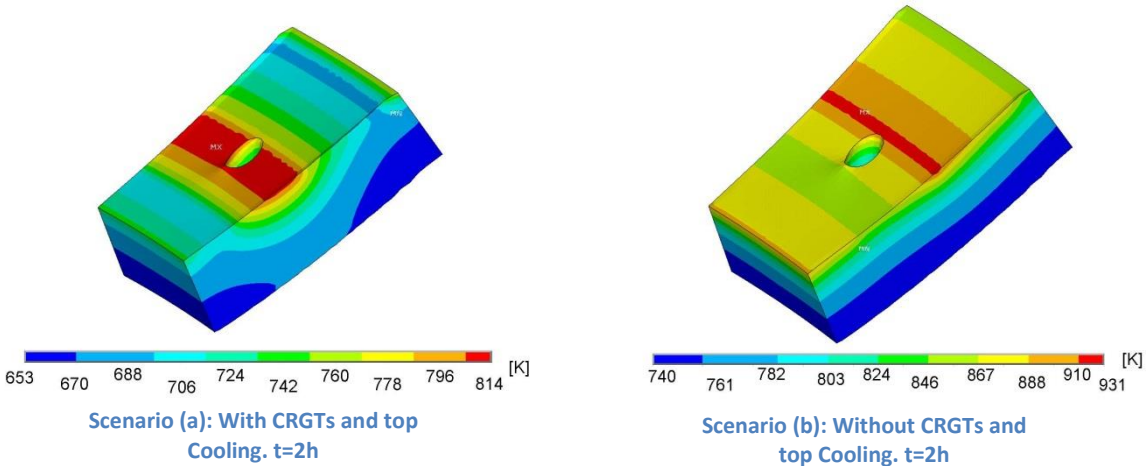

Figure 35: Temperature distribution at the surroundings of the IGT farthest to the center at 2 hours, for the scenario (a) With CRGTs and top cooling and (b) Without CRGT cooling

Figure 36 and 37 show the change in the distance between the selected pairs of nodes in the flow limiter for scenarios (a) and (b) respectively. It can be observed how for this IGT the distance between some of the selected pairs decreases, thus clamping the tube and avoiding its failure. For scenario (a) with CRGT and top cooling (Figure 36) the clamping is expected to happen around 1.2 hours. Therefore there is still a very small chance of tube ejection (since it is inside the welding failure timing window). For the scenario (b) Without CRGTs, on the other hand, the clamping occurs even earlier, around 0.6 hours (Figure 37). From these results we can conclude that failure of the farthest IGT is not expected in any of the postulated cooling scenarios due to clamping of the tube in the flow limiter.

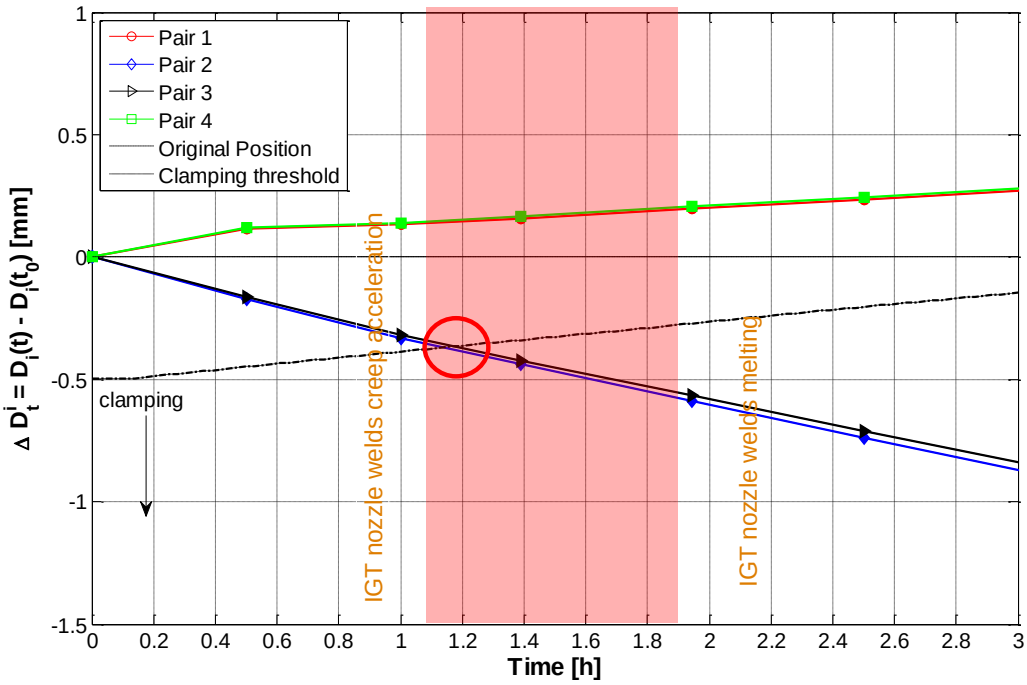

Figure 36: Distance of the diametrical opposite pairs of nodes selected in the flow limiter as a function of time for the farthest IGT form the center (a) With CRGTs and top cooling. It can be observed that the clamping of the IGT occurs at 1.2 hours, avoiding its ejection and failure.

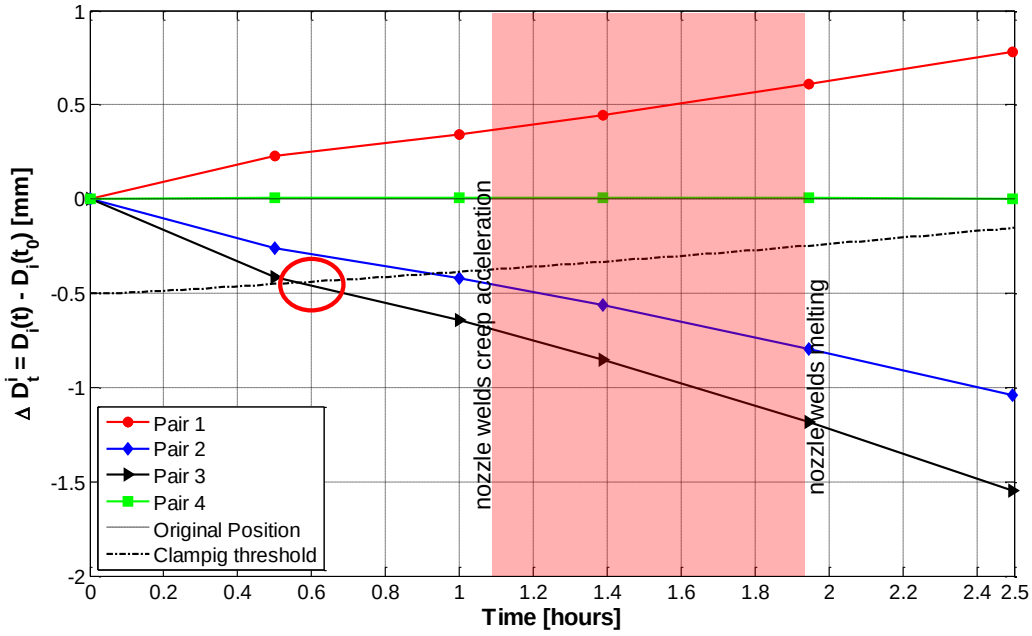

Figure 37: Distance of the diametrical opposite pairs of nodes selected in the flow limiter as a function of time for the farthest IGT form the center (b) Without CRGT cooling. It can be observed that the clamping of the IGT occurs at 0.6 hours, avoiding its ejection and failure.

3.2 Task II: Study of the Vessel Wall Failure using 3D Quadrant Geometries with penetrations

In Task I of the present work we have analyzed the possibility IGT failure in terms of tube ejection, which is expected to be the earliest mode of failure. On the other hand, to have earlier IGT failure does not eliminate the possibility of later failures of the global vessel wall or other penetrations as it is rather a local effect. For this reason in the Task II of the present work we provide a detailed 3D analysis of the vessel wall failure. In order to carry out this analysis, the debris bed heat transient and melt pool formation are simulated using the PECM implemented in 3D geometry models of a quadrant of the reactor lower head. Then, the obtained thermal load is applied to 3D structural models of a quadrant of the vessel wall, which takes into account the CRGTs penetrations. Furthermore, Task II is divided into two parts. The results corresponding to the first part -detailed comparison between these quadrant models and the slices models used previously- are included in the conference Paper attached in Appendix I, and we will not go through them in this section to avoid repetition. In this section we will present the result corresponding to the second part of Task (II), where simulations were performed for a total of 4 scenarios, combination of two different amounts of debris located in the lower plenum -1.9 m and 0.7 m height debris beds- and CRGTs cooling or no CRGTs implemented as SAM strategy. These four scenarios are defined as:

I) Scenario I: 1.9 m Debris bed with CRGTs and top cooling.
II) Scenario II: 1.9 m Debris bed without CRGTs and top cooling.
III) Scenario III: 0.7 m Debris bed with CRGTs and top cooling.
IV) Scenario IV: 0.7 m Debris bed without CRGTs and top cooling.

In the first subsection, we show the results corresponding to the thermal transient of the debris bed and melt pool formation, including the thermal load to the vessel. Then, we present the results corresponding to the structural analysis, showing the timing and mode of failure for the considered scenarios.

3.2.1 Debris Bed and Melt Pool Heat Transfer Solution

Scenarios I and II- Debris bed of 1.9 m height

In this section we present the results corresponding to the scenarios with a debris bed of 1.9 m (around 200 tons), which corresponds with almost the whole core relocated and quenched in the lower plenum.

Figure 38 shows the average temperature in the debris bed volume as a function of time for scenarios I and II. It can be observed how the temperature increases from the initial conditions

(470K) up to temperatures higher than 2000 K in less than 2-3 hours. The higher the temperature, the higher is the difference between cooling scenarios, i.e. higher effectiveness of the CRGTs and top cooling. The reason of this behavior is the higher thermal conductivity of the melt material in comparison to the solid and porous debris bed. The longer is the transient, the thinner are the crust layers surrounding the CRGTs and higher the conductivity of debris/melt pool hence more heat is effectively evacuated through such cooled CRGTs.

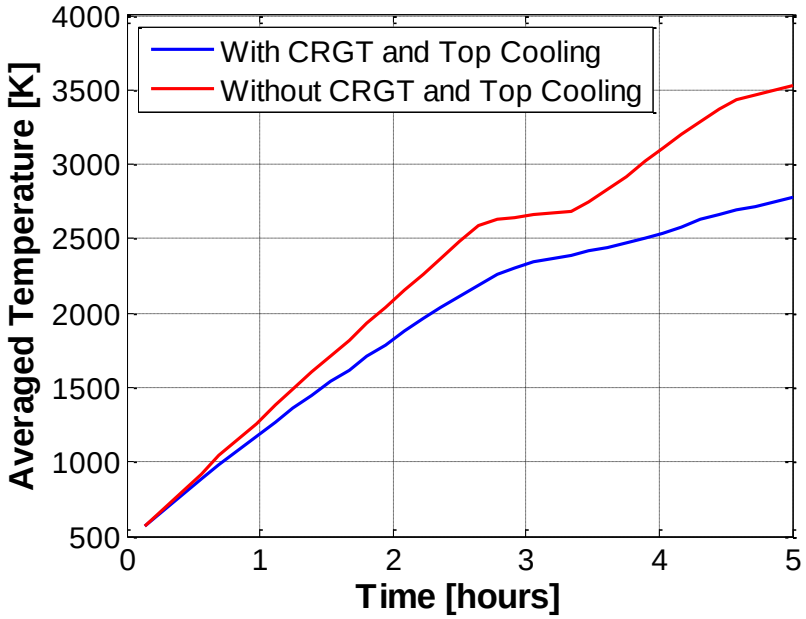

Figure 38: Average temperature in the debris bed/melt pool volume as a function of time for a 1.9 m height debris bed and two scenarios; With CRGTs and top cooling (blue) and (b) Without CRGT cooling (red).

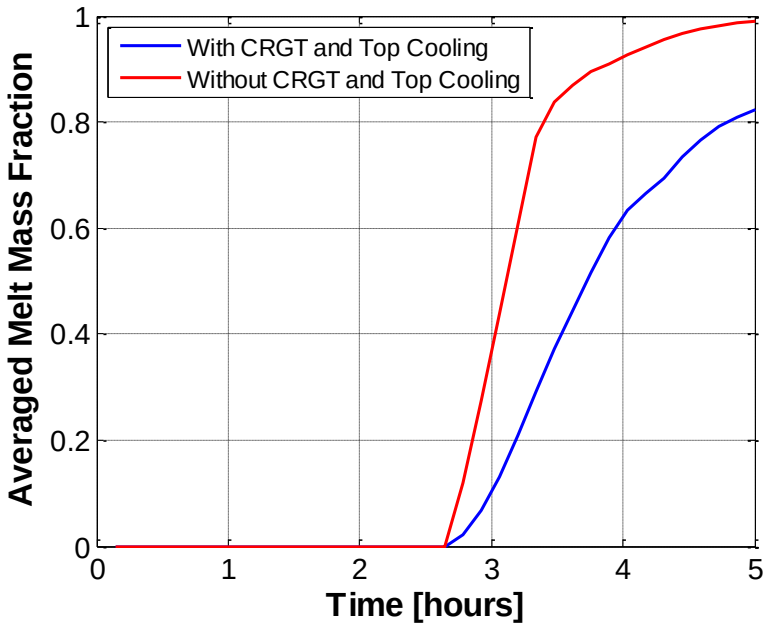

Figure 39: Average melt mass fraction in the debris bed/melt pool volume as a function of time for a 1.9 m height debris bed and two scenarios; With CRGTs and top cooling (blue) and (b) Without CRGT cooling (red).

Figure 39 shows the averaged melt mass fraction as a function of time for the studied case of 1.9 m debris bed. It can be observed that melt starts appearing around 2.7 hours after the debris bed dry-out for both cooling scenarios. However in the scenario without CRGTs cooling the melting of the debris occurs much faster, almost 100% of the debris is re-melted again in 5 hours, while only 80% if CRGTs cooling is implemented. Nevertheless, at this time the vessel wall has already failed in both scenarios, as it will be seen in the structural analysis.

Snapshots of the 3D quadrant melt mass fraction solution at 3.47 hours are shown in Figure 40. At this time around 90% of the debris has been melted in scenario II while 50% in scenario I. It is very interesting to observe the formation of crust layers around the CRGTs and at the top of the debris bed when CRGTs and top cooling is implemented, as well as the formation of a large melt pool at the periphery, where no CRGTs are present –Figure 40(a)-. The thermal load from this peripheral melt pool will be the cause of failure of the vessel wall in this scenario, as it will be seen in the structural analysis. Also it is interesting to see in these figures the formation of isolated melt pools between the cooled CRGTs. At the time of failure not all liquid melt will be available for release. In scenario (II) on the other hand all the debris bed and CRGTs are melted leading to the formation of a unique molten pool.

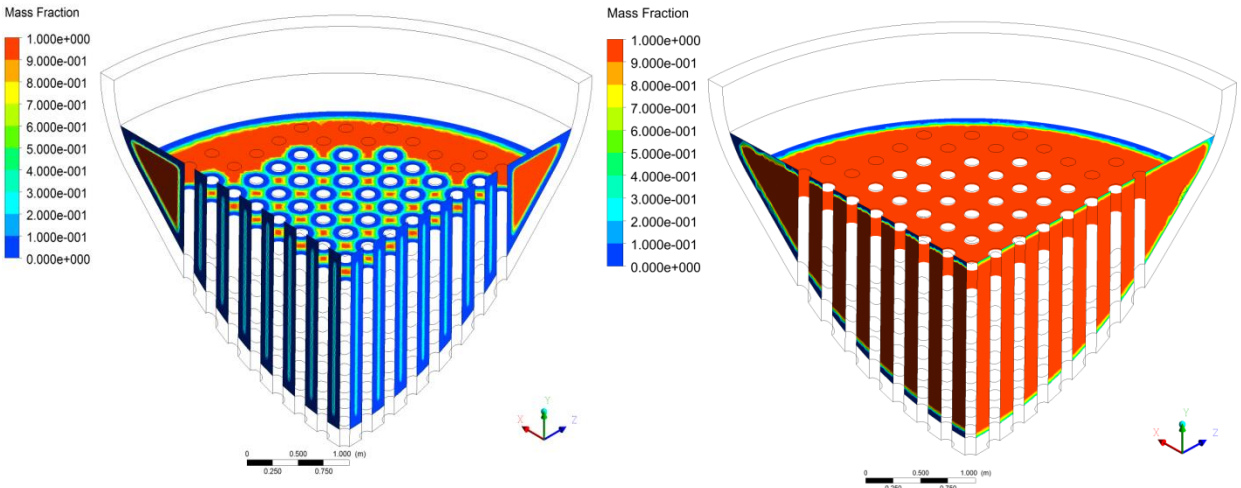

(a) Scenario (I) 1.9 m With CRGTs and top Cooling. t=3.47h

(b) Scenario (II) 1.9m Without CRGTs and top Cooling. t=3.47h

Figure 40: Snapshots the melt mass fraction in the debris bed at t=3.47 h, for the scenario (a) With CRGTs and top cooling and (b) Without CRGT cooling. In the figure blue represents solid debris, red represents molten debris.

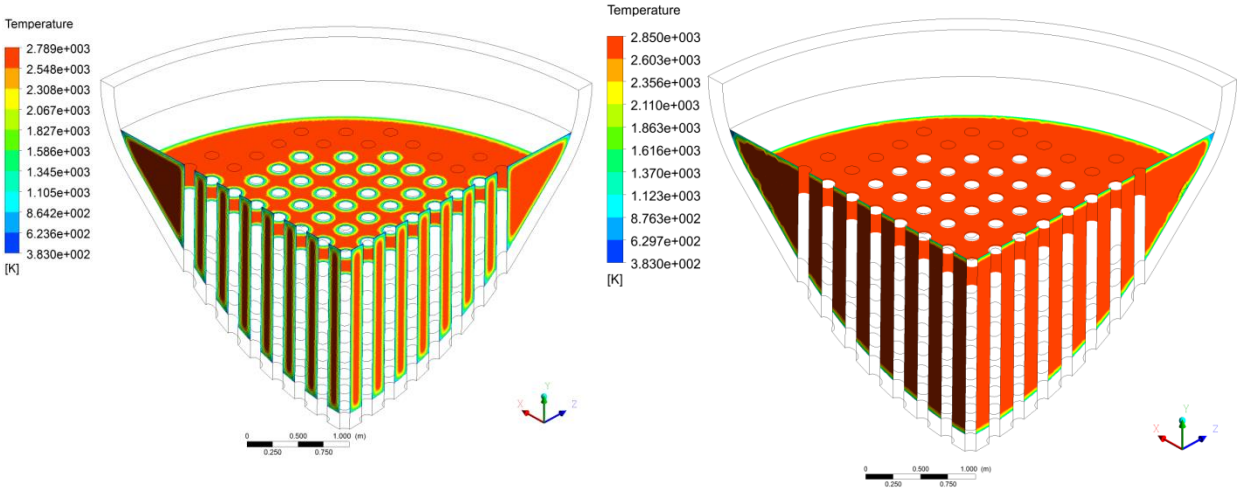

(a) Scenario (I) 1.9 m With CRGTs and top Cooling. t=3.47h

(b) Scenario (II) 1.9m Without CRGTs and top Cooling. t=3.47h

Figure 41: Snapshots of the temperature distribution in the debris bed at t=3.47 h, for the scenario (a) With CRGTs and top cooling and (b) Without CRGT cooling

Figure 41 shows the temperature distribution at 3.47 hours, which is consistent with the melt distribution shown in the Figure 40. There is not a large difference in the maximum temperature

reached in scenarios (I) and (II) (2850 and 2790 K respectively). We attribute this feature to the fact that in scenario (II) –without cooling- the decay energy is mainly spent in melting the debris instead of increasing the temperature. This can be observed in the results the red lines in Figure 35 and 36, where in the time window between 2.8 and 3.5 hours the melt mass fraction significantly increases while the temperature is almost constant.

It is important to note at this point, that the snapshots presented in Figures 40(a) and 41(a) correspond to the 3D quadrant model for 1.9 m debris bed height implemented in a fine mesh while the plots of Figure 38, 39 and 42 as well as the thermal load to the vessel were obtained from a model with a coarser mesh (see Table 8). The finer mesh model was built in order to be able to check locally the thickness of the crust layers. Comparison of these two meshes showed that the refinement of the mesh does not have a noticeable effect on the results and thermal load to the vessel. Thus, both models are consistent.

Finally, the Figure 42 represents the thermal load to the vessel wall at 3.47 hours. In the figure the average temperature on the vessel surface is plotted as a function of the angle from the center line. The temperature was averaged along one slice of the 3D quadrant solution, in order to illustrate the spatial influence of the CRGTs in the vessel wall temperature. The "noise" in the temperature profile is attributed to the averaging process; due to the variable number of mesh nodes in the angle-steps taken in the slice of the 3D Quadrant. For the scenario I (blue)-, the figure shows how the temperature is much lower in the CRGTs penetration region (900 K, 1000K from 0 to 40 degrees) and how increases up to 1200 K in the non-penetrated region (where the peripheral melt pool melt pool appeared). Then the average temperature drops to 500K due to the top cooling. On the other hand, for the scenario II (red), the temperature is around 1100 K in the penetrated region. For the non-penetrated region the temperatures are almost the same for scenarios (a) and (b).

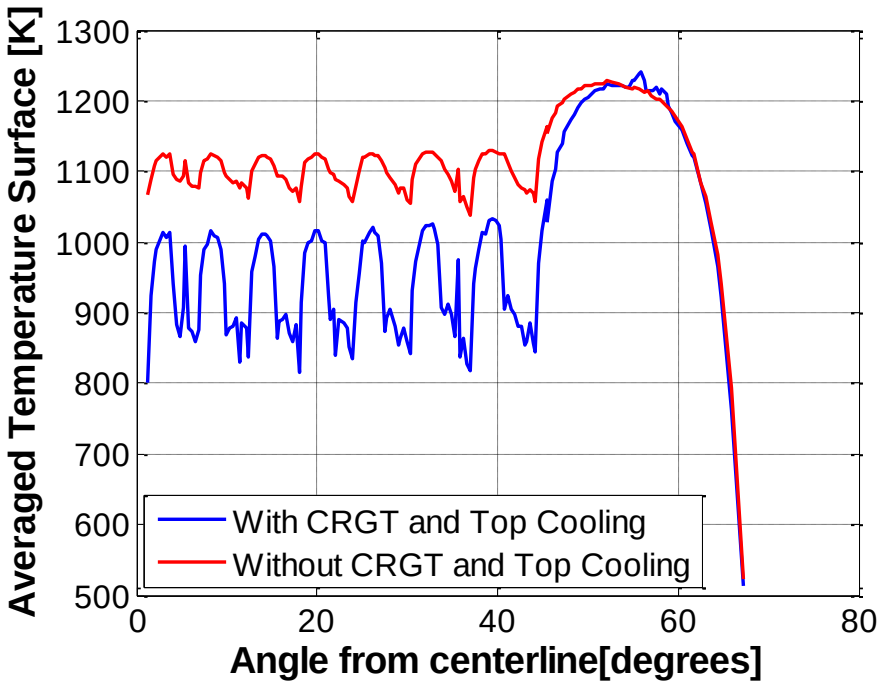

Figure 42: Temperature distribution on the vessel surface as a function of the angle from the center line at time 3.47 h. For the scenario (a) With CRGTs and top cooling (blue) and (b) Without CRGT cooling (red).

Scenarios III and IV - 0.7 m Debris bed height

In this section we present the results corresponding to the scenarios where a lower amount of the core is melted and relocated in the lower plenum, forming a debris bed of 0.7 m (around 30 tons).

Figure 43 shows the average temperature in the debris bed volume as a function of time. It can be observed how the temperature increases more slowly for both cooling scenarios in comparison with the cases with 1.9 m debris bed (Figure 38), reaching a maximum temperature of 2750 K instead of the 3500K reached with the larger debris bed in the non CRGT cooling scenario (Figure 38). Furthermore, it seems that the temperatures and melt mass fractions reach equilibrium at some point for the scenario with 0.7m and CRGTs and top cooling -blue- meaning that the balance between the internal generated heat and the evacuated through CRGT and top cooling is equalized. However it must be pointed that at that time the vessel wall will be probably failed.

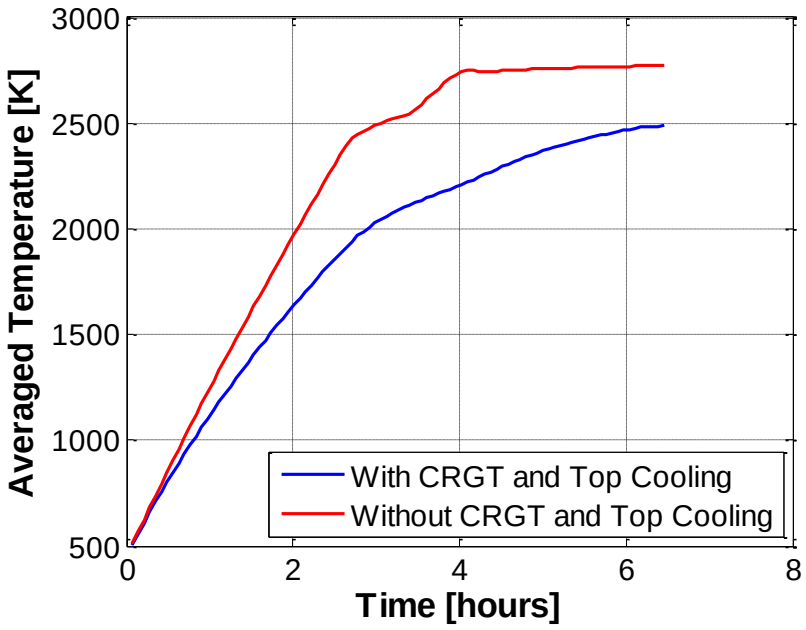

Figure 43: Average temperature in the debris bed/melt pool volume as a function of time for a 0.7 m height debris bed and two scenarios; With CRGTs and top cooling (blue) and (b) Without CRGT cooling (red).

The effectiveness of the CRGTs cooling seems to be higher in this case with lower amount of debris bed as can be observed in Figure 44. When CRGTs is implemented the melt mass fraction at 5 hours is 50% while it was more than 80% in the case with 1.9 m debris bed. The formation of the melt pool starts around 2.8 hours, for both cooling scenarios, as it also happened in the case with 1.9 m debris bed.

Figure 45 and 46 show snapshots of the melt mass fraction and temperature distribution respectively in the debris bed/melt pool at 3.61 h for scenarios (a) With CRGTs and top cooling and (b) Without CRGT cooling. For the cooling scenario (a), it can be observed the formation of unitary melt pools between the cooled CRGTs surrounded by crust layers -Figure 45(a)- as it also happened in the case with 1.9 m height debris bed -Figure 40(a)-. However, with this lower amount of relocated core there is no peripheral melt pool since all the debris bed is penetrated by the cooled CRGTs. This fact will have a key influence in the mode of failure of the vessel wall, since without thermal load in the upper part of the vessel lower head the expected type of failure will be ballooning instead of localized creep (as it happened with 1.9 m debris bed).

Finally, in the case without cooling –Figure 45(b) and 46(b) - we can observe the formation of a unique melt pool including the melted CRGTs and wrapped by a crust layer around the boundaries -blue in Figure 45 (b)-. This crust layer is thicker than the one obtained in the case with a debris bed of 1.9 m –Figure 41 (b)-. We attribute this result to the fact of having a larger cooled surface to heated volume ratio in the case with a debris bed of 0.7 m height.

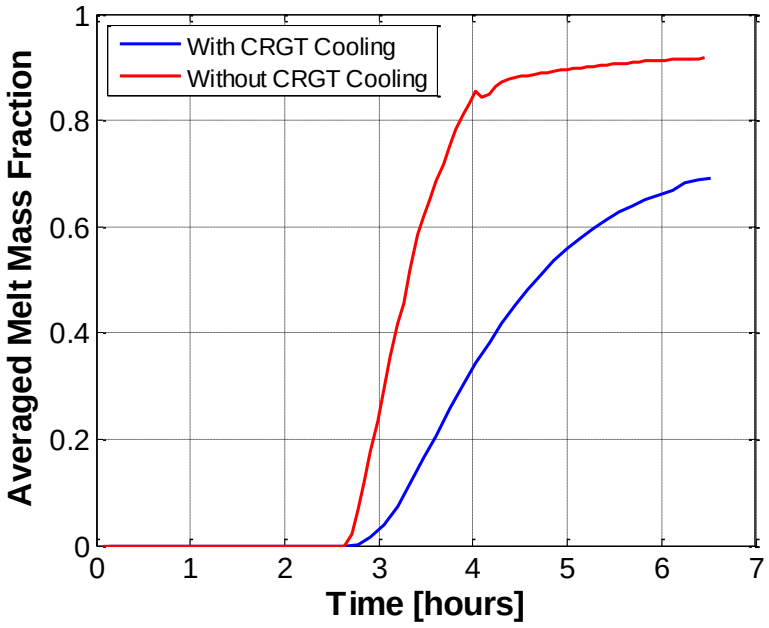

Figure 44: Average melt mass fraction in the debris bed/melt pool volume as a function of time for a 0.7 m height debris bed and two scenarios; With CRGTs and top cooling (blue) and (b) Without CRGT cooling (red).

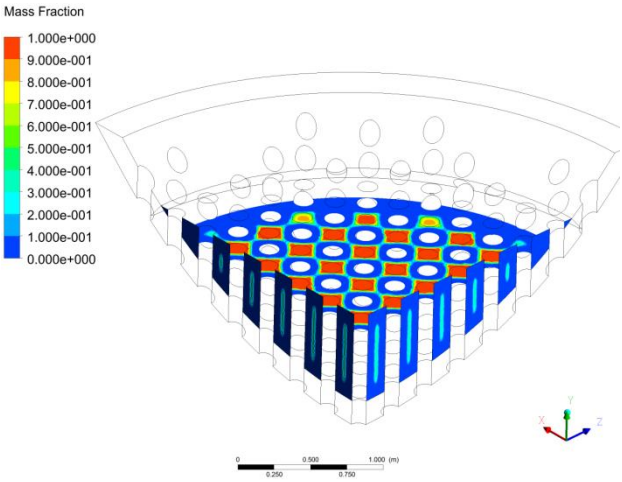

Scenario (a): With CRGTs and top Cooling. t=3.61h

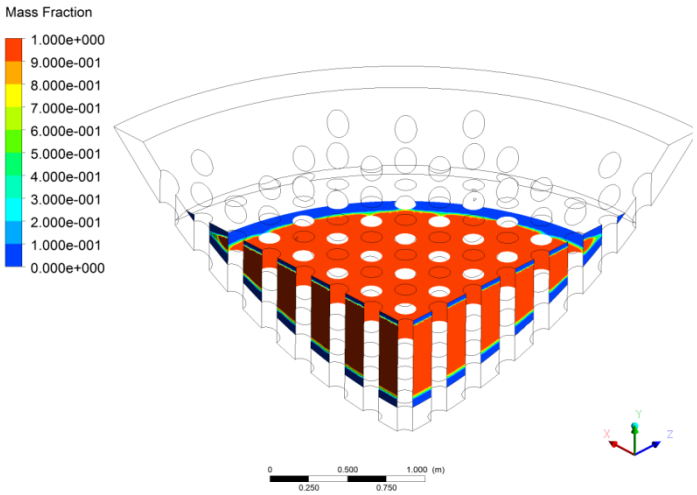

Scenario (b): Without CRGTs and top Cooling. t=3.61h

Figure 45: Snapshots the melt mass fraction in the debris bed at t=3.61 h, for the scenario of 0.7 m debris bed for (a) With CRGTs and top cooling and (b) Without CRGT cooling. In the figure blue represents solid debris, red represents molten debris.

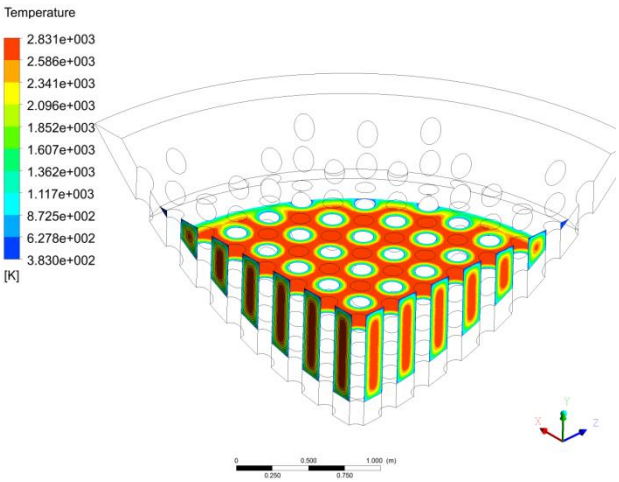

Scenario (a): With CRGTs and top Cooling. t=3.61h

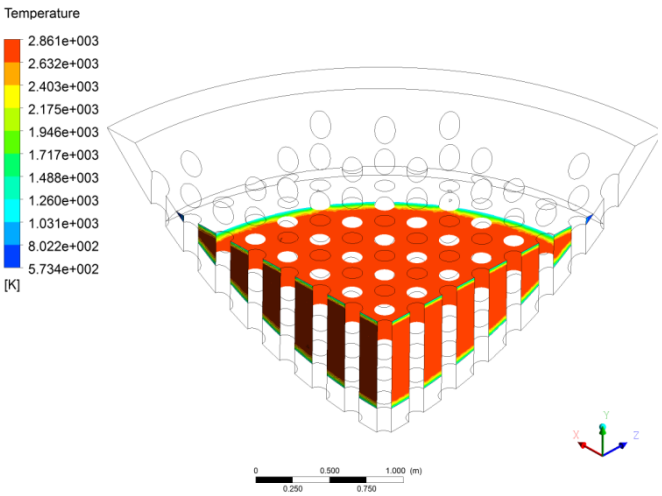

Scenario (b): Without CRGTs and top Cooling. t=3.61h

Figure 46: Snapshots of the temperature distribution in the debris bed at t=3.61 h, scenario of 0.7 m debris bed for (a) With CRGTs and top cooling and (b) Without CRGT cooling

3.2.2 Structural Creep Analysis

Scenarios (I) and (II) - Debris bed of 1.9 m height

In this section we present the results corresponding to the full transient structural creep analysis performed in ANSYS for the case of 1.9 m debris bed and for the scenarios (I) With CRGTs cooling and top cooling, and (II) Without CRGTs cooling. The results show that the timing and mode of failure may be quite different in these two scenarios, as we will explain in this section.

Figure 47 shows the creep maximum strain as a function of time for the two considered scenarios. In the plot it is possible to observe the creep behavior that is present in all the performed simulations. During the first hours the creep strain presents very low rates until a certain time when accelerated creep stage is reached. After this point the creep strain suddenly grows in a few minutes up two rates higher than 20% strain –threshold of the quantitative reliable results provided by the model- and the failure of the vessel wall is considered imminent.

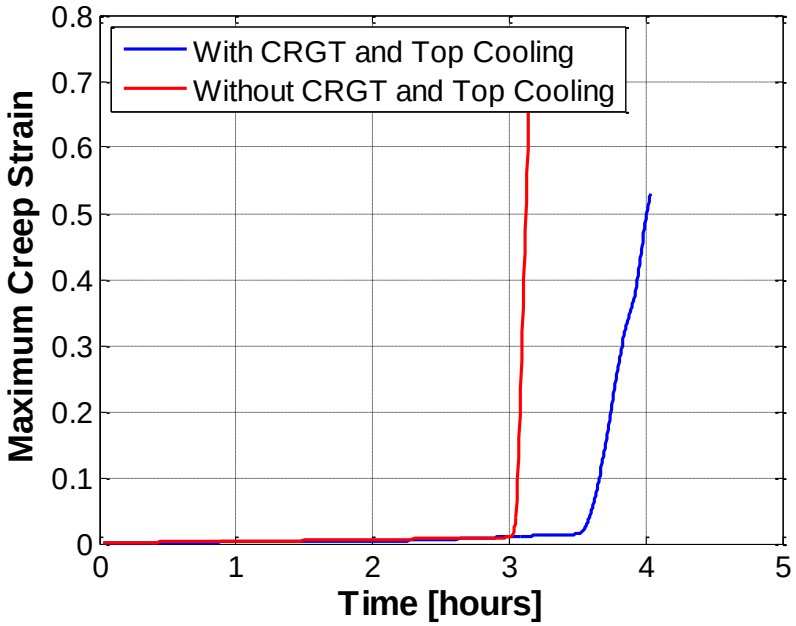

Figure 47: Maximum creep strain as a function of time for scenarios I (blue) and II (red),

As can be seen in Figure 47, accelerated creep is reached around 40 minutes earlier in the scenario without CRGTs cooling (red). In this case the accelerated creep occurs in the non-cooled CRGTs penetrations at 3.1 hours while in the cooling case the failure is produced by localized creep at the periphery of the pool at 3.75 hours.

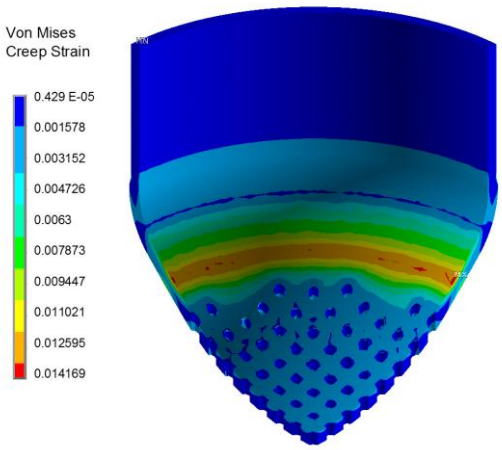

(a) **Von Mises creep strain distribution at 3.47h. Scenario (I)**

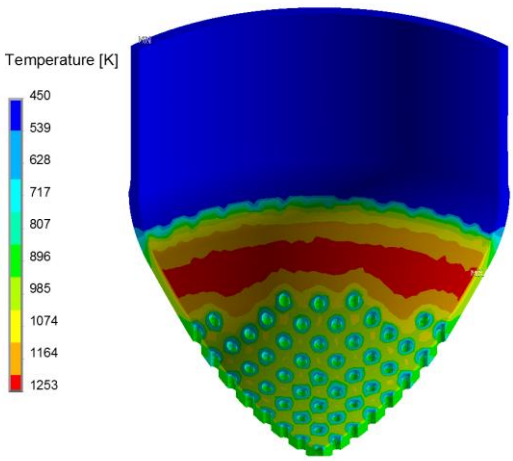

(b) Temperature distribution at 3.47h, Scenario (I)

Figure 48: Snapshot of the Von Mises creep strain (a) and Temperature (b) at t=3.47 h. For Scenario (I); 1.9m debris bed With CRGTs and top Cooling

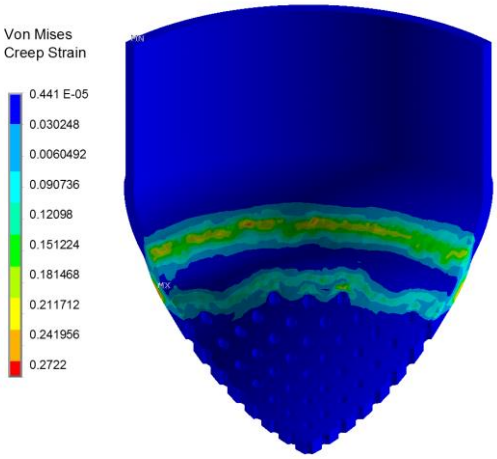

(a) Von Mises creep strain distribution at 3.75h. Scenario (I)

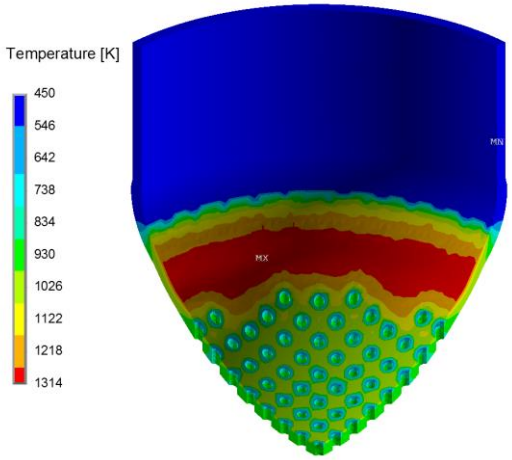

(b) Temperature distribution at 3.75h, Scenario (I)

Figure 49: Snapshot of the Von Mises creep strain (a) and Temperature (b) at t=3.75 h. For Scenario (I); 1.9 m debris bed With CRGTs and top Cooling

Figure 48 and 49 shows snapshot of the von Mises creep strain and temperature distribution at 3.47h and 3.75h respectively for the scenario when CRGTs and top cooling is implemented. The highest creep strain is reached at the periphery of the pool, where the influence of CRGT cooling is lower, leading to higher temperatures on the vessel wall surfaces (as show in Figure 42). At t=3.47 h, the maximum creep strain is only 1.4 %, which is still far from the adopted 20 % creep strain as a failure criterion. It should be said that this was the time of failure predicted by the simulations carried out previously at KTH using 2D slice structural axisymmetric model [26]. The reason of this different result is attributed to a lower thermal load to the vessel wall obtained when using slice models. Detailed comparison and discussion of these differences between the

models are provided in Appendix I. Nevertheless, in the 3D quadrant structural analysis the maximum creep strain reaches 19% at 3.75 h (Figure 49a). At this time we consider that the failure of the vessel wall is imminent. Therefore we conclude that the failure will occur around 3.75h at the periphery of the lower head vessel wall, where temperatures up to 1300 K are reached. According to the melt pool heat transfer calculations, 50 % of the debris bed is melted at this time but the wall is still covered with a crust of 5 cm. It can be expected that deformation of the vessel in the failure region and thermal loads will lead eventually to the failure of the crust and melt release. However, remaining crust can also serve as a protective refractory layer hindering intensive ablation of the wall in the vicinity of the opening.

On the other hand, for the scenario (II) Without CRGTs and top cooling, very high maximum strains are reached earlier in the CRGTs penetrations, as can be seen in Figure 50(a). This figure shows that at 3.13 hours the maximum creep strain has already reached 60% at some of the peripheral penetrations, even if the temperature at these zones is more than 200 K lower than on the wall of the periphery (Figure 50(b)). It seems that the CRGTs penetrations in the vessel wall play as concentrators of stresses, hence higher creep strain rates are reached. This fact was prevented when CRGTs cooling was implemented since the temperature at CRGTs surroundings was maintained lower than 700 K (Figure 45(b)) while the non-cooling scenario presents temperatures up to 1000K. It is interesting to observe that at this time (3.13 hours) the debris bed is still in a mushy state (maximum melt mass fraction is 0.7).

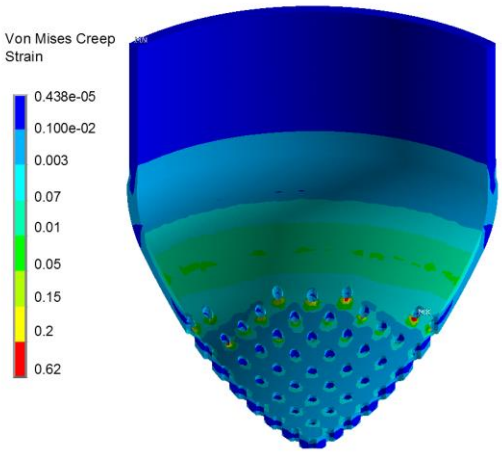

(a) Von Mises creep strain distribution at 3.13h. Scenario (II)

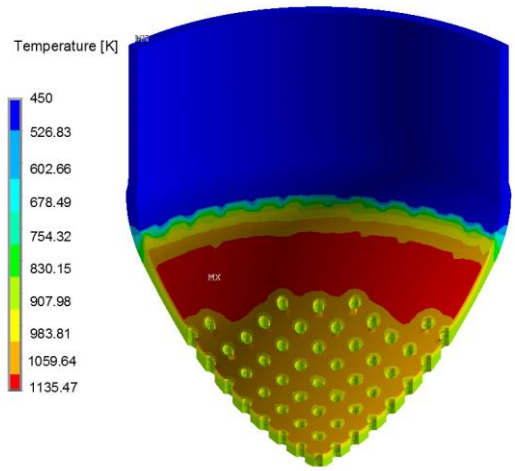

(b)Temperature distribution at 3.13h, Scenario (II)

Figure 50: Snapshot of the Von Mises creep strain (a) and Temperature (b) at t=3.47 h. For Scenario (II); 1.9 m debris bed Without CRGTs and top Cooling

This behaviour continues over the time, reaching creep strains above 20% for almost all the CRGTs penetrations as is showed in Figure 51(a). This snapshot corresponds to the creep stain solution at 3.7 hours. Very high Von Mises creep strains up to 200% are reached locally at the CRGTs penetrations surroundings, meaning that the vessel wall has no structural consistency

anymore in these local regions and failure is expected through them. High creep strains are also reached at the vicinity of the top periphery –Figure 51(a)- as it happened with the cooling scenario (I). For this reason, localized creep failure at the top periphery is also expected in scenario (II) from 3.7 h.

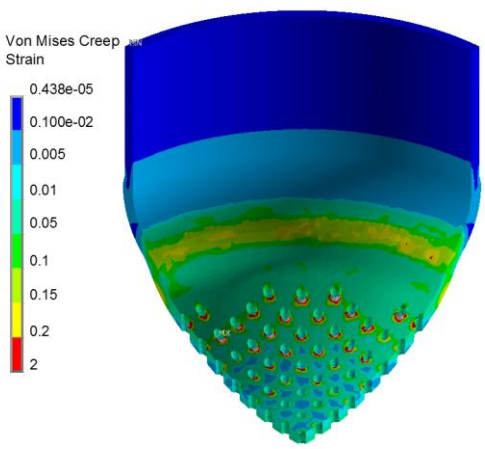

(a) Von Mises creep strain distribution at 3.7h. Scenario (II)

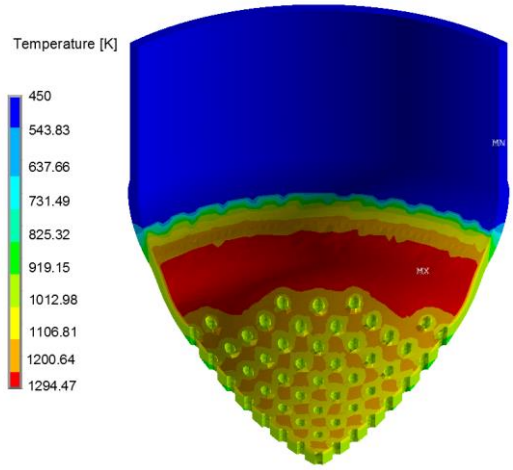

(b) Temperature distribution at 3.7h, Scenario (II)

Figure 51: Snapshot of the Von Mises creep strain (a) and Temperature (b) at t=3.7 h. For Scenario (II); 1.9 m debris bed Without CRGTs and top Cooling

Scenario (III) and (IV) Debris bed of 0.7 m height

In this section we present the results corresponding to the case of 0.7 m debris bed and for the scenarios; (III) With CRGTs and top cooling, and (IV) Without CRGTs cooling.

Figure 52 shows snapshot of the von Mises creep strain (a) and temperature distribution (b) at 4.7h. At this time 20% creep strain is reached at the vessel of the wall, thus we consider that the failure of the vessel wall is imminent. We identify this type of failure as "Ballooning mode", due to the mode of deformation, which is consistent with the results previously obtained using 2D axisymmetric models [26]. However, the failure is expected to happen earlier according to our 3D quadrant model -at 4.7 hours- compared to the results of the 2D structural models (failure was predicted at 4.9 hours as can be seen in Table 1). A possible reason of this difference could be vessel wall weakening due to the CRGTs penetrations (not resolved in the 2D structural models). It is interesting to note that the maximum creep strains are reached at the bottom of the vessel instead of at the periphery as occurs in the case with 1.9 m debris bed. This happens as a result of not having thermal load in the non-penetrated periphery region, since the size of the melt pool is

smaller. Besides, the failure occurs around 1 hour later than in the case with 1.9 m debris bed as a consequence of the lower weight load and thermal load to the wall.

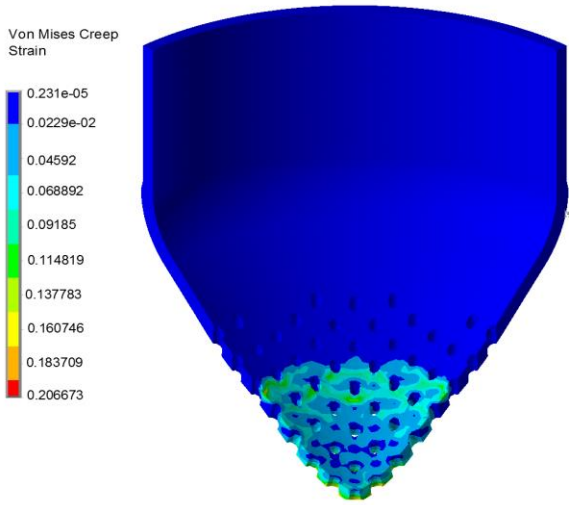

(a) **Von Mises creep strain distribution at 4.7. Scenario (III)**

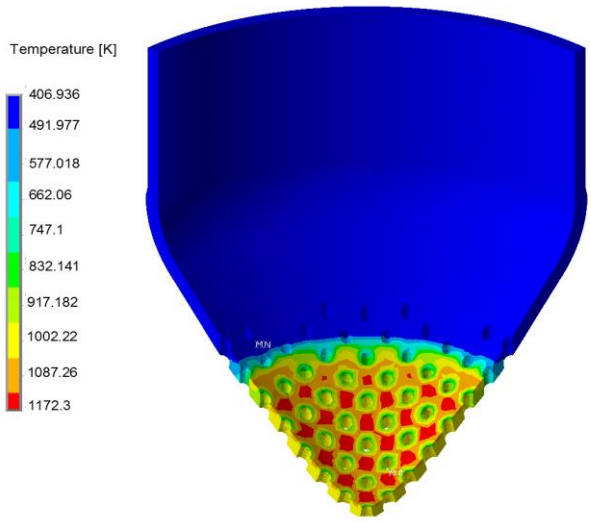

(b) Temperature distribution at 4.7h, Scenario (III)

Figure 52: Snapshot of the Von Mises creep strain (a) and Temperature (b) at t=4.7 h. For Scenario (III); 0.7 m debris bed With CRGTs and top Cooling.

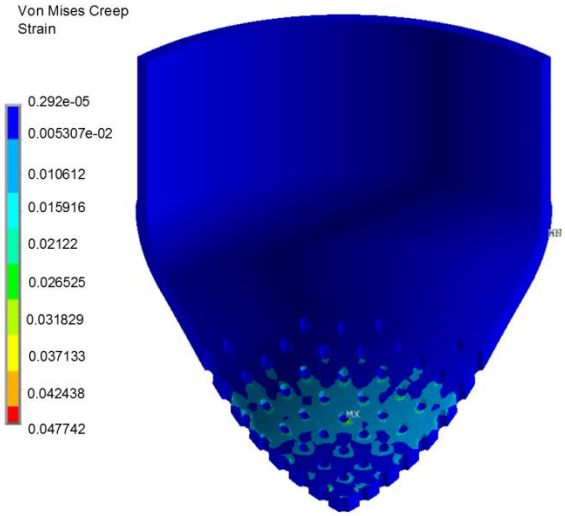

(a) **Von Mises creep strain distribution at 3.32 Scenario (IV)**

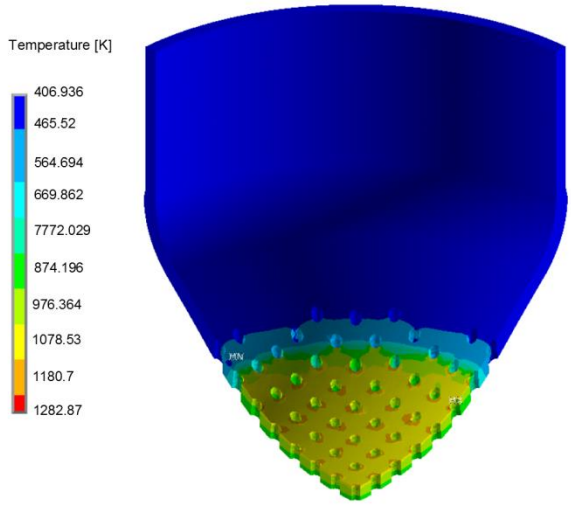

(b) Temperature distribution at 3.32h, Scenario (IV)

Figure 53: Snapshot of the Von Mises creep strain (a) and Temperature (b) at t=3.3 h. For Scenario (IV); 0.7 m debris bed Without CRGTs and top Cooling.

Lastly, we show in Figure 53 a snapshot of the von Mises creep strain (a) and temperature distribution (b) at 3.32 h for the scenario (IV); 0.7 m height debris bed without CRGTs cooling. The deformation trend is consistent with the one of scenario (III), that is, ballooning mode. However, it can be observed that the maximum creep strain takes place at the non-cooled CRGTs penetrations, as it occurred in scenario (II), where the highest temperatures (up to 1300K) are reached. Thus earlier failure though the non-cooled CRGTs penetrations than global wall failure is also expected in this scenario. It should be said that in this case the failure through the penetrations is expected later than in scenario (II) due to the lower weight load and the absence thermal load in the peripheral penetrations -where high creep strains were reached earlier with the 1.9 m debris bed, as can be seen in Figure 47.

Summary of the Vessel Wall Failure and Melt Ejection Mode

Finally, we provide in this section a short summary and comparison of the results obtained in the four scenarios studied in the second part of the work. Figure 54 shows snapshots of the Von Mises creep strain and displacement of the wall structures at representative times (close to of failure) for the four mentioned scenarios. Note that the time and mode of failure differs from the studied cases. Three modes of failure were identified; localized creep failure -Scenario (I)-, ballooning type failure –Scenario (III)- and failure through creep at the multiple CRGTs penetrations –Scenarios (II) and (IV)-, when CRGTs cooling is not supplied.

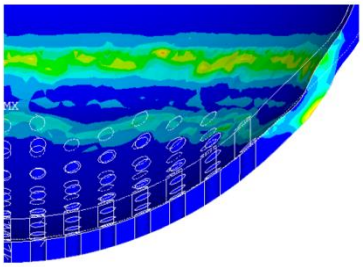

Scenario (I) at 3.75 hours. Failure through "localized creep" at the top periphery of the vessel wall.

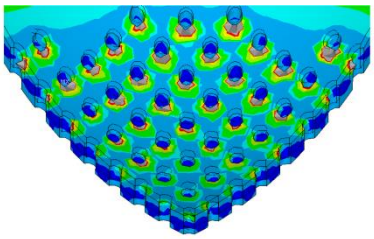

Scenario (II) at 3.6 hours. Possible failure by accelerated creep at the CRGTs penetrations

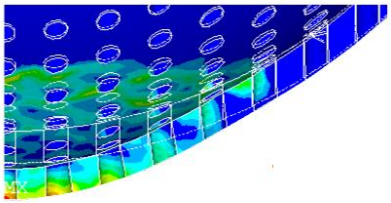

Scenario (II) at 4.7 hours. Failure through the vessel wall by "ballooning" of the vessel bottom.

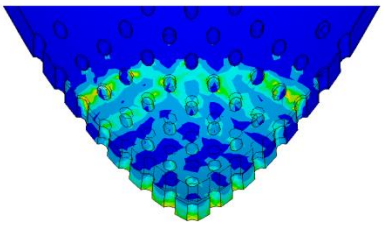

Scenario (IV) at 3.83 hours. Possible failure by accelerated creep at the CRGTs penetrations

Figure 54: Snapshots of the Von Mises creep strain and displacements for the scenarios considered in the present work at the respective times close to failure. Three different modes of failure have been identify; (i) "Localized creep" in Scenario (I), (ii) "Balloning" in scenario (III), and (iii) failure by creep at the CRGTs penetrations in Scenatios (II) and (IV).

The time of failure varies from 3.13 h for the scenario (II); 1.9 m debris bed without CRGTs cooling to 4.64 h for the scenario (III) 0.7 debris bed with CRGTs cooling. It should be noted that, despite the possible early failure through the CRGTs penetrations in scenarios (II) and (IV), later failure through "localized creep" and "ballooning mode" is also respectively expected, since the deformation of the global vessel is mainly determined by the amount of relocated debris bed. This can be seen in Figure 55, where the vertical displacement of the bottom of the vessel as a function of time is showed. The plot shows when accelerated creep is reached in the vessel wall, leading to a sudden vertical displacement of the bottom of the vessel. Scenarios corresponding to 1.9 m height debris bed –red and blue- follow the same displacement trend, while in the scenarios with smaller debris bed the ballooning failure occurs later.

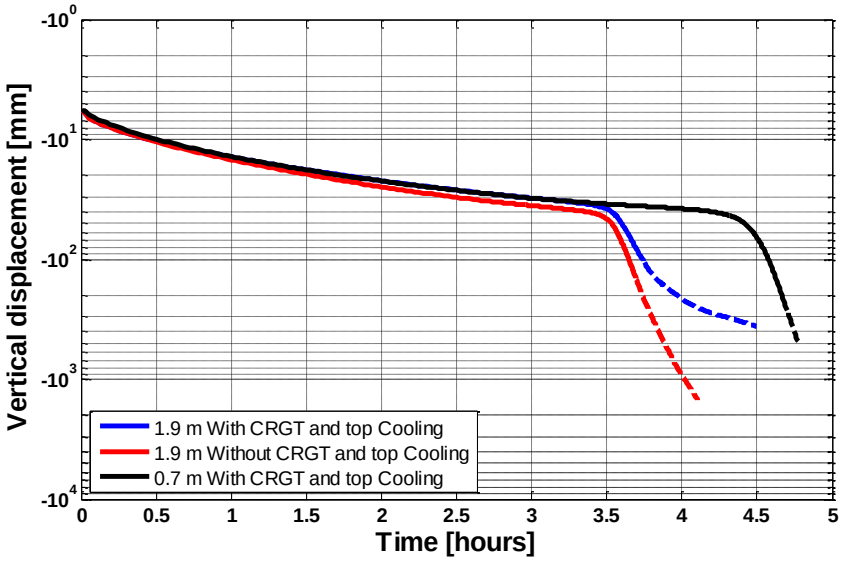

Figure 55: Vertical dislpacement of the bottom of the vessel as a function of time for the scenarios considered in the present work. The solid lines represent the reliable predicted region by the creep model (below 20% creep strain) while the dashed line results are reliable only in a qualitative way

Finally, Table 10 shows a summary of the debris bed conditions close to the times of failure predicted by the quadrant models in the present work. It is interesting to compare Table 1 with Table 1, which showed the results obtained in previous calculations using slide models. The results mainly differ in the scenarios corresponding to the cases where CRGTs cooling is not supplied, as the early creep failure through the CRGTs penetrations due to stress concentration could not be predicted by the 2D slice models.

Regarding the influence of the amount of debris relocated in the lower plenum on the time of failure, it is interesting to observe that despite the much lower amount of debris corresponding the 0.7 m scenario -15% of the one located in the scenario with 1.9m- the failure of the vessel is expected to happen less than one hour later. That means that failure of the vessel will occur even without large amounts of the core relocated in the lower plenum. Nevertheless the amount of

available melt for being released is evidently much lower –order of 10 times lower- for the scenarios with lower debris bed.

Table 10: : Summary of time and mode of vessel wall failure as well as the state of the melt pool at this time for the different scenarios studied in the present work.

Scenario	Debris Bed Height (mass) [m] [tons]	CRGTs Cooling	Time at max ~20 % creep strain, t_1 [h]	Mode of Creep Failure	Amount of liquid melt at t_1 (and after 30 min) [ton]	Average melt superheat at t_2 (and after 30 min) [K]
(I)	1.9	Yes	3.75	**Localized creep**	100 (140)	60 (125)
(II)	1.9	No	3.13	**Through CRGTs penetrations**	90-mushy melt-(175)	40 (100)
(III)	0.7	Yes	4.64	**ballooning**	16 (19)	33 (177)
(IV)	0.7	No	*	*	*	*

*The computational simulation is in progress.

Concerning the effectiveness of CRGTs cooling, it is clear the implementation of this strategy delays the failure of the vessel wall -30 min for 1.9 m debris bed and for 0.7 debris bed- as well as prevents the failure through the CRGTs vessel penetrations. However the global failure of the vessel is not avoided. Furthermore, the later the failure occurs, the larger amount of melt and superheated temperatures available for being released (as can be seen in Table 10), which is unfavorable for the point of view of ex-vessel coolability. Thus is not completely clear that the implementation of CRGTs will be always favorable from the point of view the ex-vessel retention strategy –at least for the considered scenarios-. This issue illustrates the complexity of the severe accident and the difficulties of the decision making in such scenarios.

4 Conclusions

In the present work a hypothetical core melting severe accident in a Nordic BWR is considered. The molten core materials are assumed to be relocated in the lower head of the reactor and quenched in the water remaining in the lower plenum. An internally heated non-coolable debris bed reheats and re-melts eventually leading to formation of a melt pool. The debris bed/melt pool inflicts thermal and mechanical loads to the vessel wall and penetrations, which will eventually lead to the vessel failure and melt ejection to the reactor cavity. The melt jet characteristics and consequently the mode and timing of vessel failure will define the subsequent accident progression, determining the success of the ex-vessel melt retention strategy.

Analysis of the in-vessel scenarios of severe accident progression was done, identifying two main modes of vessel failure: (i) Failure due to IGT ejection, and (ii) Failure of the vessel wall due to creep. 3D thermo-mechanical calculations taking into account the vessel penetrations were performed in order to reduce the uncertainties and predict the timing and characteristics of these failure modes.

The work was therefore divided in two parts; (i) Study of IGT failure and (ii) Study of the vessel wall failure using 3D quadrant geometries with penetrations. The mode of failure depends on the accident scenario. E.g. among other factors, it depends on the amount of melt relocated in the lower head or implemented SAM strategy (CRGTs cooling, activation of ECCS systems, etc.). Therefore, several scenarios were considered in the calculations in terms of amount of debris bed relocated in the lower head (200 tons or 30 tons) and CRGTs cooling along with cooling of the melt from the top implemented as SAM strategy, with the aim to investigate the influence of these factors on the mode of failure.

Concerning the study of the IGTs failure - Task (I) of the present work - the PECM was implemented in a unitary volume of the debris bed including one IGT and four CRGTs assuming 1.9 m debris bed depth. The IGT welding failure is predicted to happen between 1h and 1.85 h after the debris bed dry out. No significant difference in timing of failure was observed between the scenarios with and without CRGTs and top cooling implemented. This result was attributed to the low thermal conductivity of the solid debris bed which avoids the efficient heat evacuation through the cooled CRGTs during the first hours of the transient. Furthermore, the IGTs melting was predicted between 1.6h and 1.8 h, also for both scenarios with/without CRGTs and top cooling, meaning that the in-vessel part of IGT is already melted at time of potential tube ejection due to the nozzle weld melting. Melt down of the in-vessel part of the CRGTs is expected to happen between 1.85 h and 2.2 h if CRGTs cooling is not implemented while it is prevented in the scenario with cooling. In addition, the temperature distribution along the debris bed in the unitary volume was investigated for development of future experimental studies of the IGT ejection.

The possibility of clamping of the IGT in the flow limiter due to the global deformation of the vessel was studied using local structural models of the penetrations' housing. We found that clamping of the farthest IGTs from the bottom center of the vessel occurs, preventing its ejection, while it does not occur for the closest to the bottom IGT. Thus we conclude that ejection of the IGT closest to the center will probably occur at sometime between 1h and 1.9 hours after the debris bed dry out, which is more than 1.5 hours earlier than global vessel failure. It is instructive to note that at this time the debris bed is still in solid state (no liquid melt yet), hence it is possible that the melt will leak out gradually while debris bed is progressively re-melted. This would be favorable from the point of view of the ex-vessel retention, as the melt release will take place by small non-superheated melt jets, which can be quenched and cooled easily in the reactor cavity with small risk of steam explosion. However, it also not excluded that solid debris and slowly dripping melt will plug the 6.5 cm diameter opening leading to accumulation of large amount of melt in the vessel, followed by massive melt release through a large opening. With massive release and a large size jet both formation of non-coolable cake debris and energetic steam explosion are quite possible. Thus for further reduction of the uncertainty investigation of the phenomena relevant to the melt release through IGT nozzle is important.

In the Tasks (II) of the present work coupled 3D thermo-mechanical analyses using a 3D quadrant model of the lower head of the geometry were performed. The aim of these studies was to resolve the debris bed heat transfer transient and the structural creep analysis of the realistic vessel lower head geometry with penetrations. This study consists of two parts. (I) The results obtained with 3D quadrant model were compared with the results obtained with the slice model previously used in the scenario of 1.9 m depth (200 tons) debris bed with CRGTs and top cooling. This study is included in Appendix I (conference paper "Coupled 3D Thermo-mechanical analysis of a Nordic BWR vessel failure and timing"). (II) Analysis of debris bed heat transfer transient and vessel wall creep failure were performed for the stated four different scenarios; 200 tons or 30 tons relocated in the lower plenum and CRGTs or no CRGTs cooling implemented as SAM strategy.

From the comparison (Appendix I) we found that the results obtained with the 3D quadrant and slice models are qualitatively consistent. Although, the former shows slightly higher melt mass fractions and temperatures in the debris bed volume and slightly lower average thermal load to the vessel wall. This difference was attributed to the fact that 3D quadrant geometry differs from the slice by (i) smaller ratio of cooled (CRGT and top) surfaces to heated debris volume, (ii) larger ratio of vessel cooled to heated debris volume, and (iii) non-axisymmetric distribution of the CRGTs. The slightly lower thermal load to the vessel wall in the 3D quadrant results in a 15 min delay compared to the 2D structural slice model. Nevertheless the mode of failure predicted for this scenario by the 3D quadrant model and 2D slice structural model was the same, localized creep in the vicinity of the top periphery of the pool.

From the comparison between the four scenarios studied using the 3D quadrant models three possible modes of vessel wall failure were identified: (i) failure through localized creep at the

vicinity of the top periphery of the melt pool, (ii) ballooning type of failure of the vessel bottom, and (iii) possible failure by creep through the CRGTs penetrations.

For the scenario (I) with 1.9 m (200 tons) debris bed height and CRGT and top cooling, the failure is expected to occur starting from 3.75 h after the dryout. The failure mode is accelerated creep of the vessel wall in the vicinity of the top periphery of the melt pool, where thermal and mechanical load from the debris bed are larger. In the scenario (II) with same amount of debris (200t tons) but without CRGTs and top cooling, it was found that accelerated creep may happen at the non-cooled CRGTs penetrations more than 30 min earlier compared to the cooling case, starting from 3.1 h after debris bed dryout. Analysis of results suggests that the CRGTs penetration act as stress concentrators in the vessel wall leading to high local strain in their vicinity. This mode of failure was not possible to predict by the 2D structural models. Accelerated creep at the CRGTs penetrations is prevented if CRGTs cooling is implemented since the temperature at the penetrations surroundings is maintained at much lower level. Although there is a possible earlier failure through the CRGTs penetrations with the non-cooling case, the global deformation of the vessel wall follows the same trend for both cooling and non-cooling cases and later creep failure at the vessel wall in the vicinity of the top periphery of the melt pool is also expected with the non-cooling case.

For the scenarios with smaller amount of debris bed 0.7m (30 tons) with cooling (III) and without cooling (IV), the calculations suggest that vessel failure can occur starting from 4.64 hours. The deformation trend of the vessel indicates ballooning type of failure, reaching large deformation rates and accelerated creep at the bottom part of the vessel wall. In the non-cooling case, the possible failure through the non-cooled CRGTs penetrations due to accelerated creep was also observed as in the case with 1.9 m debris bed without cooling.

Apparently the consequences of identified modes of vessel failure in terms of size of the breach, amount of melt which can be released at once and melt superheat will be different.

For the cases where CRGTs and top cooling of the debris bed was implemented it is instructive to note the presence of small melt pools between the cooled CRGTs separated from each other by the crust. Such spatial configuration of the melt and crust reduces amount of liquid melt which is available for release given certain failure location. Location of the vessel wall failure in case of large (200 tons) debris bed is quite high which also can limit amount of liquid melt available for ejection. Moreover it was found that at the time of vessel wall failure the wall is still covered with a crust layer which may have also an influence on the mode of melt release.

Further investigations will be needed to clarify the effect of (i) mentioned above phenomena, (ii) more realistic properties of the debris bed (heterogeneous mixture of oxidic and metallic debris, spatial distribution of the debris bed, etc.), (iii) coolability of the porous debris bed, (iv) chemical reactions (e.g. oxidation of metallic melt) etc. on mode and timing of melt ejection from the vessel.

5 Bibliography

[1] International Atomic Energy Agency -IAEA-.

[2] Swedish Radiation Safety Authority (SSM), "Forskning 2012:12 APRI-7 Risk Importance. En lägesrapport om forskningen inom området svåra haverier under åren 2009-2011," 2012.

[3] P. Kudinov and M.V. Davydov, "Development and validation of conservative-mechanistic and best estimate approaches to quantifying mass fractions of agglomerated debris," *Nuclear Engineering and Design,* 2013.

[4] P. Kudinov, A. Karbojian, C.-T. Tran, and W. Villanueva, "Experimental Data on Fraction of Agglomerated Debris Obtained in the DEFOR-A Melt-Coolant Interaction Tests with High Melting Temperature Simulant Materials," *Submitted to Nuclear Engineering and Design,* 2013.

[5] P. Kudinov, A. Karbojian, C.-T. Tran, and W. Villanueva, "The DEFOR-A Experiment on Fraction of Agglomerated Debris as a Function of Water Pool Depth," in *Proceedings of The 8th International Topical Meeting on Nuclear Thermal-Hydraulics, Operation and Safety (NUTHOS-8),* Shanghai, China, October 10-14 2010.

[6] P. Kudinov and M. Davydov, "Development and Validation of the Approach to Prediction of Mass Fraction of Agglomerated Debris," in *Proceedings of The 8th International Topical Meeting on Nuclear Thermal-Hydraulics, Operation and Safety,NUTHOS-8*, Shanghai, China, October 10-14 2010.

[7] S. Yakush, P. Kudinov, and T.-N. Dinh, "Multiscale Simulations of Self-organization Phenomena in the Formation and Coolability of Corium Debris Bed," in *Proceedings The 13th International Topical Meeting on Nuclear Reactor Thermal Hydraulics (NURETH-13), Paper N13P1143, .* Kanazawa City, Ishikawa Prefecture, Japan, September 27-October 2, 2009,..

[8] S. Yakush and P. Kudinov, "Effects of Water Pool Subcooling on the Debris Bed Spreading by Coolant Flow," in *Proceedings of ICAPP 2011, Paper 11416*, Nice, France, May 2-5 2011.

[9] B. Pershagen, Light Water Reactor Safety, Nyköping: Pergamon Press, 1989.

[10] W. Villanueva, C. T. Tran and P. Kudinov, "Effect of CRGT cooling on modes of global vessel failure of a BWR lower head," in *Proceedings of the 20th International Conference on Nuclear Engineering ICONE20*, Anaheim, CA, USA, August 2012.

[11] C-T Tran, T.N. Dinh, "The effective convectivity model for simulation of melt pool heat transfer in light water reactors pressure vessel lower head, Part II: Model assessment and application," *Progress in Nuclear Energy*, vol. 51, pp. 860-871, 2009.

[12] B.R Seghal, Nuclear Safety in Light Water Reactors: Severe Accident Phenomenology, Ed. Elsevier Inc. , 2012.

[13] R.O. Gauntt, J.E. Cash, R.K. Cole, C.M. Erickson, L.L. Humphries, S.B. Rodriguez and M.F. Young, "Melcor Computer Code Manual, Core (Cor)Package Reference Manuals,," NUREG/CR-6119, 2005.

[14] Chi Thanh Tran, The Effective Convectivity Model for Simulation and Analysis of Melt Pool Heat Transfer in a Light Water Reactor Pressure Vessel Lower Head, Doctoral Thesis in Energy Technology, Stockholm, Sweden, 2009.

[15] R.O. Gauntt, L.L. Humphries, "Final Results of the XR2-1 BWR Metallic Melt Relocation," Sandia National Laboratories Albuquerque NUREG/CR-6527, August 1997.

[16] E.L. Tolman, P. Kuan and J.M. Broughton, "TMI-2 Accident Scenario Update," *Nuclear Engineering and Design*, vol. 108, pp. 45-54, 1998.

[17] A. Karbojian, W.M. Ma, P. Kudinov, T.N. Dinh, "A Scoping Study of Debris Bed Formation in the DEFOR Test facility," *Nuclear Engineering and Design*, 2009.

[18] S.A. Hodge, "BWR Reactor Vessel Bottom Head Failure Modes," in *CONF-890546-3*, Dubronvik, Yugoslavia, December 1989.

[19] B.R. Sehgal, "Stabilization and Termination of Severe Accidents in LWRs," *Nuclear Engineering and Design*, vol. 236, pp. 1941-1952, 2006.

[20] T.G. Theofanous, C. Liu, S. Addition, S. Angelini, O. Kymalainen, T. salmassi, "In-vessel Coolability and Retention of a Core Melt," October 1996.

[21] C-T Tran and T.N. Dinh, "The effective convectivity model for simulation of melt pool heat transfer in light water reactors pressure vessel lower head, Part I: Physical processes, modeling and model implementation," *Progress in Nuclear Energy*, vol. 51, pp. 849-859, 2009.

[22] J. L. Rempe, S. A. Chavez, G. l. Thinnes C. M. Allison, G.E. Korth, R. J. Witt, J. J. Sienicki, S. K. Wang, L. A. Stickler, C. H. Heath and S. D. Snow, "Light Water Reactor Lower Head Failure," NUREG/CR-5642, Idaho Falls, 1993.

[23] W. Villanueva, C.T. Tran, and P. Kudinov, "A Computational study on instrumentation guide tube failure during a severe accident in boiling water reactors," in *The 14th International Topical Meeting on Nuclear Reactor Thermal Hydraulics, NURETH-14*, Toronto, Ontario, Canada, September 25-29, 2011. .

[24] B.R. Sehgal, A. Theerthan, A. Giri, A. Karbojian, H.G Willschütz, O. Kymäläinen, S. Vandroux, J.M. Bonnet, J. M Seiler, K. Ikkonen, R. Sairanen, S. Bhandari, M. Bürger, M. Buck, W. Widmann, J. Dienstbier, Z. Techy, R. Taubner, T.G. Theofanous,T.N. Dinh, "Assesment of reactor vessel integrity (ARVI)," *Nuclear Engineering and Design*, vol. 221, pp. 23-53, 2013.

[25] H.G. Willschütz, E. Altstadt, B.R. Segha andl F.P. Weiss, "Coupled thermal structural analysis of LWR vessel creep failure experiments," *Nuclear Engineering and Designs*, vol. 208, pp. 265-282, 2001.

[26] W. Villanueva, C.-T Tran, and P. Kudinov, "Coupled thermo-mechanical creep analysis for boiling water reactor pressure vessel lower head," *Nuclear Engineering and Design*, vol. 249, pp. 146-153, 2012.

[27] W. Villanueva, C. T. Tran and P. Kudinov, "Assessment with coupled thermo-mechanical creep analysis of combined CRGT and external vessel cooling efficiency for a BWR," in *The 14th International Topical Meeting on Nuclear Reactor Thermal Hydraulics, (NURETH-14)*, Toronto, Ontario, Canada, September 2011.

[28] http://www.fluent.com/.

[29] http://ansys.com/.

[30] V.A. Bui, T.N. Dinh, "Modeling of heat tranfer in heated-generating liquid pools by an effective diffusivity-convectivity approach," in *2nd European Thermal-Science Conference pp. 1365-1372*, Rome, Italy, 1996.

[31] U. Steinberner and H. H. Reineke, "Turbulent buoyancy convection heat transfer with internal heat sources," in *Proceedings of the 6th International Heat Transfer Conference, 2, 305-310*, Toronto, Canada,, 1978.

[32] C-T Tran, W. Villanueva, P. Kudinov, "A Study on the Integral Effect of Corium Material Property Melt Pool Heat Transfer in a Boiling Water Reactor," in *The 9th International*

Topical Meeting on Nuclear Thermal-Hydraulics, Operation and Safety (NUTHOS-9) N9P0289, Kaohsiung, Taiwan, September 2012.

[33] Konstantin Naumenkko, Holm Altenbach, Modeling of Creep for Structural Analysis, Springer, 2007.

[34] O. Kymäläinen, H. Tuomisto, T.G. Theofanous, "In-Vessel Retention of Corium at the Loviisa Plant," *Nuclear Engineering and Design* , vol. 169, pp. 109-130, 1997.

[35] http://www.solidedgeu.com/.

Appendix I

COUPLED 3D THERMO-MECHANICAL ANALYSIS OF A NORDIC BWR VESSEL FAILURE AND TIMING

Claudio Torregrosa[1], Walter Villanueva[1], Chi-Thanh Tran[2], and Pavel Kudinov[1]
[1]Division of Nuclear Power Safety, Royal Institute of Technology (KTH), Stockholm, Sweden
[2]Vietnam Atomic Energy Institute (VINATOM), Hanoi, Vietnam
Emails: cltm@kth.se, walter@safety.sci.kth.se, thanh@safety.sci.kth.se, and pavel@safety.sci.kth.se

ABSTRACT

An in-vessel stage of a severe core melting accident is considered in a Nordic-type Boiling Water Reactor (BWR). The decay heated debris bed that is formed in the lower head of the reactor vessel after core degradation and relocation inflicts thermal and mechanical loads which induce creep. Mode and timing of the vessel failure determine melt ejection mode and ex-vessel accident progression. Cooled from inside Control Rod Guide Tubes (CRGTs) are considered as possible element in severe accident management strategy. In this work the debris bed heat-up, melt pool formation, and heat transfer to the vessel wall are simulated by the Phase-change Effective Convectivity Model (PECM). A coupled thermo-mechanical creep analysis is carried out with ANSYS code where transient heat transfer characteristics are used as boundary conditions. The focus of the present study is on comparison of the results obtained with (i) PECM in 3D slice model of the debris bed coupled with ANSYS 2D axisymmetric vessel wall model, and (ii) PECM in 3D quadrant model of the bed coupled with ANSYS 3D quadrant model of the vessel. The most important questions are (i) how actual 3D geometry with non-axisymmetric distribution of CRGTs can affect melt pool heat transfer; (ii) how penetrations in the vessel wall (resolved in 3D quadrant model) can affect creep characteristics and eventually timing of failure. Based on the results of the analysis, we can conclude that the melt mass fraction and averaged temperatures provided by the 3D quadrant model are consistent with previously obtained results using 3D slice geometry models. Although, the former shows slightly higher melt mass fractions and temperatures. The thermo-mechanical creep analysis also shows that results of 2D and 3D models are consistent, however later timing of the vessel is obtained in the 3D model compared to the 2D model. The differences are attributed to the fact that the 3D quadrant geometry differs from the slice by (i) ratios of vessel wall surface and cooled surface (CRGT and top) to the debris volume and (ii) non-axisymmetric positions of the CRGTs.

1. INTRODUCTION

In case of severe core-melt accident in a nuclear reactor, the core is assumed to melt down due to lack of cooling. The debris of decay-heated core relocates to the bottom of the vessel. The debris is quenched in the water pool located in the lower head, and then is reheated and re-melted again. At this point, a pool of corium melt is formed in the lower head of the vessel, inflicting thermal

and mechanical loads to the vessel penetrations and walls which eventually can lead to failure of the vessel and melt ejection.

Ex-vessel melt coolability is proposed as a means to terminate progression of a severe accident in Nordic BWRs. The success of this strategy depends strongly on the melt ejection characteristics which determine formation and coolability of a debris bed in the flooded cavity [1], [2], [3], [4], [5], [6], [7]. A non-coolable debris will be reheated, re-melted, and will attack the containment basemat, threatening the containment integrity. Besides, there is a risk of energetic molten fuel-coolant interactions (steam explosion), e.g., if the melt jet size and superheat are large. Thus ex-vessel accident progression depends on the melt release mode which is determined by the mode and timing of vessel failure. Therefore it is important to quantify and reduce the uncertainties of in-vessel accident progression and vessel failure modes.

Rempe et al. [8] have classified the possible modes of vessel failure in two main groups, (i) vessel wall failure, and (ii) vessel penetrations failure through the Instrumentation Guide Tube (IGT), drain line, or Control Rod Guide Tube (CRGT). The vessel wall failure is expected to happen due to creep acceleration caused by high temperature load on the internal vessel surface from decay heat generating melt pool. In the previous study [9] we have analyzed such failure mode and timing and their dependence on the melt pool depth. Two main modes of vessel wall failure were identified, a ballooning and a localized creep. These studies were performed using a 2-D structural analysis of the RPV, with the thermal load boundary conditions obtained from the PECM 3D-slice model of the melt pool (Figure 1b). Vessel wall failure due to creep was predicted to happen around 3.5 h after formation of dry debris bed of 1.9 m height (~200 tons). Cooling through CRGTs was taken into account in the analysis. The accelerated creep was reached at the periphery of the melt pool where the vessel is not penetrated by cooled CRGTs.

Multiple penetrations (IGT and CRGT) in a BWR vessel can fail under thermal load from the debris. In Nordic BWRs the welding of the IGT and CRGT to the penetration nozzle is located deep inside the bed. When the welding fails, the tubes can be ejected out of the vessel. However there is a possibility of IGT clamping inside the vessel wall due to the global deformation of the vessel. Such clamping can possibly prevent ejection of IGT and therefore delay or prevent this mode of vessel failure. In order to clarify this hypothesis, previous studies [10] have been performed considering 3D unit volume structural models of an IGT section. We found that the failure of the closest IGT to the centre of the vessel is one of the dominating vessel failure modes, while there is a chance that the farthest IGT can be clamped. However these results were obtained by applying boundary conditions from the 3D slice-geometry models and 2D axisymmetric structural models to the unit volume IGT geometry. Similarly to IGT, CRGT failure can be addressed with such analysis too. However, if CRGT cooling is implemented as SAM strategy CRGT mode of vessel failure is unlikely to happen [11].

The aim of this paper is to clarify the uncertainties in the previous analyses [9], [10], [11], [12], [13] of vessel failure modes and timing obtained with a 3D slice geometry of the debris bed and a 2D axisymmetric model of the vessel which do not take into account the influence of the (i) vessel penetrations (not resolved in the 2D structural model), and (ii) non-axisymmetric distribution of the CRGTs on the melt pool heat transfer behaviour and on the structural analysis. The task for this work is to perform a coupled thermo-mechanical analysis of melt pool heat transfer and the vessel deformation and creep using a 3D quadrant model of the lower head

geometry taking into account actual positions of CRGTs and penetrations. Furthermore, results of present analysis can provide more accurate boundary conditions for the local temperatures deformations for future studies of the IGTs and CRGTs failures. In this work we consider specific scenario with 200 tons of core debris melted and relocated into the lower plenum where cooling through CRGTs and from the top of the debris bed is provided. In order to clarify the dominant mode of failure different accident scenarios have to be considered, but in this work our primary concern is to establish a procedure for future analysis of the other possible scenarios. A comparison provided in the paper suggests qualitative consistency of the results obtained with slice and quadrant geometry models and shows quantitative differences between the solutions.

2. COMPUTATIONAL APPROACH

First, transient formation of the melt pool and thermal load from the melt pool to the vessel wall is calculated with the PECM (which is implemented in FLUENT® using a 3D quadrant geometry model). Then, the coupled thermo-mechanical creep analysis of the reactor pressure vessel is implemented in another 3D quadrant structural model in ANSYS® with imposed temperature distribution on internal vessel walls predicted by PECM which will be discussed shortly. The coupling between FLUENT and ANSYS is only performed in one way, i.e., we consider that the global deformation of the vessel has negligible effect on the melt pool heat transfer predicted by the PECM. In this section we will provide specifications of the 3D quadrant model developed in this paper as well as a short description of the slice model used in the previous studies ([9], [10], [11], [12], [13]).

2.1 Implementation of the PECM in the Quadrant Geometry

2.1.1 PECM Model

In order to get the thermal load for the boundary conditions of the ANSYS structural model, the PECM was implemented in a 3D quadrant geometry of the BWR lower plenum, as is showed in Figure 1. The PECM has been developed based on the concept of effective convectivity which was pioneered by Bui and Dinh [14]. The PECM is a model that describes the turbulent natural convection heat transfer in an internally heated fluid volume, as decay-heated debris bed. In this model, the convective terms of the energy conservation equation are described using directional characteristic heat transfer velocities to transport the heat; therefore the need of solving Navier-Stokes equations is eliminated. This assumption makes this model much more computationally-efficient than conventional CFD codes. Furthermore, the PECM uses reduced characteristics velocities as a function of the melt mass fraction to describe the phase change heat transfer and represent the natural convection heat transfer at mushy zones [15]. The characteristic velocities are determined using heat transfer correlations based on Rayleigh number, namely the upward, sideward and downward Steinberner-Reineke correlations [16]. The PECM is implemented in the commercial code FLUENT, to utilize all advantages of a CFD commercial code solver such as the pre- and post-processing.

2.1.2 Geometry and Boundary Conditions of the Quadrant Model

The quadrant geometry model of the BWR lower plenum developed in the present work includes the penetrations of the 35 CRGTs corresponding to a quarter of the total number of CRGTs present in the RPV. It is assumed that the debris bed formed in the lower head is initially in solid

state as it has quenched in the remaining water filling the space below the core. Then the debris bed is heated up, dried out and re-melted due to the absence of sufficient cooling. In this work we assume that the Instrumentation Guide Tubes (IGTs) are melted and plugged by corium melt during the re-melting of the debris and therefore do not have an influence on melt pool heat transfer. In the studied scenario, CRGT cooling from inside by water flow is implemented at some point in time before CRGT failure is to occur. The water is assumed to be ejected from the CRGTs providing a water layer and thus cooling at the top of the debris bed. Dirichlet type isothermal boundary conditions with water saturation temperature (383 K) are applied to the top and the upper part of the vessel inner wall. The CRGT walls are assumed to be at 450 K, while the initial temperature of the debris bed is also at 450 K. Other surfaces assume Neumann boundary conditions. The external surface of the vessel wall is covered with insulation therefore a small heat flux (20 W/m^2) is allowed. Symmetry boundary conditions were applied to the edges of the quadrant (Figure 1).

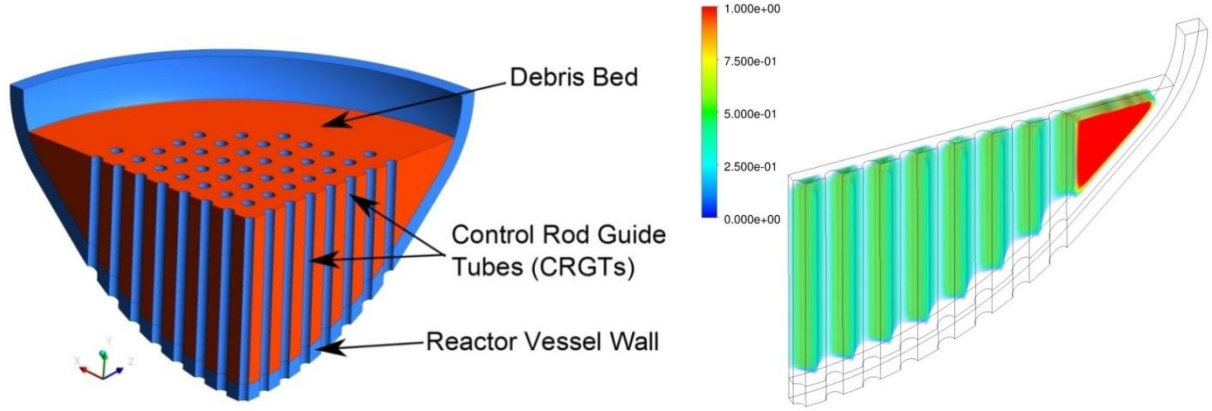

(a) (b)

Figure 1: (a) Geometry of the 3D quadrant used in FLUENT where the PECM is implemented to calculate the melt pool progression and thermal loads to the vessel wall, and (b) 3D Slice geometry used in [9] where the PECM was implemented. The snapshot at t=3.47 h shows the melt mass fraction for the case with 1.9 m height melt pool.

Table 1: Mesh data of the FLUENT models for both 3D-Slice geometry (used in previous calculations) and the 3D-Quadrant geometry presented in this paper

Feature	**3D-Slice**	**3D-Quadrant**
Number of elements	293,750	3,899,924*
Number of Nodes	332,222	1,204,059*
Type of element:	Hexahedra	Tetrahedra: 2713254 Wedges: 763810 Polyhedra: 422860
Typical calculation time	12 hours	4 days

*The numbers of elements and nodes in the 3D quadrant are taken at a specific time but are representatives, since adaptive mesh was chosen and these numbers may change during the calculations.

The 3D-slice geometry model from [9], which will be used for comparison with new results, consists of a segment of BWR lower plenum filled with decay-heated corium and containing 8 cooled CRGTs as shown in Figure 1b. The boundary conditions applied in this model were the

same as those in our 3D quadrant geometry model (Section 2.1.2). Table 1 summarizes the mesh data for both the 3D-slice and 3D quadrant model.

2.2 Implementation of Structural Analysis in the Quadrant Geometry

In order to perform the structural analysis of the RPV lower plenum, finite element mechanical calculations were performed using a 3D ANSYS model. The model also represents a quadrant of the vessel's lower plenum including the CRGTs penetrations as the one implemented in FLUENT for the thermal load calculations (see Figure 2).The calculation was performed using full transient analyses and strong structural-thermal coupling [17]. We use SOLID226 element type and a mesh consisting of 117362 nodes and 71343 elements with an average edge length of 0.05 m. A typical run with this mesh on a 4 Intel Cores 3GHz windows platform takes about 14 days.

2.2.1 Material

The vessel was considered to be made of carbon steel SA533B1 with material properties such as density, elastic modulus (linear isotropic), thermal conductivity (isotropic), specific heat, and coefficient of thermal expansion (that are all functions of temperature) taken from [8]. The Poisson's ratio is set to 0.3. The elastic modulus is highly dependent on temperature, which decreases 2 orders of magnitude as the temperature increases from 300 to 1050 K. Consequently, the strain due to creep will increase significantly at high temperatures as the elastic response of the material is inversely proportional to the elastic modulus. For this reason creep is considered the main cause of failure of the reactor pressure vessel wall and it has to be taken into account in the structural calculations.

2.2.2 Creep Model

For our analysis, a modified time hardening (primary) creep model is chosen in ANSYS (same as the one used in 2-D structural calculations in [9]). The coefficients of the equivalent strain model for the primary creep stage as a function of temperature were fitted against the experimental creep data for SA533B1 from [8], please see [9] for more details. However this creep model is not able to identify a creep limit as it only predicts the equivalent creep strain for the primary creep stage. Instead of defining a creep limit a range of strain which can be considered reliably predicted by the model was defined. Beyond this range the results are only considered as indicative in a qualitative way. The limit of this reliably predicted range was set at 20% strain [9]. We adopt the time necessary to reach 20% strain as the minimum estimated vessel wall failure time. Indeed, the structure in such state is very close to its mechanical failure ([12], [13]).

2.2.3 Geometry and Boundary Conditions

The thermal boundary conditions on the inner surface of the vessel wall that is in contact with debris are provided by the PECM calculation of a 3D quadrant model. Other boundary thermal conditions are the same as in section 2.1.2. The pressure inside the vessel is set at 0.3 MPa (corresponding to the pressure after the actuation of the vessel depressurization systems). Also the hydrostatic pressure due to the weight of the debris bed was taken into account. The displacement boundary conditions and geometry of the ANSYS model are summarized in

Figure 2. We do not apply displacement boundary conditions on the CRGT penetrations as we consider that they are not strongly attached to the structures of the lower part of the reactor cavity and therefore they will move with some freedom while the vessel is deformed.

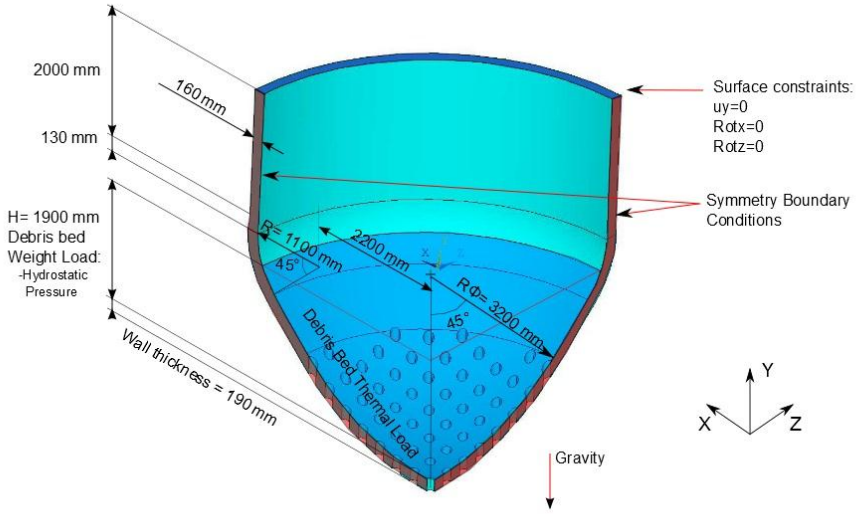

Figure 2: Geometry and boundary conditions of the 3D quadrant structural model of the vessel's lower head implemented in ANSYS.

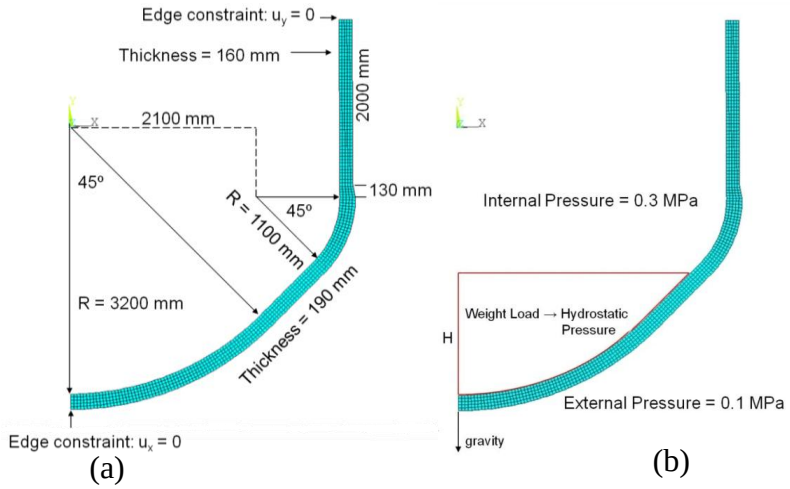

Figure 3: 2D structural model previously used in [9] for the analysis of the creep mechanical failure of the vessel wall (a) 2D axisymmetric geometry and mesh (b) schematics of mechanical load on the reactor vessel.

The 2D structural ANSYS model developed in [8], [9] only takes into account the edge of one slice of the reactor vessel lower head, as shown in Figure 3. In this 2D model the vessel was considered axisymmetric and the CRGTs were not included, therefore their influence on the reactor vessel wall deformation could not be studied. The thermal boundary conditions were provided by averaging the temperature profile obtained on the vessel surface of the 3D slice PECM model (Figure 1b). Except for this feature, the rest of boundary conditions such as pressure inside the vessel or hydrostatic pressure due to the 1.9 m debris bed were the same as

that implemented in our 3D quadrant model. Lastly in Table 2, we present some relevant data of the mesh of both 3D quadrant ANSYS model used in this paper and the 2D ANSYS model previously used [9].

Table 2: Mesh data of the ANSYS models for both 2D (used in previous calculations) and the 3D-Quadrant geometry presented in this paper

Feature	2D	3D-Quadrant
Number of elements	850	71,343
Number of Nodes	2901	117,362
Type of element	Quad Plane223	SOLID226
Average edge length	0.04 m	0.05 m
Approximated run time	0.78h	14 days

Ratios of different parts of the debris bed surface to the total volume of the debris V_T for the quadrant and slice geometries are presented in Table 3. Note that while total surface to volume ratio is very close in both models, there are significant differences for different parts of the total surface. On one hand, the ratio of cooled surfaces (CRGTs plus top of the bed) to the volume is slightly larger (~11%) for the slice geometry. Thus the average temperature of the debris is expected to be slightly lower in the slice geometry with respect to that in the quadrant. On the other hand, the ratio of the vessel wall surface in contact with the debris bed to the total volume of the debris is considerably larger (~45%) in the quadrant geometry. Thus, on average, later heating up of the wall is expected in the quadrant model.

Table 3: Ratios of the debris bed surfaces to the total volume V_T of the debris

Ratios	Quadrant	Slice	Quadrant/Slice
CRGT surface / V_T, m^{-1}	3.98	4.84	0.82
Top debris bed / V_T, m^{-1}	1.04	0.79	1.32
Total cooled surface / V_T, m^{-1}	5.02	5.63	0.89
Vessel wall in contact with the debris bed / V_T, m^{-1}	1.40	0.97	1.45
Total debris bed surface / V_T, m^{-1}	6.42	6.60	0.97

3. RESULTS AND DISCUSSION

A coupled thermo-mechanical creep analysis of the pressure vessel lower head is performed considering a pool melt of 1.9 m height and CRGT cooling implemented as SAM strategy. First, the transient formation of the melt pool and thermal load from the melt pool to the vessel wall are calculated with the PECM in the 3D quadrant geometry proposed model. We consider that at time 0 the debris bed is present in its solid state at a temperature of 450 K. From this point the temperature of the debris bed starts increasing due to the decay heat.

Figure 4a shows the average temperature of the debris bed as a function of time for the 3D slice model [9] and 3D quadrant model. Figure 4b shows the melt mass fraction present in the debris bed as a function of time, also for both models. Figure 5 shows the averaged melt superheat temperature which is one of the important parameters for both steam explosion and debris agglomeration [2], [3], [4], [5]. Generally, we found that results of both the 3D quadrant and the

3D slice models are quite consistent and they follow the same trends with some small quantitative differences.

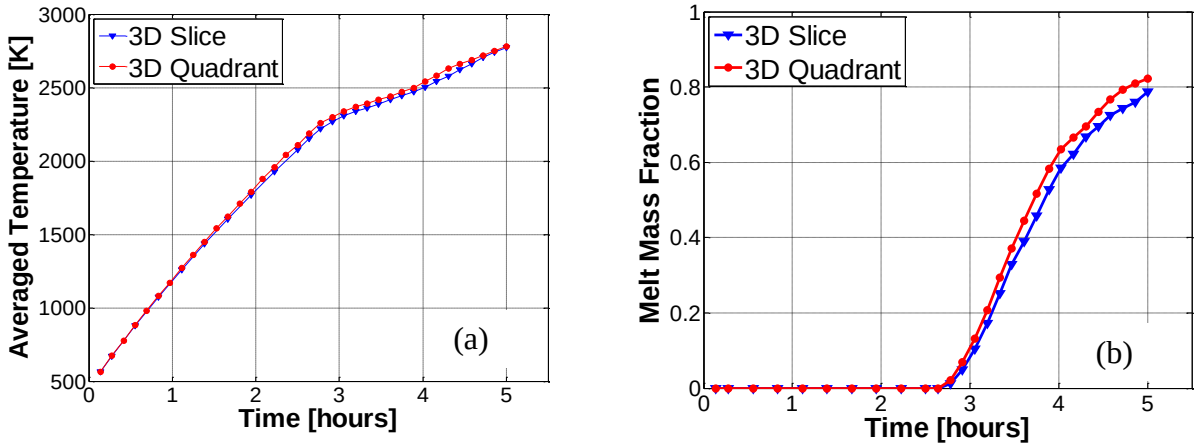

Figure 4: (a) Averaged temperature in the debris bed as a function of time for both, 3D slice model [9] and the 3D Quadrant model presented in this paper (red), and similarly, (b) Averaged melt mass fraction present in the debris bed a as a function of time.

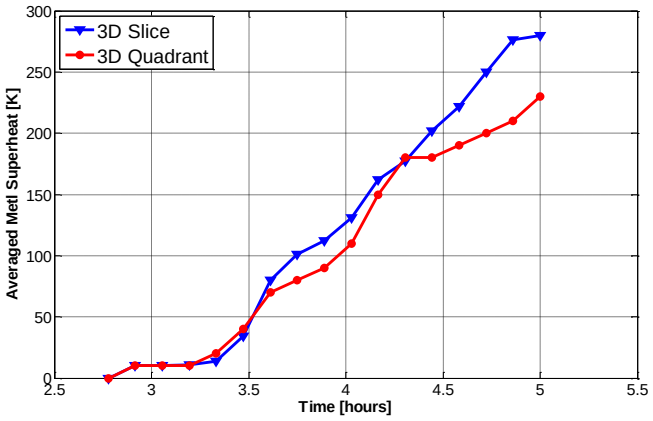

Figure 5: Averaged melt superheat in the debris bed as a function of time for both, 3D slice model from [9] (blue) and the 3D Quadrant model presented in this paper (red). The melting temperature of the corium is considered to be 2750 K.

The debris bed starts melting around at 2.6 hours. The amount of melt increases with time due to the decay heat. While both average temperature and fraction of liquid melt are larger in case of 3D quadrant model, the averaged liquid melt superheat temperature is lower. For instance, the 3D quadrant predicts 5 % more of melt mass fraction present in the debris bed at the time of vessel wall creep failure found by the 2D structural model (~3.5 hours). Apparently, fraction of liquid melt is growing faster than the temperature of the melt. One possible explanation for obtaining higher melt mass fractions could be in the axisymmetric geometry assumption of the 3D slice model. This assumption implies that there are always 8 cooled CRGTs symmetrically distributed, which is not the case in reality as shown in Figure 6a. There are some slices of the reactor vessel where there are only 7 or even 6 CRGTs. In the regions with smaller number of cooled CRGTs results show larger amount of molten corium. Figure 6 shows the melt mass

fraction on a XZ cutting plane at 1.2 m from the bottom of the melt pool at t=3.5 h for (a) 3D quadrant and (b) 3D Slice. The results are quite similar in both models. It is also interesting to observe the formation of isolated melt pools between the cooled CRGTs as well as in the periphery region, where the CRGTs are not present.

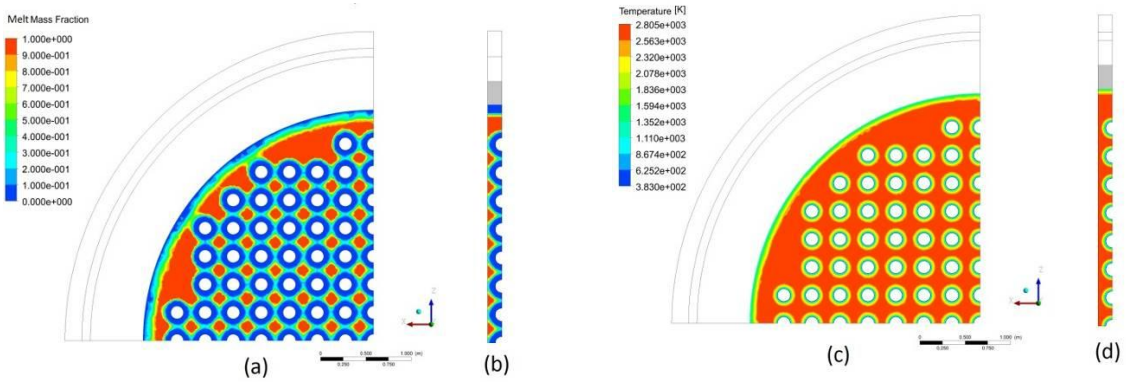

Figure 6: (a)-(b) Melt mass fraction and (c)-(d) temperature profile on the XZ plane located at 1.2 m from the bottom of debris bed and at time t=3.47 hours; (a) and (c) corresponds to the 3D quadrant geometry while (b) and (d) corresponds to the 3D slice geometry. Note the non-axisymmetric distribution of the CRGTs and its influence on the melt formation.

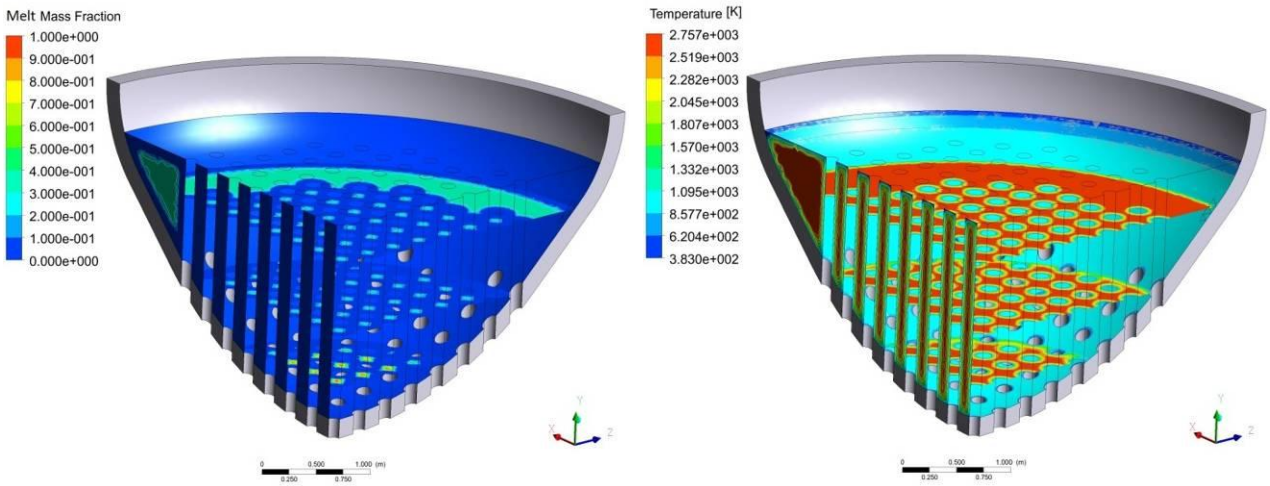

Figure 7:(a) Melt mass fraction and (b) temperature profile at t=2.91 h on levels 0.3, 1, and 1.5 m from the bottom of the melt pool, on the vessel surface, and in vertical a cross section.

In Figure 7, 8, and 9, the melt mass fraction (a) and temperatures (b) at three different horizontal cutting planes of the debris bed corresponding to 0.3, 1, and 1.5 meters from the bottom of the melt pool, as well as one vertical cutting plane and the vessel wall surface are shown. The three figures are snapshots at times 2.91 h, 3.47 h, and 4.72 h respectively. In Figure 7a (at 2.91 h) we can observe how the debris bed starts to melt at the periphery regions where the CRGTs are not present, leading to the formation of mushy zones (blue). The temperature in these zones is around 2756 K, above the solidus temperature of 2750 K (see Figure 7b). The temperature drops at the surroundings of the CRGTs as well as near the debris bed top surface and vessel surface. It

is also interesting to observe that the maximum melt mass fraction (red) at this time (2.91 h) is observed at the isolated regions between the CRGTs, close to the bottom of the debris bed, since this part is farthest from the top cooled surface (Figure 7a).

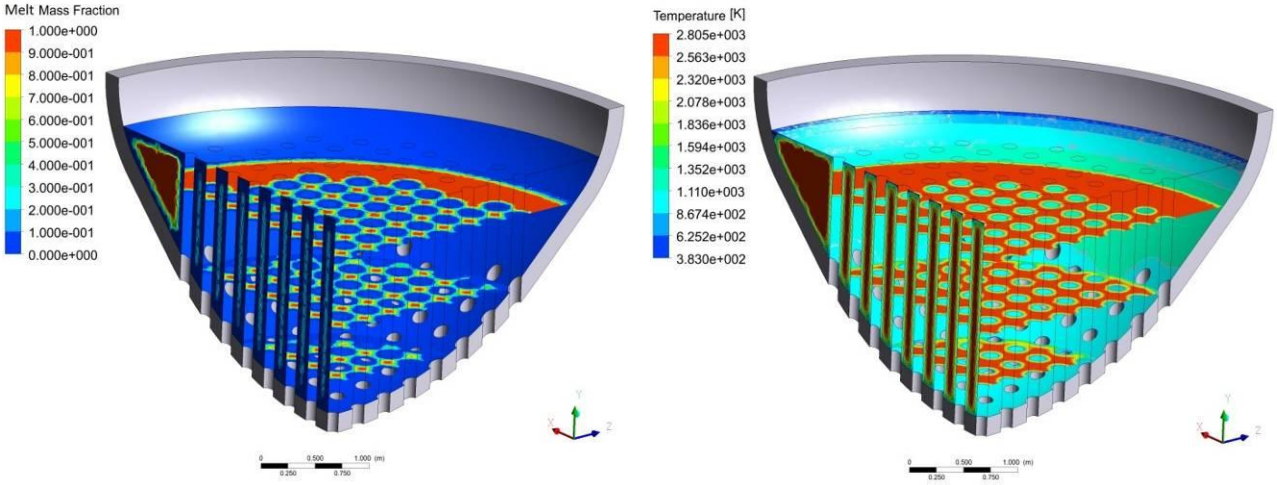

(a) (b)

Figure 8: (a) Melt mass fraction and (b) temperature profile at t=3.47 hours on levels 0.3, 1, and 1.5 m from the bottom of the melt pool, on the vessel surface, and in vertical a cross section.

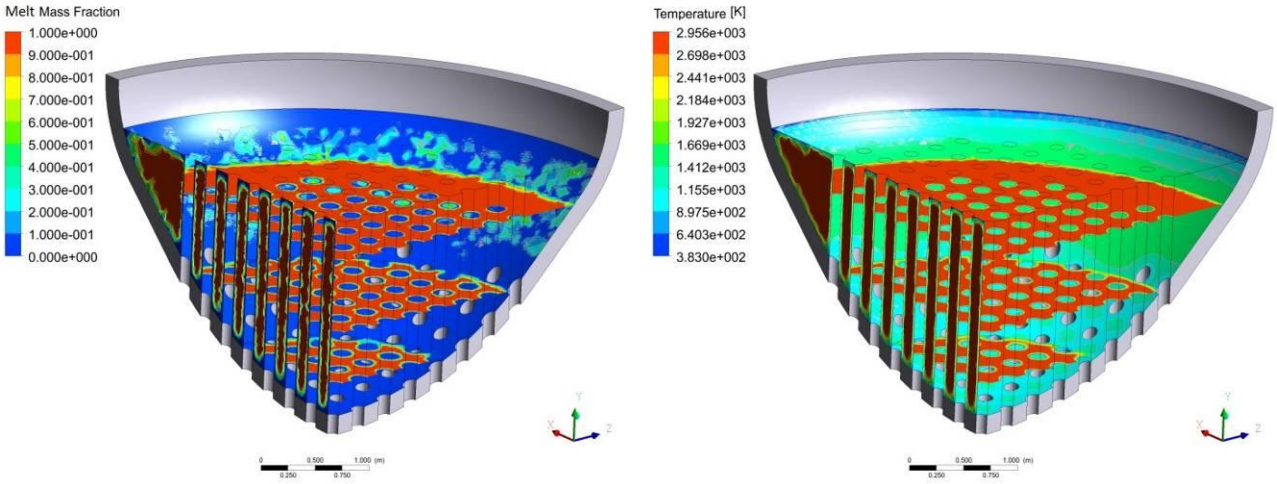

(a) (b)

Figure 9: (a) Melt mass fraction and (b) temperature profile at t=4.72 h on levels 0.3, 1, and 1.5 m from the bottom of the melt pool, on the vessel surface, and in vertical a cross section.

At time 3.47 h, the debris bed is completely melted at the periphery regions, leading to the formation of a melt pool with a triangular section, as can be observed on the vertical cutting plane in Figure 8a. Isolated melt pools are also observed in the regions between CRGTs. However the zones close to the vessel surfaces and the cooled CRGTs are still in solid state (blue) leading to the formation of a crust layer near these surfaces. The thermal load on the vessel has increased considerably at this time (Figure 8b), especially at the periphery where the vessel wall temperature reaches 1222 K (as shown more clearly in Figure 10b).

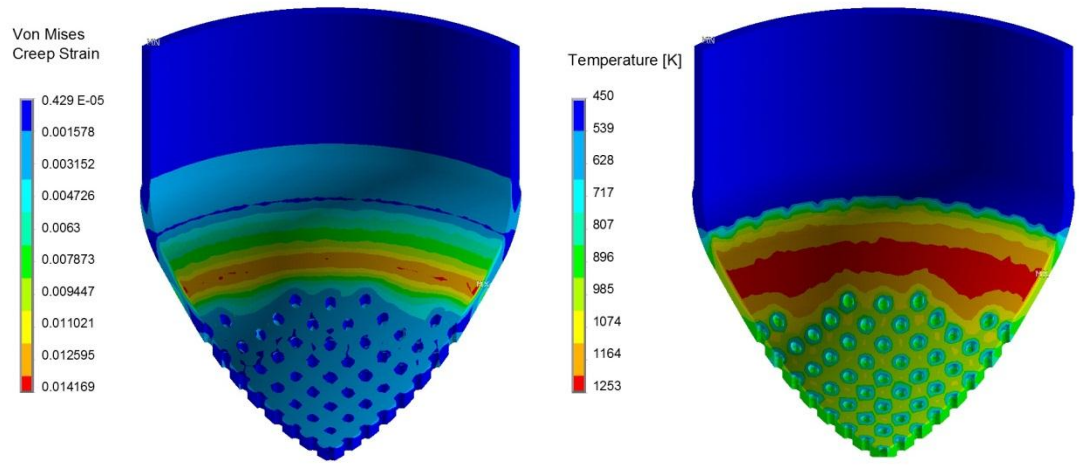

(a) (b)

Figure 10: Snapshot of the (a) Von Mises creep strain and (b) Temperature at t=3.47 h.

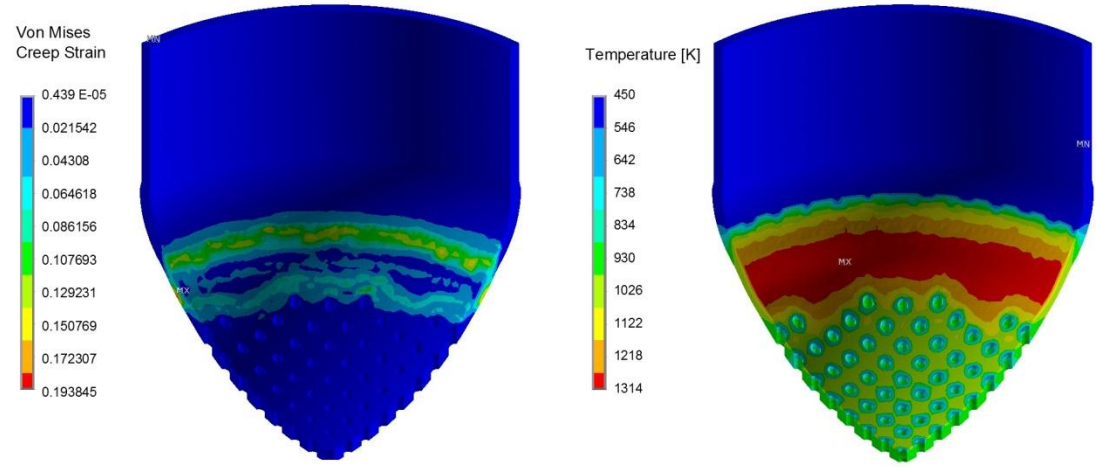

(a) (b)

Figure 11: Snapshot at t = 3.74 h of (a) Von Mises creep strain and (b) Temperature.

Figure 9 shows the melt mass fraction and temperature profile at t= 4.72 h. At this time all the individual melt pools between the CRGTs are connected, forming a single melt pool together with the one at the top periphery of the pool. The crust layer presented near the vessel wall and CRGTs surfaces becomes thinner each time, to the point that some mushy zones reach the vessel's wall in several regions at the periphery (light blue colour on the vessel's surface in Figure 9a). The thermal load to the vessel wall continues to increase, reaching about 2000 K. According to the creep analysis performed in the 3D structural model the vessel wall has already failed at that time.

Once the temperature profiles as a function of time on the vessel surface are obtained from the PECM calculations, they were applied as thermal boundary conditions for the structural analysis. Figure 10, 11, and 12 show the Von Mises creep strains and temperature distributions in the vessel's wall at t=3.47 h and t=3.74 h, and 3.8 h respectively. High creep strains are reached at the periphery of the pool, where the influence of CRGT cooling is lower, leading to temperatures

on the vessel wall surfaces up to 1342 K (see Figure 12b). These results are in accordance with the behaviour predicted in [9] using 2D structural analysis, where it was found that the vessel wall will fail by localized creep at the top periphery of the melt pool.

Figure 10a shows that at 3.47 h, the maximum creep strain is only 1.4 %, which is still far from the adopted 20 % creep strain as a failure criterion. However, the maximum creep strain will follow an accelerated increase after some point. It is assumed that once the creep starts to accelerate, the failure of the vessel wall is imminent. Figure 11a shows that the maximum creep strain at 3.74 hours is 19 % while Figure 12a shows that at 3.8 h has reached 27 %. The creep accelerates even further in just a matter of few minutes. Comparison of the vessel wall failure timing obtained with 3D quadrant and 2D structural models suggest that 15 minutes later failure is expected according to the case of 3D quadrant geometry. The reason for this change in timing could be attributed to (i) larger ratio of cooling surface to heated volume (leading to lower thermal load to the vessel's surface) in 3D quadrant geometry, and (ii) the fact that temperatures applied on the 2D structural model of the vessel are generated using averaging of the 3D temperature distributions obtained from the PECM 3D slice model. Note that later failure is predicted in the quadrant geometry despite the higher melt mass fractions and averaged temperatures (Figure 4). Another possible reason for later failure can be attributed to the spatial distribution of the stresses in the 3D quadrant model, e.g. if there are few relatively cold "strings" inside a quite thick vessel which can hold the load, then the bottom of the vessel may not displace as much. More detailed analysis of the reasons for observed differences is a topic for future research.

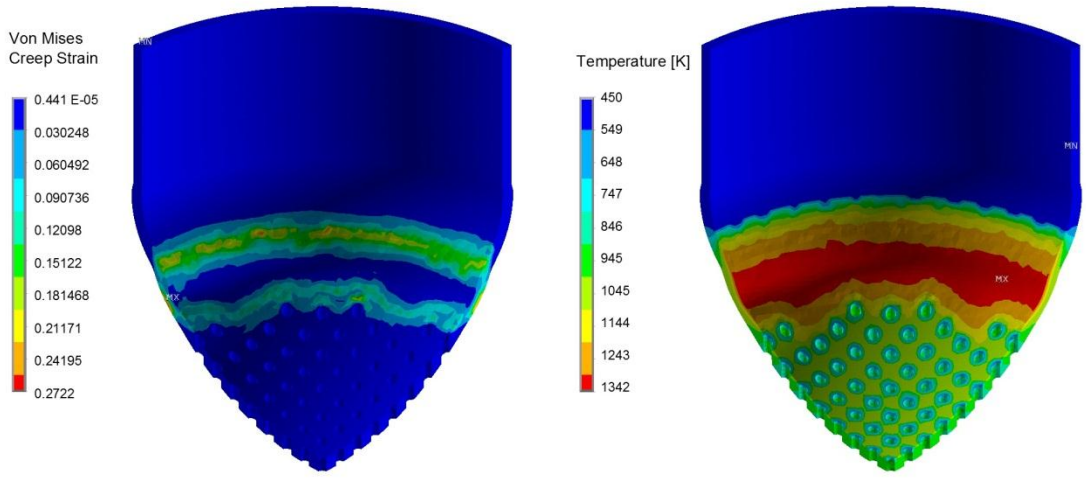

(a) (b)

Figure 12: Snapshot at t = 3.8 h of (a) Von Mises creep strain and (b) Temperature.

Figure 13 shows the un-deformed and deformed edge of the 3D quadrant model in comparison with the 2D axisymmetric model in [9]. It can be observed how the bottom of the vessel is displaced vertically due to the thermo-mechanical load of the melt pool and the gradual loss of structural strength at the localized creep region. It is also very interesting to point out the horizontal displacement of the CRGTs penetrations in the 3D quadrant model due to the global deformation of the vessel (Figure 13c). These horizontal displacements will play a major role in future studies of CRGTs and IGTs failure and possibility of clamping. The magnitude of the

radial displacement of penetrations is more pronounced in the peripheral CRGTs, where clamping can happen more likely. Generally, the global deformation of the vessel in the 3D model is very similar to that in the 2D model. Thus we also expect that the IGT failure studies carried out previously [10] still hold, where it was found that the farthest IGT from the centre can be clamped before the melting of its nozzle weld, while the IGT located at the bottom is not clamped the entire time. This is to be confirmed in the future analysis.

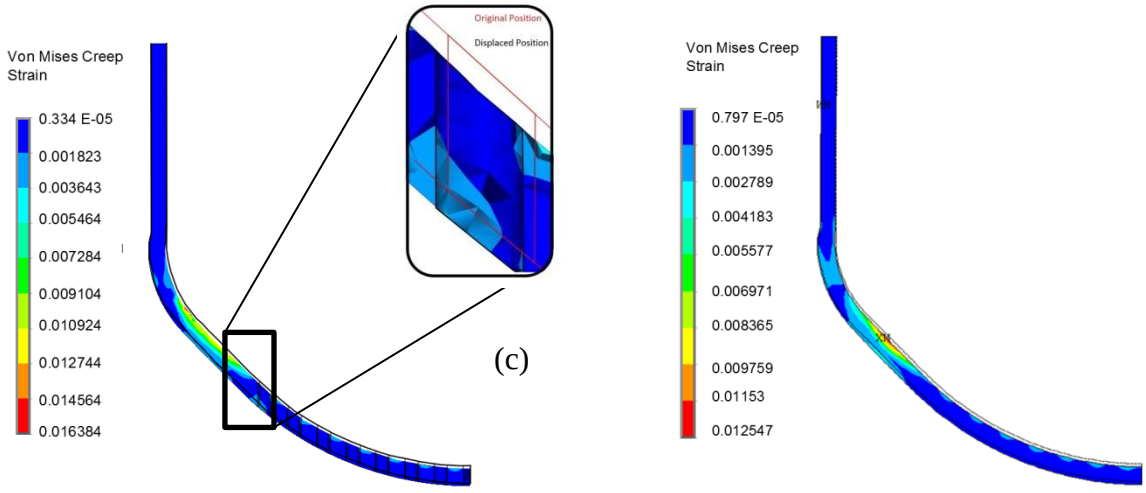

(a) (b)

Figure 13: Un-deformed and deformed edges of the XY plane for (a) 3D quadrant model and (b) 2D structural model in [9] at t = 3.05 h. A close-up of the displacement at the farthest CRGT predicted by the 3D quadrant model is shown at (c).

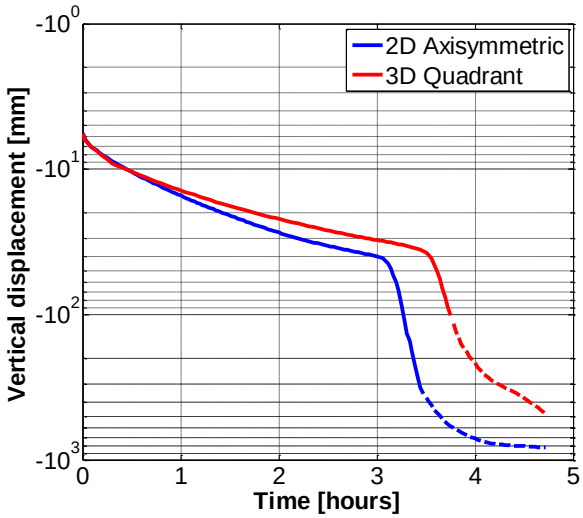

Figure 14: Vertical displacement of the canter of the vessel for the 3D Quadrant geometry and the 2D axisymmetric geometry.

Figure 14 shows the vertical displacement of the vessel bottom centre for the 3D Quadrant model (red) and the 2D structural model (blue). The displacement follows a similar trend for both models, showing their overall consistency. However, accelerated creep strain starts later for the

3D quadrant model (around 3.74 hours instead of the 3.5 hours predicted by the 2D structural model [9]).

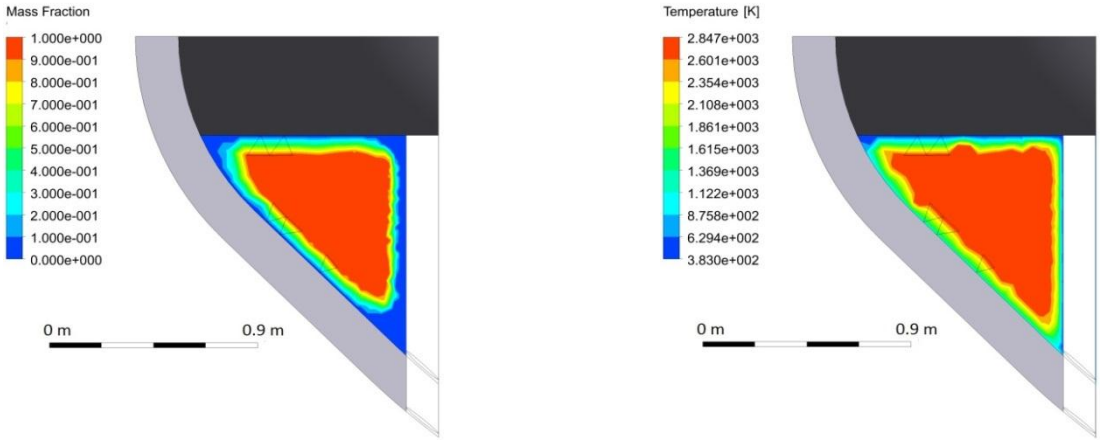

(a) (b)

Figure 15: (a) Melt mass fraction and (b) temperature profile at t = 3.75 h of the melt pool close to the zone where localized creep failure is expected to happen.

Lastly, Figure 15 shows the melt mass fraction and temperature profile at t = 3.75 h in the debris bed close to the zone where localized creep failure is expected to take place. The effect of grid resolution in the vicinity of melt-crust interface has not been investigated yet and will be done in future work. Nevertheless, it should be mentioned that at the time of vessel failure the wall is still covered with a crust. It can be expected that deformation of the vessel in the failure region and thermal loads will lead eventually to the failure of the crust and melt release. However, remaining crust can serve as a protective refractory layer hindering intensive ablation of the wall in the vicinity of the opening.

4. CONCLUSIONS

The present study addressed in-vessel stage of a hypothetical severe accident in a Nordic BWR, after relocation of core debris (~200 tons) into the lower head of reactor pressure vessel forming a 1.9 m deep debris bed. It was assumed that CRGT cooling is implemented as an element of SAM strategy. Coupled thermo-mechanical analysis was carried out for (i) melt pool formation and heat transfer using the PECM implemented in a FLUENT and (ii) vessel wall creep using ANSYS with thermal loads predicted by the PECM.

Main focus of the present study is on comparison of the results obtained with (i) PECM in 3D slice model of the debris bed coupled with ANSYS 2D axisymmetric vessel wall model, and (ii) PECM in 3D quadrant model of the bed coupled with ANSYS 3D quadrant model of the vessel taking into account penetrations in the vessel. The most important questions are (i) how actual 3D geometry with non-axisymmetric distribution of CRGTs can affect melt pool heat transfer; (ii) how penetrations in the vessel wall (resolved in 3D quadrant model) can affect creep characteristics and eventually timing of failure.

The results of the melt pool formation and heat transfer simulations show that the melt mass fraction and averaged temperatures provided by the 3D quadrant geometry are qualitatively

consistent with previously obtained results using 3D slice geometry. Although, the former shows slightly higher melt mass fractions and temperatures attributed to the fact that 3D quadrant geometry differs from the slice by (i) smaller ratio of cooled (CRGT and top) surfaces to heated debris volume and (ii) non-axisymmetric distribution of the CRGTs.

Structural analysis suggests that higher creep strains are reached in the vessel in the vicinity of the top periphery of the melt pool, where thermal and mechanical load from the debris bed are larger. These observations are qualitatively consistent with the previously obtained results using a 2D axisymmetric model. We found that creep starts to accelerate ~15 minutes later in the 3D model than in the 2D model. The main reason for this behaviour is believed to be on average lower thermal load to the vessel's surface due to the larger ratio of vessel surface in contact with debris to the total volume of debris in the 3D Quadrant Model. Other possible reasons for later failure also have to be considered in the future analysis.

Failure location is far from the area with the penetrations. Thus local weakening of the wall by the penetrations doesn't affect failure timing too much, and can only slightly delay the failure (compared to 2D analysis) by reducing the mass of the vessel wall. It is instructive to note though that the influence of penetrations for the ballooning type of failure at the bottom of the vessel [9] might be more significant.

Obtained results provide boundary conditions for detailed analysis of vessel penetrations failure. The displacements (both in horizontal and vertical directions) of the vessel penetrations due to the global vessel deformation can be significant and should be taken into account in future analysis. The developed methodology will be applied in the future for the studies of other accident scenarios, such as no cooling through the CRGTs, different amounts of debris.

5. ACKNOWLEDGEMENTS

We acknowledge the financial support from the Swedish Nuclear Radiation Protection Authority (SSM), Swedish Power Companies, European Commission (SARNET-2), Nordic Nuclear Safety Program (NKS), and Swiss Federal Nuclear Safety Inspectorate (ENSI) under the APRI- MSWI program at the Royal Institute of Technology (KTH), Stockholm, Sweden. Authors are grateful to Professor Sevostian Bechta from KTH for very useful comments and discussions.

6. REFERENCES

[1] P. Kudinov, A. Karbojian, W. Ma, and T.-N. Dinh "The DEFOR-S Experimental Study of Debris Formation with Corium Simulant Materials", *Nuclear Technology*, 170(1), pp. 219-230, 2010.

[2] P. Kudinov and M.V. Davydov, "Development and validation of conservative-mechanistic and best estimate approaches to quantifying mass fractions of agglomerated debris," *Nuclear Engineering and Design*, accepted, 2013.

[3] P. Kudinov, A. Karbojian, C.-T. Tran, and W. Villanueva, "Experimental Data on Fraction of Agglomerated Debris Obtained in the DEFOR-A Melt-Coolant Interaction Tests with High Melting Temperature Simulant Materials," Submitted to *Nuclear Engineering and Design*, 2013.

[4] P. Kudinov, A. Karbojian, C.-T. Tran, and W. Villanueva, "The DEFOR-A Experiment on Fraction of Agglomerated Debris as a Function of Water Pool Depth," Proceedings of

The 8th International Topical Meeting on Nuclear Thermal-Hydraulics, Operation and Safety (NUTHOS-8), Shanghai, China, October 10-14, N8P0296, 2010.

[5] P. Kudinov and M. Davydov, "Development and Validation of the Approach to Prediction of Mass Fraction of Agglomerated Debris," Proceedings of The 8th International Topical Meeting on Nuclear Thermal-Hydraulics, Operation and Safety (NUTHOS-8), Shanghai, China, October 10-14, N8P0298, 2010.

[6] S. Yakush, P. Kudinov, and T.-N. Dinh, "Multiscale Simulations of Self-organization Phenomena in the Formation and Coolability of Corium Debris Bed," Proceedings The 13th International Topical Meeting on Nuclear Reactor Thermal Hydraulics (NURETH-13), September 27-October 2, 2009. Kanazawa City, Ishikawa Prefecture, Japan, Paper N13P1143, 2009.

[7] S. Yakush and P. Kudinov, "Effects of Water Pool Subcooling on the Debris Bed Spreading by Coolant Flow," Proceedings of ICAPP 2011, Nice, France, May 2-5, Paper 11416, 2011.

[8] J. L. Rempe, S. A. Chavez, G. l. Thinnes C. M. Allison, G.E. Korth, R. J. Witt, J. J. Sienicki, S. K. Wang, L. A. Stickler, C. H. Heath and S. D. Snow, "Light Water Reactor Lower Head Failure", Report NUREG/CR-5642, Idaho Falls, 1993.

[9] W. Villanueva, C. T. Tran and P. Kudinov "Assessment with coupled thermo-mechanical creep analysis of combined CRGT and external vessel cooling efficiency for a BWR", Proc. of The 14th International Topical Meeting on Nuclear Reactor Thermal Hydraulics (NURETH-14), Toronto, Ontario, Canada, September 25-30, 2011.

[10] W. Villanueva, C.T. Tran, and P. Kudinov, "A Computational study on instrumentation guide tube failure during a severe accident in boiling water reactors", Proc. of The 14th International Topical Meeting on Nuclear Reactor Thermal Hydraulics (NURETH-14), Toronto, Ontario, Canada, September 25-29, 2011.

[11] W. Villanueva, C.T. Tran and P. Kudinov, "Effect of CRGT cooling on modes of global failure of a BWR vessel lower head" Proceedings of The 20th International Conference on Nuclear Engineering (ICONE20), Anaheim, CA, USA, July 30 – August 3, 2012.

[12] W. Villanueva, C.-T. Tran, and P. Kudinov, "Coupled Thermo-Mechanical Creep Analysis for Boiling Water Reactor Pressure Vessel Wall Lower Head," Proceedings of The 8th International Topical Meeting on Nuclear Thermal-Hydraulics, Operation and Safety (NUTHOS-8), Shanghai, China, October 10-14, N8P0248, 2010.

[13] W. Villanueva, C.-T Tran, and P. Kudinov, "Coupled thermo-mechanical creep analysis for boiling water reactor pressure vessel lower head," *Nuclear Engineering and Design*, 249, pp. 146-153, 2012.

[14] V. A. Bui and T.-N. Dinh, "Modeling of heat transfer in heated-generating liquid pools by an effective diffusivity-convectivity approach", Proceedings of 2nd European Thermal-Sciences Conference, Rome, Italy, 1365-1372, 1996.

[15] C.-T. Tran, T.-N. Dinh, "The effective convectivity model for simulation of melt pool heat transfer in a light water reactor pressure vessel lower head. Part I: Physical processes, modeling and model implementation", *Progress in Nuclear Energy*, 51, pp. 849-859, 2009.

[16] U. Steinberner and H. H. Reineke, "Turbulent buoyancy convection heat transfer with internal heat sources", Proceedings of the 6th International Heat Transfer Conference, Toronto, Canada, 2, 305-310, 1978.

[17] ANSYS 12.1, User's Manual, ANSYS®, Inc., 2009.